**The Thesis Committee for Yuhao Sun**

**Certifies that this is the approved version of the following thesis:**

# Investigation of Buoyant Plumes in a Quasi-2D domain: Characterizing the Influence of Local Capillary Trapping and Heterogeneity on Sequestered $CO_2$ – A Bench Scale Experiment

**APPROVED BY**

**SUPERVISING COMMITTEE:**

**Supervisor:** _____

**Steven L Bryant**

_____

**Timothy A Meckel**

# Investigation of Buoyant Plumes in a Quasi-2D domain: Characterizing the Influence of Local Capillary Trapping and Heterogeneity on Sequestered $CO_2$ – A Bench Scale Experiment

**by**

**Yuhao Sun, B.S.C.E.**

**Thesis**

Presented to the Faculty of the Graduate School of

The University of Texas at Austin

in Partial Fulfillment

of Requirements

for the Degree of

**Master of Science in Engineering**

**The University of Texas at Austin**

**May 2014**

**Acknowledgement**

First of all, I would like to express my sincerest gratitude to my advisor Professor Steven Bryant for his guidance on research as well as on personal life. As the most wonderful and helpful supervisor in every possible way, he demonstrated fervent passion towards scientific research and meticulous academic attitude, which have influenced me deeply. I would also like to thank Dr. Meckel for his precious time in reading the thesis and offering valuable suggestions and solutions to some research problems. Their patience, encouragements and supports let me know the research work is meaningful and beneficial to the humankind.

Special thanks go to the Department of Energy National Energy Technology Laboratory who funded this project #DE-FE0004956, and the related sponsors of the Geologic $CO_2$ storage Joint Industry Project at the University of Texas at Austin.

I am extremely grateful to Glen Baum and Gary Miscoe who provided anything I needed for the research works; to Daryl Nygaard who helped me with the design, construction and modification of the experimental apparatus; to Roger Terzian and Joanna Castillo for their IT-related assistance; and to Sophia Ortiz for ordering the materials needed for the lab work and administrative assistance. Without their generous helps, this research would not be possible.

My heartfelt gratitude goes to my parents and other family members who have offered their best and unyielding supports throughout the journey of my academic life.

Last by not least, I would like to thank my dearest Fiancé Xin Hu for always being on my side. She took great care of me when research work turned hectic. Her love, patience and understanding have strengthened my life with hope, and made a lot of hard times bearable.

## Abstract

**Investigation of Buoyant Plumes in a Quasi-2D domain: Characterizing the Influence of Local Capillary Trapping and Heterogeneity on Sequestered $CO_2$ – A Bench Scale Experiment**

Yuhao Sun, M.S.E

The University of Texas at Austin, 2014

Supervisor: Steven L Bryant

Leakage of stored bulk phase $CO_2$ is one risk for sequestration in deep saline aquifers. As the less dense $CO_2$ migrates upward within a storage formation or in layers above the formation, the security of its storage depends upon the trapping mechanisms that counteract the migration.

The trapping mechanism motivating this research is local capillary trapping (LCT), which occurs during buoyancy-driven migration of bulk phase $CO_2$ within a saline aquifer with spatially heterogeneous petrophysical properties. When a $CO_2$ plume rising by buoyancy encounters a region where capillary entry pressure is locally larger than average, $CO_2$ accumulates beneath the region.

One benefit of LCT, applied specifically to $CO_2$ sequestration and storage, is that saturation of stored $CO_2$ phase is larger than the saturation for other permanent trapping mechanisms. Another potential benefit is security: $CO_2$ that occupies local capillary traps remains there, even if the overlying formation that provides primary containment were to be compromised and allow leakage.

Most work on LCT has involved numerical simulation (Saadatpoor 2010, Ganesh 2012); the research work presented here is a step toward understanding local capillary trapping at the bench scale. An apparatus and set of fluids are described which allow examining the extent of local capillary trapping, i.e. buoyant nonwetting phase immobilization beneath small-scale capillary barriers, which can be expected in typical heterogeneous storage formation. The bench scale environment analogous to $CO_2$ and brine in a saline aquifer is created in a quasi-two dimensional experimental apparatus with dimension of 63 cm by 63 cm by 5 cm, which allows for observation of plume migration with physically representative properties but at experimentally convenient ambient conditions. A surrogate fluid pair is developed to mimic the density, viscosity and interfacial tension relationship found at pressure and temperature typical of storage aquifers.

Porous media heterogeneity, pressure boundary conditions, migration modes of uprising nonwetting phase, and presence of fracture/breach in the capillary barrier are studied in series of experiments for their influences on LCT. A variety of heterogeneous porous media made of a range of sizes of loosely packed silica beads are used to validate and test the persistence of local capillary trapping mechanism. By adjusting the boundary conditions (fluid levels in reservoirs attached to top and to bottom ports of the apparatus), the capillary pressure gradient across the domain was manipulated. Experiments were conducted with and without the presence of fracture/potential leakage pathway in the capillary seal.

The trapped buoyant phase remained secure beneath the local capillary barriers, as long as the effective capillary pressure exerted by the trapped phase (proportional to column height of the phase) is smaller than the capillary entry pressure of the barrier. The local capillary trapping mechanism remained persistent even under forced imbibition, in

which a significantly higher hydraulic potential gradient, and therefore a larger gradient in capillary pressure, was applied to the system. The column height of buoyant fluid that remained beneath the local capillary barrier was smaller by a factor corresponding to the increase in capillary pressure gradient. Mimicking a breach of the caprock by opening valves at the top of the apparatus allowed buoyant mobile phase held beneath the valves to escape, but buoyant phase held in local traps at saturations above residual, and therefore potentially mobile, was undisturbed.

This work provides systematic validation of a novel concept, namely the long-term security of $CO_2$ that fills local (small-scale) capillary traps in heterogeneous storage formations. Results from this work reveal the first ever unequivocal experimental evidence on persistence of local capillary trapping mechanism. Attempts to quantify the nonwetting phase saturation and extent of LCT persistence serve as the initial steps to potentially reduce the risks associated with long-term storage security.

**CONTENTS**

**LIST OF TABLES:**

**LIST OF FIGURES:**

# Chapter 1 Introduction

## 1.1 Problem Statement

### 1.1.1 Energy demand, fossil fuel consumption and the "carbon problem".

The world population has exceeded 7 billion in 2011 (US Census Bureau), and more than six billion people in the world today burn organic fuel to empower their daily activities. Simply put, more population demands more energy.

The Intergovernmental Panel on Climate Change (IPCC) suggests that the supply of world's primary energy will continue to be dominated by fossil fuels until the middle of the 21st century at least (IPCC 2005). In the United States, the Department of Energy (US DOE) projects that the nation's consumption of fossil fuels will continue to play a major role. Figure 1.1 below shows that fossil fuels will contribute to about 80% share of total energy use by 2040, which is very similar to the global scenario.

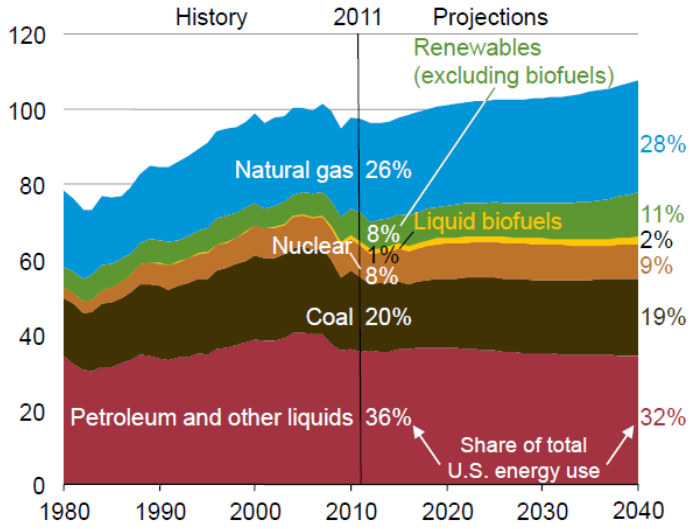


Figure 1.1: US primary energy use by fuel, 1980-2040 (quadrillion Btu). Natural gas leads the rise in primary energy consumption and conventional fossil fuels still dominates the total share. (Figure from United States Energy Information Administration Annual Energy Outlook 2013)

During combustion, these carbon-based fuels release not only gigantic amount of energy which empowers the human civilization, but also billions of tons of carbon dioxide, which is a green house gas, as end product into the atmosphere. Figure 1.2 below shows a greenhouse gas flow chart.

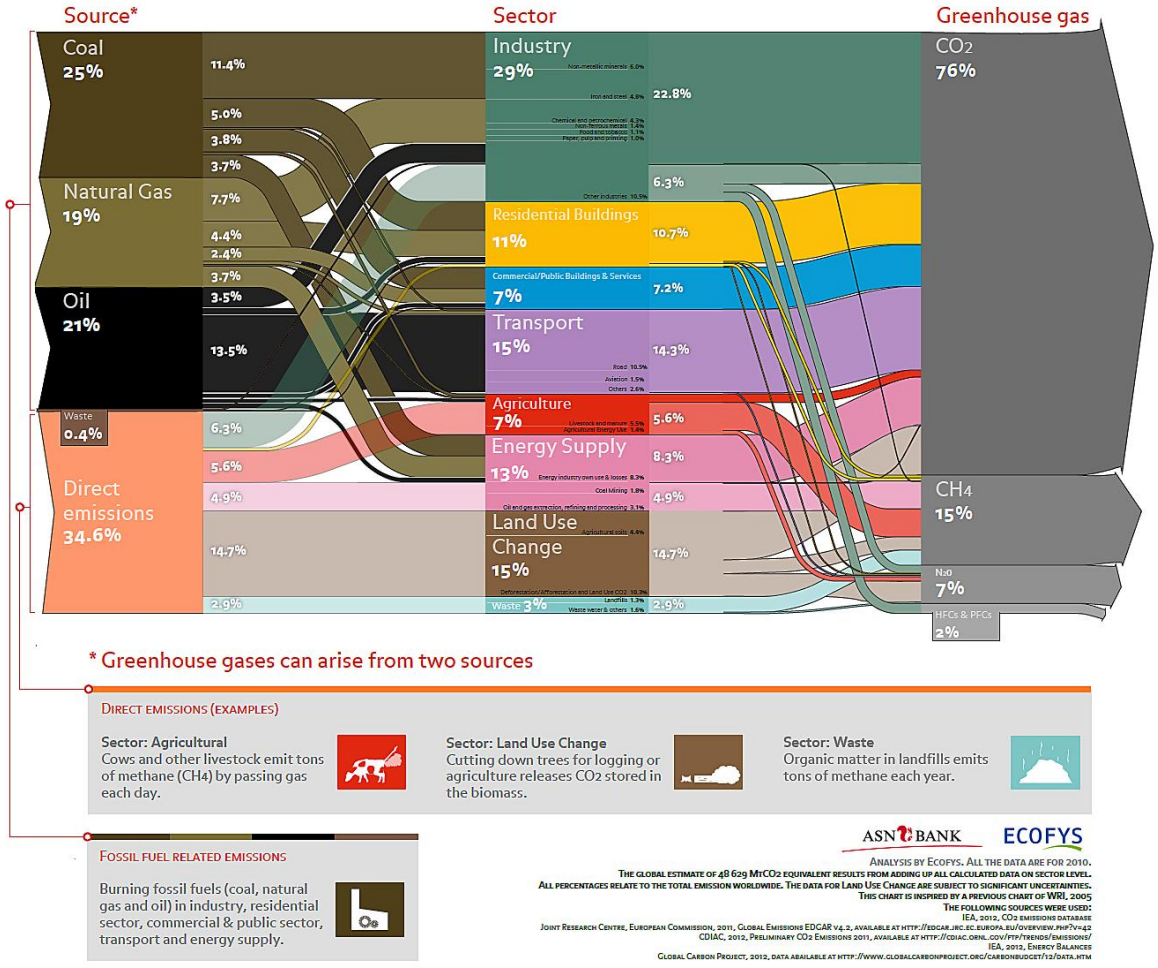


Figure 1.2: World greenhouse gas flow chart. All data is for year 2010. The global estimate of 48629 $MtCO_2$ equivalents is a result from adding up all calculated data on sector level. All percentages relate to the total emission worldwide. The data for Land Use Change are subject to significant uncertainties. IEA 2012, $CO_2$ emissions database (Figure from ASN Bank & Ecofys 2010)

The growing energy demands of the ever-increasing population are forecast with increasing economic progress. The size of the economy and efficiency of energy utilization determine the $CO_2$ emissions rate. While developed countries, for instance the US, Europe, Japan, remain responsible for large quantities of $CO_2$ emissions over the years, rising developing economies such as China and India emerge as the new major contributors. Figure 1.3 below lists major $CO_2$ emitters.

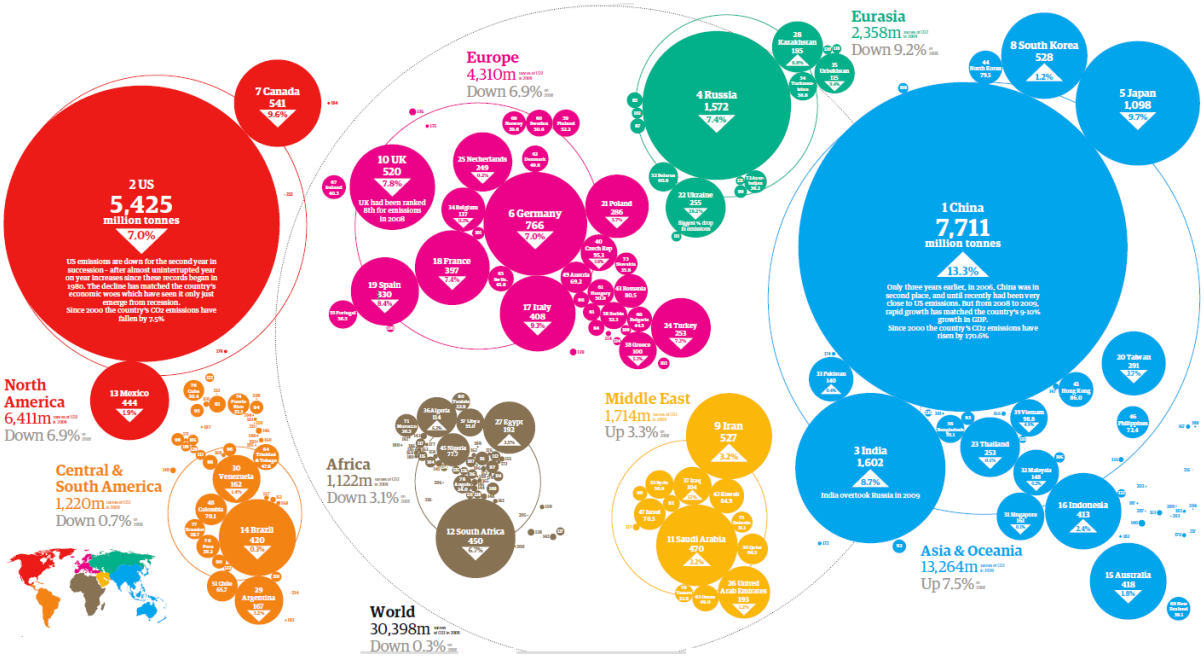


Figure 1.3: $CO_2$ emissions by country (Figure from World $CO_2$ emissions from consumption of energy, US EIA; World $CO_2$ emissions data by country, London Guardian 2010).

Figure 1.4 below shows the $CO_2$ emission sources for the US.

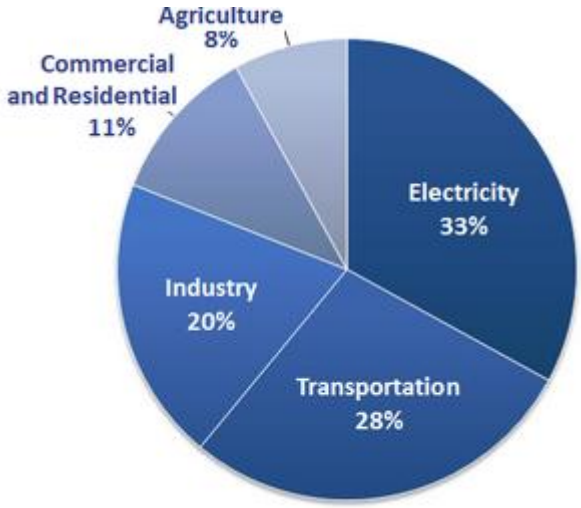


Figure 1.4: US $CO_2$ emissions by source in 2011. Electricity production generates the largest share of emissions followed by transportation and industry. (Figure from Inventory of U.S. Greenhouse Gases and Sinks, United States Environmental Protection Agency, EPA)

### 1.1.2 Greenhouse effect and global warming

The Earth's atmosphere plays a crucial role in maintaining the suitable temperature to sustain lives on the planet. The Earth surface temperature is kept relatively constant due to the balance of radiation fluxes. A schematic to help understand "greenhouse effect" is shown below in Figure 1.5.

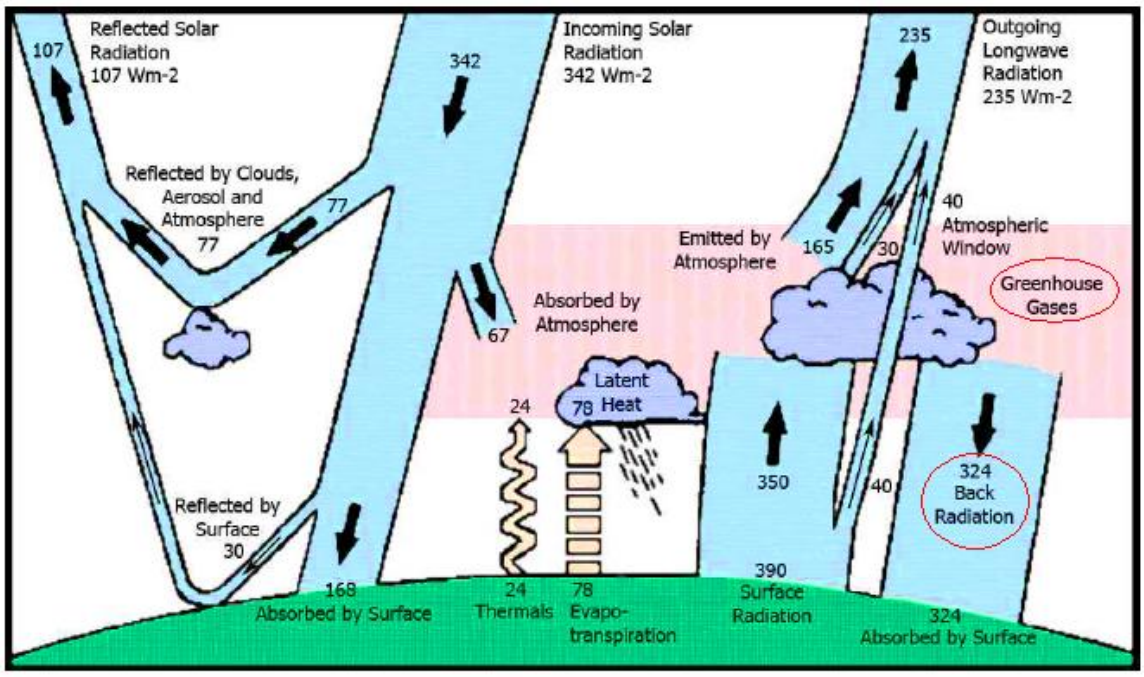


Figure 1.5: The detailed budget of radiation fluxes (numbers next to text boxes; units of $W/m^2$) on the Earth. The incoming solar radiation is equal to the sum of reflected solar radiation and the outgoing long wave radiation. This radiation balance maintains the constant surface temperature of the Earth. (Adapted from Figure 7 in Kiehl and Trenberth 1997)

Increasing concentration of $CO_2$ in the atmosphere from anthropogenic sources enhances the back radiation, producing net warming by strengthening the natural "greenhouse effect". Therefore the surface temperature keeps increasing.

The large amount of anthropogenic emission of $CO_2$ into the atmosphere is correlated with a surge in atmospheric concentration of $CO_2$ which is unprecedented in the last several hundred thousand years. Figure 1.6 shows the correlation between the Earth's temperature variation and atmospheric $CO_2$ concentration.

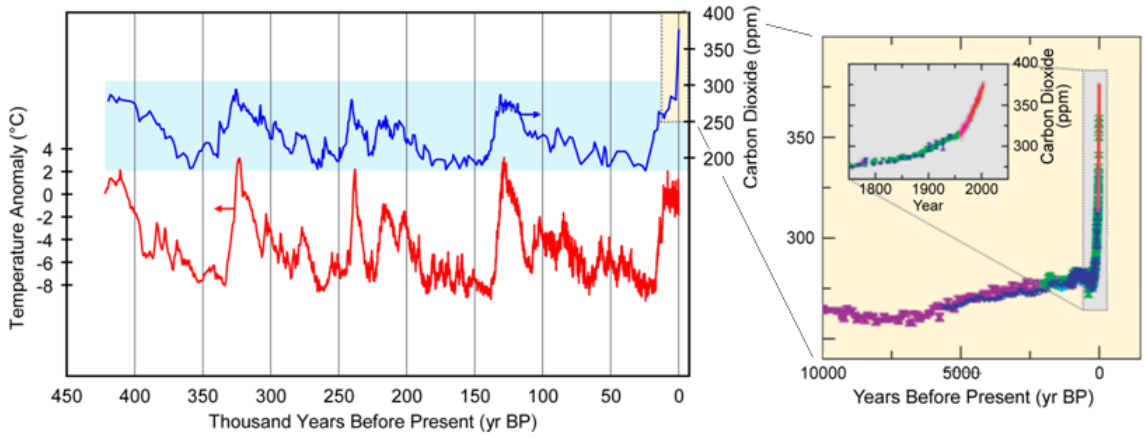


Figure 1.6: $CO_2$ concentration and temperature variation during recent geologic time. (Figure and data from NOAA, National Climate Data Center, Vostok Ice Core $CO_2$ data)

The simplest explanation for the spike of $CO_2$ concentration in the past one thousand years is that it is a direct consequence of human activities. Since the Industrial Revolution in the 19$^{th}$ century, $CO_2$ concentration increased substantially and went far beyond the pre-industrial level of 280 parts per million and soon approaches 400 parts per million (398.6 parts per million now (NOAA, February 2014)) , with the fastest growth in the past ten years (about 2 ppm per year). Significant surges have also occurred in levels of methane ($CH_4$) and nitrous oxide ($N_2O$). From Figure 1.6 above, there is a strong correlation between the concentration of $CO_2$ and the temperature anomaly: the higher the concentration of $CO_2$, the higher the Earth's surface temperature.

In 2007, a report by Intergovernmental Panel on Climate Change (IPCC) concluded that the planet is warming up based on then-existing data and models. Over the past century, the Earth average surface temperature has risen about 0.74℃. Figure 1.7 below shows that increased surface temperature is not an isolated case, but a global phenomenon.

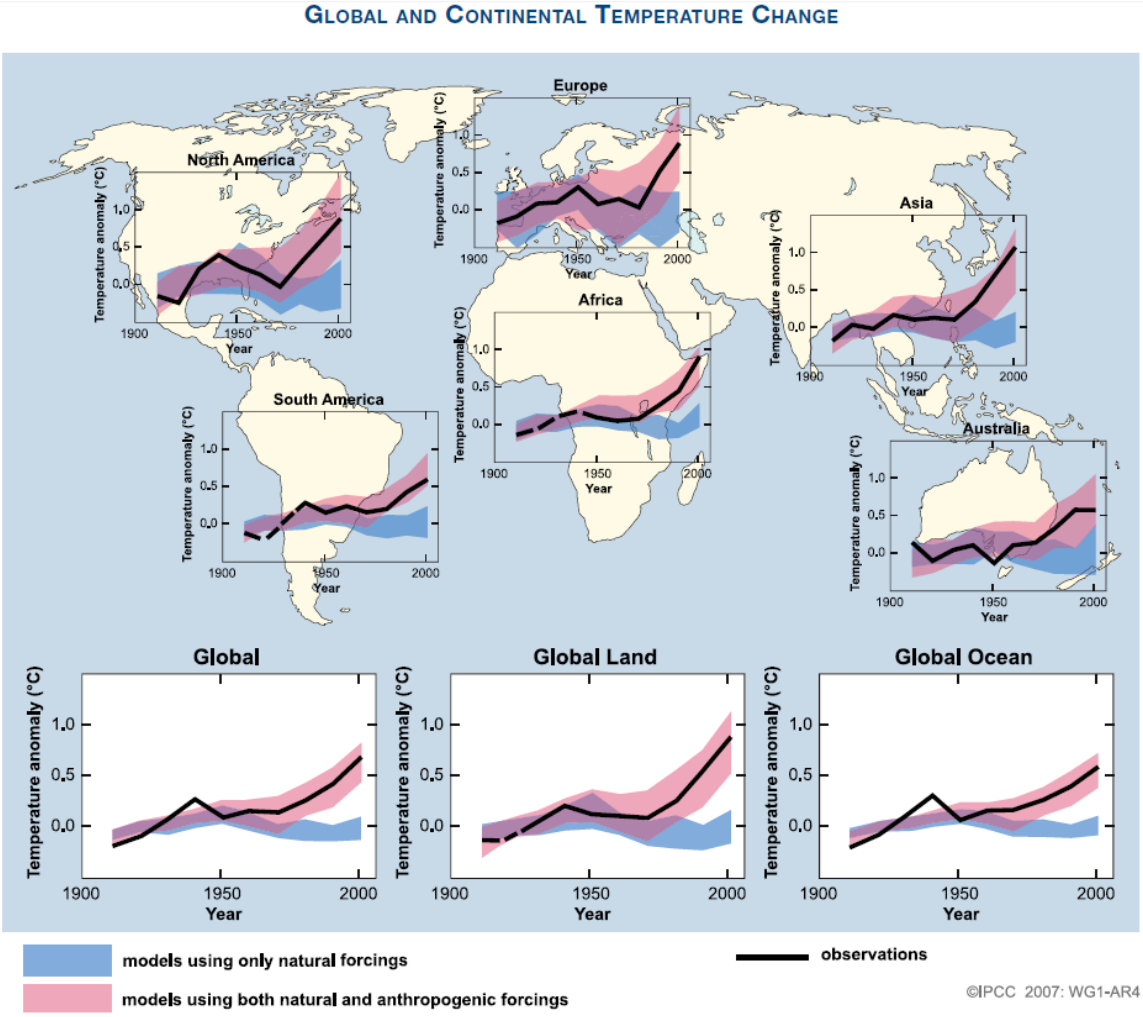


Figure 1.7: Comparison of observed continental- and global-scale changes in surface temperature with results simulated by climate models using natural and anthropogenic forcings. Decadal averages of observations are shown for the period 1906 to 2005 (black line) plotted against the center of the decade and relative to the corresponding average for 1901–1950. Lines are dashed where spatial coverage is less than 50%. Blue shaded bands show the 5–95% range for 19 simulations from five climate models using only the natural forcings due to solar activity and volcanoes. Red shaded bands show the 5–95% range for 58 simulations from 14 climate models using both natural and anthropogenic forcings. (Figure from IPCC 2007 Report)

Realizing the consequences of accelerated global warming, scientists and policy makers have attempted vigorously to reduce the $CO_2$ concentration to a reasonable range. While the Kyoto Protocol's first commitment period ended in 2012 (UNFCCC), the world has yet to come up with an effective agreement which could legally bind every country involved. Despite all the efforts put in, global energy-related $CO_2$ emissions in 2012 increased 1.4% last year, reaching a record high level of 31.6 gigatonnes (IEA).

## 1.2 Impacts of greenhouse effect

Some impacts due to the increased green house gas concentration may not be instantly apparent because of the slow interaction between the inherent climate, ecological and socio-economic systems. Nonetheless, many consequences associated with the increased concentration of greenhouse gases have become obvious.

### 1.2.1 Climate change

The increased average surface temperature heats up the ocean and pumps more energy into tropical storms via evaporation, making them stronger and more devastating. History data has shown that while ocean temperature increased over the past decades, the number of category 4 and 5 storms has increased significantly in the past 35 years. Aggravated evaporation due to warmer temperature can lead to heavy rainfall in some areas, devastating many communities from floods. U.S. national annual precipitation has increased almost 10% since the beginning of the $20^{th}$ century. More regions became vulnerable in front of heavy downpours.

In 2005 Hurricane Katrina caused economic losses of 125 billion dollars, and remained the costliest hurricane in the U.S. history. The 2012 Hurricane Sandy swept the Northeast region of the U.S., disrupted the energy system and left New York City and nearby areas with heavy economic losses.

Warmer temperatures also increase the probability of drought and wildfire because greater rate of evaporation carries more water from the land surfaces. The western United States has experienced higher frequency of drought in the last 30 years. In 2006 alone, nearly 100000 fires were reported and 10 million acres of land was burned, 125% above the 10 year average (NRDC). Firefighting expenditures have totaled up to one billion dollars per year; losses of human properties and lives are beyond evaluation. Figure 1.8 below reports recent extreme weather in the US.

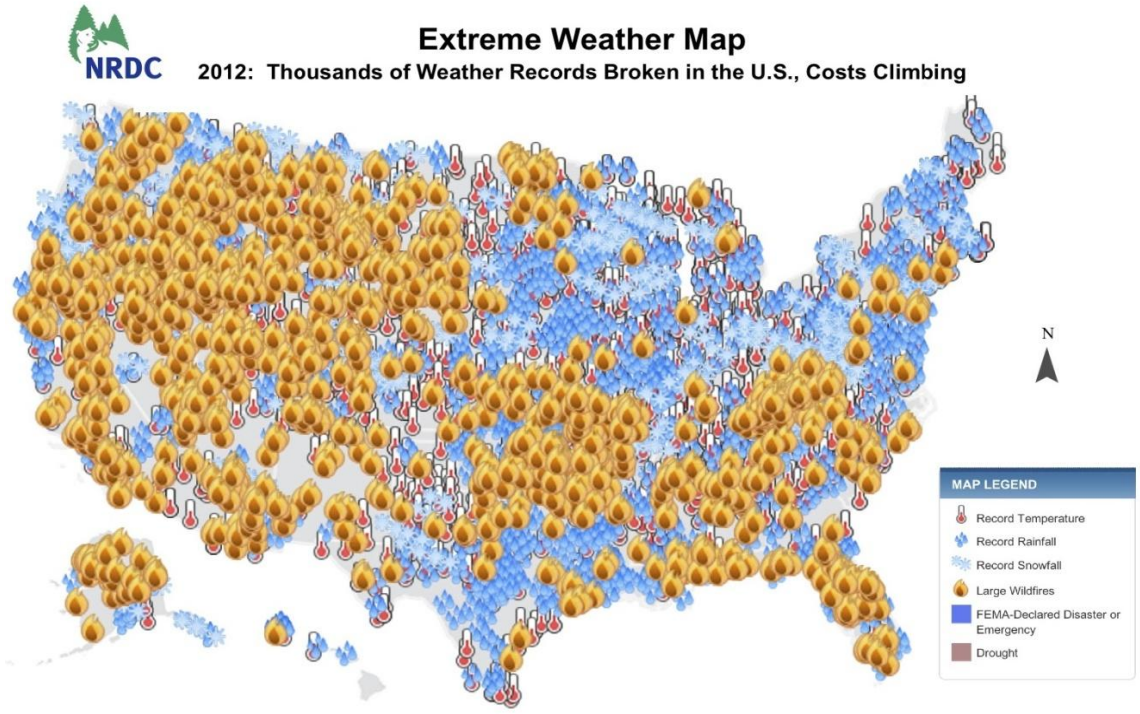


Figure 1.8: U.S. Extreme Weather Map 2012. Climate change increases the risk of many types of record-breaking extreme weather events that threaten communities across the country. In 2012, there were 3572 monthly weather records broken for heat, rain, and snow in the U.S., which is even more than the 3251 records broken in 2011, according to information from the National Climate Data Center. Some of the newly-broken records had stood for 30 years or more. (Figure from National Climatic Data Center (NCDC))

### 1.2.2 Sea level rise and escalating hazards for coast

Global warming process results both thermal expansion of the oceans and melting of most mountain glaciers and partial melting of the West Antarctic and Greenland ice caps. Coastal wetlands, barrier islands, and low-lying areas are subject to greater risk of flooding. Global sea level has already risen by an average of 6 inches in the past century, and this rise is accelerating.

The polar ice cap is now melting at the alarming rate of 9% per decade. Arctic ice thickness has decreased 40% since 1960s. Scientists at the U.S. Center for Atmosphere Research have warned that the Arctic could be ice-free in the summer by 2040 and all of the glaciers in Glacier National Park will disappear by 2070, if the current rate of global warming sustained. IPCC predicts that 10 to 23 feet (4-6 meters) of rise of the sea level will be observed by 2100, but recent data has shown that this rise is even faster than the upper end of the range predicted. This additional 4-6 meters of rise in sea level will cause severe inundation of low-lying coastal areas, including parts of many major populous regions or cities such as New Orleans, Florida coasts, coastal cities of Europe, and delta region of Asia etc.

### 1.2.3 Acidification of ocean, ecosystem disruption and species extinction

As the concentration of $CO_2$ in the atmosphere keeps increasing, the ocean will continue to become more acidic as more and more $CO_2$ dissolves into the water. Species with calcium carbonate shells and vital to ocean ecosystems, for example coral reefs, will suffer. Scientists warned that a 3.6 degree Fahrenheit increase in temperature would eliminate 97% of coral reefs on the planet.

Scientists have also noticed that over 2000 flora and fauna species moved toward the poles (presumably cooler regions) at an average rate of 3.8 miles per decade (Oregon

DFW). Similarly, species in alpine areas are moving to higher (cooler) elevation at a rate of 20 feet per decade in the second half of the 20th century.

The IPCC has warned that if the global average temperature increases by more than 2.7 to 4.5 degrees Fahrenheit, 20% to 30% of plant and animal species will be at the risk of extinction. For instance, some Antarctic penguin populations have decreased by 33% in the past 25 years due to deterioration of sea-ice habitat. USGS predicts that 2/3 of world's polar bears sub-population will be drowned or starved to death by mid-century due to melting of the Arctic ice cap.

The results are loss of biodiversity and disruption of coexistence of different species in a shared ecosystem.

### 1.2.4 Change in water resources and food production

If most of us don't feel the direct adverse impacts from extinction of species and loss of biodiversity due to climate change, the following consequences will certainly warn us. Water shortage will exacerbate as the temperature continues to rise. Elevating global temperature triggers greater evaporation rate from surface land and extends dry-season, hence alters the water cycle. People are likely to face more severe water shortages. More than one fifth of the global population currently lives near rivers and depends on glacier or snow water. These communities (including the western United States) will be the first group hit with decreased water resources over this century. The Intergovernmental Panel on Climate Change (IPCC) expects water resource competition becoming keener in areas such as western U.S. and sub-Sahara Africa, when decreased mountain snowpack reduces summer river flow. The areas are also expected to receive less precipitation. All combined will yield less usable water supplies.

Ironically, frequency and intensity of storm events are predicted to increase due to global warming and climate change. Intense rain events often deliver excessive water at once, causing water overflow instead of absorbing by the ground and making it harder to manage and conserve. Extreme floods washed away the plants holding off the soil; vicious cycle continues when the eroded soil becomes more vulnerable to flooding and erosion in the future.

The changing water resource is likely to impact heavily on global food production. Food production in some rain-fed arable land could be reduced by half by 2020. Seasonally dry tropical land near the equator will be prone to this reduction of water resources. Food shortage problem in African countries may worsen due to deterioration of arable land. Intensified monsoon hurricanes endanger the arable land in South Asia, South-East Asia and India.

Globally, warmer temperature increases the risks of crop epidemics and pest outbreaks. Faster growth of insects and bacteria due to warmer temperature trigger wider-spread diseases among the crop species, making it more difficult and more costly for pesticide control. Similar to other species which responded to global warming, insects and bacteria are also moving toward the Earth's poles, invading new habitats and breaking local ecological balances.

Prolonged drought due to global warming will impose an even higher pressure to the burdened irrigation system, adding extra costs to achieve the same or even lower productivity. In the state of Texas, 6.17 million irrigated acres make up more than 10% of the irrigated acres in the United States. This number is expected to increase along with rising temperature and growing population. A major part of irrigation was done using groundwater. Nonetheless, statewide groundwater supplies are expected to decrease 32% by 2060, making it more costly to irrigate the farm lands (TWDB 2012).

Not only the crop plantations' lives are at stake, but the livestock is also threatened. Rising temperature in the water system combined with overfishing may deplete the fish supply. Cattle feeding will become more difficult because of reduction in pasture and water resources. This is especially true in the western states of United States.

### 1.2.5 Human health and safety concerns

Global warming also imposes some direct threats to human health and safety. More frequent and severe heat waves have caused a great number of heat-related deaths. Much of North America experienced a severe heat wave in July 2006, which claimed lives of 140 people; some of them even owned air conditioners. In the fight against the 2013 Arizona blaze wildfire, 19 firefighters lost their life (Yan 2013).

The increasing cases of smog pollution in some areas, intensified pollen allergies and asthma are thought to link with global warming. Rising temperatures increase surface level ozone smog production, a serious threat to asthmatics. The terrible smog in January 2013 Beijing is partially due to the increasing $CO_2$ concentration in the air by burning coal without emissions controls in the power plants.

As mentioned above, hotter weather disrupts the ecosystem by alternating periods of drought and floods. This effect has contributed to more widespread outbreaks of diseases such as malaria, dengue fever, and diarrheal. Disease-carrying mosquitoes are moving to and surviving in formerly inhabitable regions due to climate change. Mosquitoes carrying dengue fever virus have appeared at 7200 feet height in Andes Mountains of Colombia, instead of its previous limitation of 3000 feet. Drinking water supplies could be contaminated by pathogens washed away by heavy rainfall from contaminated soils, farms and streets. Food borne bacteria grow much faster with warmer

temperature. People living in poverty with inferior sanitation condition will be hit hardest by the global surge in infectious illness.

## 1.3 Possible solutions

With the climate change being the single biggest environmental and humanitarian crisis of our time, the importance of taking care of heat-trapping anthropogenic $CO_2$ emission must be emphasized. Solutions have been proposed and implemented to mitigate the adversity brought by global warming.

IPCC has suggested a list of possible adaptation and mitigation options for reducing emissions.

### 1.3.1 Better energy usage efficiency

Use of coal (the dirtiest energy source) has been generally criticized. Replacements with more efficient and cleaner energy resources, such as natural gas, are recommended. To move to a clean energy economy, definite and enforceable emission goals should be set and met. Achieving this requires a combination of work from three sectors: technological (scientists and engineers), legislative (policy makers and regulators), and commercial (society and market).

An instructive example is automobile standards and emission regulations which have become increasingly stringent over the last 20 to 30 years. The role played by technology advancement and legislative consensus should not be underestimated. The market and general public have responded accordingly. More fuel-efficient, emission reduced cars are on the road now. Burning a gallon of gasoline pumps about 20 pounds of $CO_2$ into the atmosphere, so there is an immediate effect on $CO_2$ emissions from introducing more efficient vehicles. Raising the average fuel economy of US automobiles

to 40 miles per gallon over the next ten years would reduce emissions in 2020 by 173 million metric tons of $CO_2$ (PSU).

### 1.3.2 Alternative fuels

Other energy resources such as wind, solar power, bio-fuels, hydro-power, and nuclear power are options in a clean energy future. Norway, for example, has its 90% energy generated by hydro power. However, due to the limitation of dependability and scaling up challenges, those energy resources could not completely replace fossil fuel in a foreseeable future without sacrificing world's economic development. In other words, generation of $CO_2$ as a post-combustion product will continue for a significant period of time.

### 1.3.3 CCUS (Carbon Capture Utilization and Storage)

Other than legislation and making policies for green house gas emission control, carbon capture and storage, or CCS technology, has long been considered as a promising alternative for reducing the $CO_2$ concentration in the atmosphere. Aiming to mitigate climate change in a long run, CCS is currently the only viable method to treat large amount of $CO_2$ generated by burning fossil fuels and from other industries.

There are essentially two parts of CCS, the capture (upstream) and the storage of captured $CO_2$ (downstream). Capture is the process of collecting waste carbon dioxide from large point sources, for example, fossil fuel (coal) based power plants, petrochemical industries, etc., and then producing a high concentration stream of $CO_2$. The captured $CO_2$ is then transported to pre-selected storage sites, normally an underground geological formation, and stored securely where it will not enter the atmosphere. Figure 1.9 below illustrates the concept of geologic carbon sequestration.

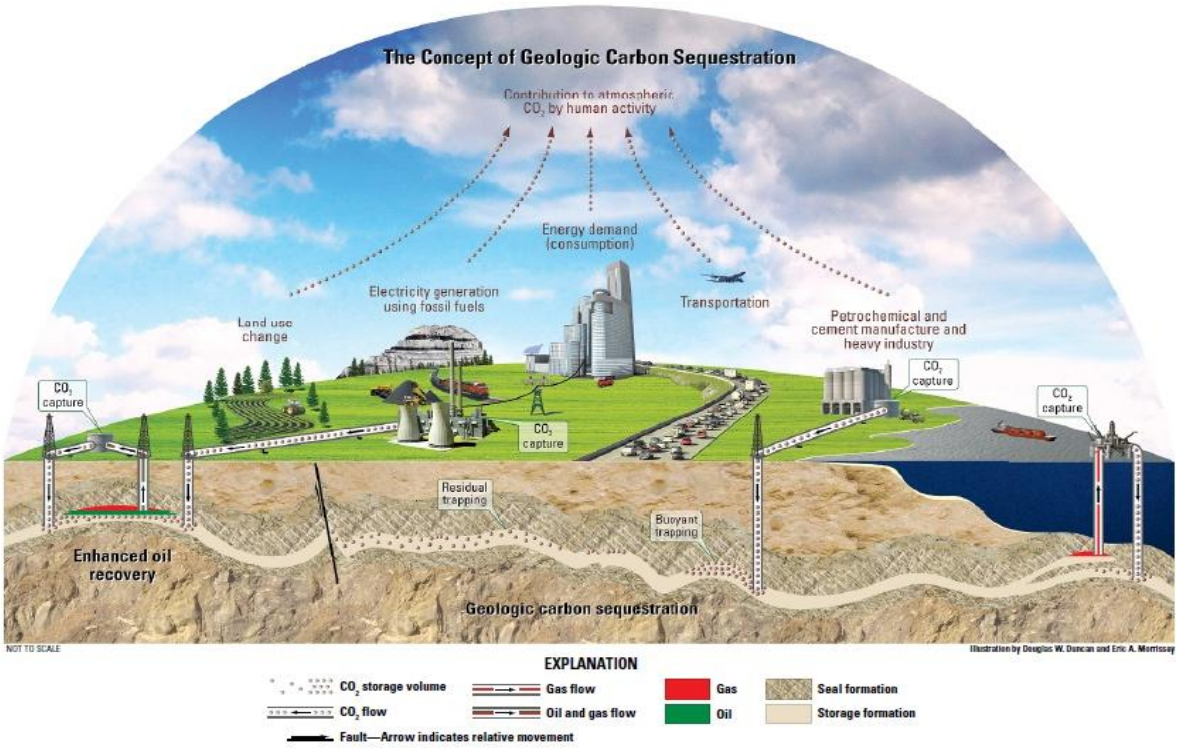


Figure 1.9: The concept of geological storage (Figure from The Concept of Geologic Carbon Sequestration, USGS, 2010)

Current storage technology involves injection of large amount of $CO_2$ into deep geologic formations with typical depth of 1 to 2 kilometers. At such depth, $CO_2$ exists as a supercritical fluid due to high temperature and high pressure. At these conditions the $CO_2$ will be less dense than brine in the deep formations. This gives the $CO_2$ a tendency to rise until stopped by a stratum that is impermeable or has pores so narrow that the meniscus between rising $CO_2$ and native brine cannot enter. The latter situation corresponds to a "capillary barrier," referring to the phenomenon of capillary pressure (pressure difference between $CO_2$ phase and brine phase) which dictates the curvature of the meniscus between the phases.

The fact that supercritical $CO_2$ can be miscible with oil (petroleum) makes it a suitable medium to extract petroleum from declining reservoirs. Oil and gas industry has been using $CO_2$ to flood (injection with high pressure) the depleting reservoirs to recover 15%-20% more oil. This technology has been in use for decades, but limited to certain reservoir suitable for $CO_2$ flooding. In the recent period when $CO_2$ geologic storage became an increasingly popular topic, $CO_2$-based enhanced oil recovery (EOR) combined with $CO_2$ storage received more and more attention. More research has been done to improve its efficiency as well as its productivity. $CO_2$ EOR is considered as a good way of utilization of $CO_2$, thus CCS becomes CCUS.

## 1.4 Research objectives

Although $CO_2$ has been injected into geological formations for several decades for various purposes, including enhanced oil recovery, the long term storage of $CO_2$ is a relatively new concept. There are still problems to be solved and questions that need to be answered before CCUS becomes a commonly used and widely accepted technology.

In typical deep saline aquifers, the $CO_2$ storage capacity and security depend on the trapping mechanisms that counteract the buoyancy-driven upward migration of the less dense $CO_2$. The mechanism motivating this thesis is local capillary trapping. Local capillary trapping occurs during buoyancy-driven migration of bulk phase $CO_2$ within a saline aquifer (Saadatpoor 2009). When the rising $CO_2$ plume encounters a region where capillary entry pressure is locally larger than average, $CO_2$ accumulates beneath the region.

Previous works by (Saadatpoor 2009, Ravi Ganesh 2012) have shown that maximum trapping by this mechanism occurs when the contact between rising $CO_2$ plumes and rock is maximized. Compact displacement front is thus favorable, and a

finger-like or channel-like displacement front is unfavorable. Heterogeneity of capillary entry pressure will severely disrupt a compact displacement front. On the other hand, the heterogeneity establishes local capillary barriers that enable permanent local trapping of rising $CO_2$ plumes. Accounting for these effects has practical implication in estimating the total storage capacity of geologically stored $CO_2$ in a saline aquifer.

Since local capillary trapping mechanism contributes significantly to the total storage capacity and potential, the research question has progressed to "is Local Capillary Trapping a secure mechanism in normal cases, and how secure/persistent is this mechanism if the overlying seal fails?" This has direct impact on the total $CO_2$ storage capacity and security.

# Chapter 2 Literature Review

## 2.1 Geologic $CO_2$ sequestration and storage

$CO_2$ storage is an essential way to minimize greenhouse gas emissions to the atmosphere if any serious efforts are to be attempted for meeting global targets in coming decades. Relying on the technology and expertise of the oil and gas industry, geologic storage is likely on the top of the list of feasible technologies. Ample space is available for $CO_2$ storage, for example in deep saline aquifers as well as in depleted oil and gas reservoirs. Transport costs could be kept low by placing projects close to the fixed $CO_2$ sources. To date, the most promising efforts to store substantial volumes of $CO_2$ have been done exclusively by oil and gas companies. This is not a coincidence, because the experiences and skill sets needed for such projects resemble those needed for oil and gas exploration and production (Bryant 2007).

### 2.1.1 Geologic $CO_2$ storage security

The question of storage safety and security is the paramount for the research on $CO_2$ geologic sequestration. Typical depths for $CO_2$ storage formation are greater than 2000 m. Assuming a hydrostatic pressure gradient of 9.8 kPa/m and geothermal gradient of 30°C/km, the pressure and temperature at such depth are around 20 MPa and 360 K respectively, and supercritical conditions for $CO_2$ are met ($P_{critical}$=7.39 MPa and $T_{critical}$=304.25 K for $CO_2$). Brine and supercritical $CO_2$ are an immiscible fluid pair, with small amounts of solubility of $H_2O$ in $scCO_2$ and of $CO_2$ in brine.

Leakage of the stored bulk phase $CO_2$ is of particular risk for sequestration in deep saline aquifers. Density of stored supercritical $CO_2$ usually ranges from 500 kg/m$^3$ to 700 kg/m$^3$, while density of formation brine is about 1000 kg/m$^3$. The density

difference between the two immiscible phases causes the less dense supercritical $CO_2$ phase to rise. This buoyancy driven movement, together with the interaction of the operation with geologic features (faults, possibly reaching the surface) and human activity (buildings, homes, extraction of subsurface fluids or minerals) will be potential factors causing $CO_2$ leakage. Oldenburg (2007) and Bryant (2007) demonstrated this idea as shown in Figure 2.1.

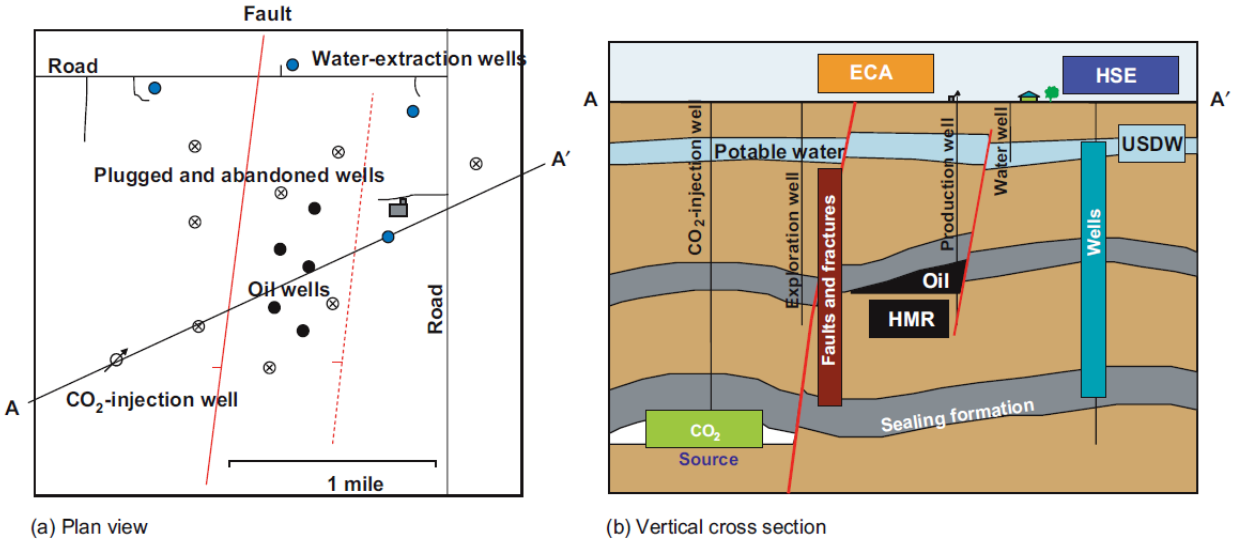


Figure 2.1: (**a**) Plan view of a geologic $CO_2$ storage site. (**b**) Side view of section AA' from (a). Schematic shows possible conduits for leakage (faults, fractures, existing wells) of $CO_2$ stored in a deep saline aquifer. In this scheme, leakage becomes a problem in three ways. One is if the $CO_2$ enters a "compartment" that has economic value, such as formations containing hydrocarbon or mineral resources (HMR) or underground sources of drinking water (USDW). Another is if the $CO_2$ affects health, safety, or environment (HSE), for example by entering basements of homes. The third is the re-entry of $CO_2$ into the atmosphere (ECA). Should the latter occur, emission credits would be reduced (Figure adapted from Oldenburg 2007, Bryant 2007).

Because of the safety concerns associated with $CO_2$ geologic storage should leakage occur, research is needed to assess the possible extent (volume) and rate (flux) of leakage. The focus of this work is on the extent. As the less dense $CO_2$ migrates upward within a storage formation or in layers above the formation, the security of its storage depends upon the trapping mechanisms that counteract the migration.

### 2.1.2 Local capillary trapping

The trapping mechanism motivating this research is local capillary trapping (LCT). $CO_2$ is a nonwetting phase relative to brine in storage aquifers. Thus when a $CO_2$ plume rising by buoyancy encounters a region where capillary entry pressure is locally larger than average and larger than the capillary pressure of the $CO_2$ plume, $CO_2$ accumulates beneath the region (Saadatpoor 2009). This concept is illustrated in the following Figure 2.2.

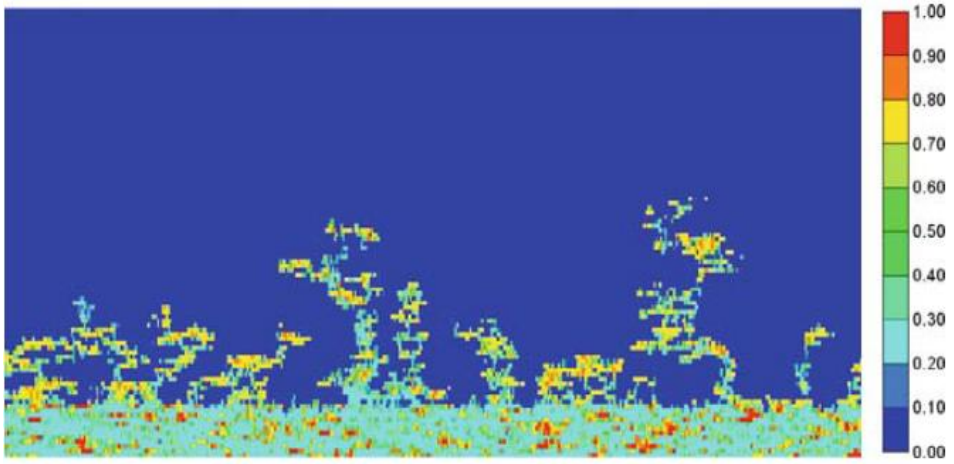


Figure 2.2: A CMG-GEM generated $CO_2$ saturation profile at 25 years after injection, when the $CO_2$ distribution is near steady state. Many grid blocks have large values of capillary entry pressure, and thus act as complete barriers to buoyancy-driven rising $CO_2$. Large saturations of $CO_2$ build up under these local barriers but do not migrate. (Figure adapted from Saadatpoor 2009)

One benefit of LCT is that saturation of stored $CO_2$ phase is larger than the saturation for other permanent trapping mechanisms. Shown in the Figure 2.3 below, with heterogeneity in capillary entry pressure, Local capillary trapping mechanism achieves a significant saturation of stored $CO_2$, comparable to other modes of storage, and simultaneously reduces the fraction of $CO_2$ that is still mobile ("free gas").

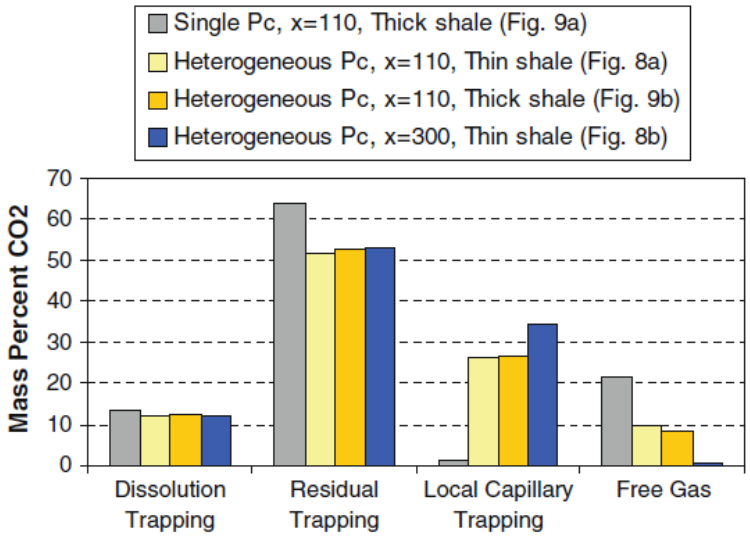


Figure 2.3: Distribution of $CO_2$ in various storage modes for single and scaled capillary pressure fields, 25 years after leak development. (Figure adapted from Saadatpoor 2009)

Another potential benefit is security: $CO_2$ that occupies local capillary traps remains there, even if the overlying formation that provides primary containment were to be compromised and allow leakage. A simulated example is presented in Figure 2.4 below.

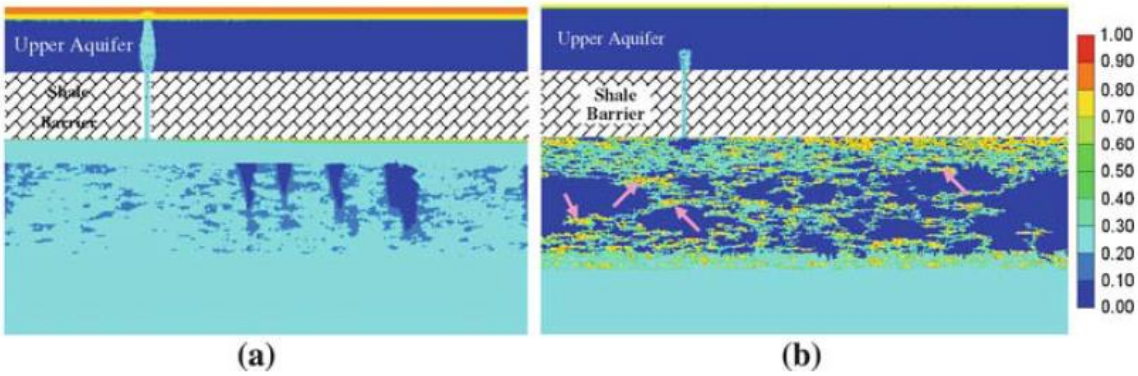


Figure 2.4: $CO_2$ saturation distribuitionat 25 years after a break opens in the top seal of the aquifer. The domain below the shale barrier is the storage volume; the $CO_2$ is assumed to have been emplaced originally in the bottom third of the storage volume, from which it then migrated under buoyancy toward to top of the storage volume. **(a)**: single reference capillary pressure curve applied to all the storage domaine. (b): scaled capillary pressure (heterogeneous capillary entry pressure distribution, different value for each grid block according to its permeability). **(b)** has larger saturations remaining in the storage volume. (Figure adapted from Saadatpoor 2009)

The question of how much pore volume in a typical storage formation can provide LCT is being actively studied. It is clear that rising $CO_2$ contacts a relatively small volume of the rock until it reaches the sealing formation providing primary containment, and that the fraction contacted depends strongly on the degree of heterogeneity in the formation and on the height of connected column the $CO_2$ can establish as it rises (Ganesh 2012).

### 2.1.3 Local capillary trapping at bench scale

Most work on LCT has involved numerical simulations (Saadatpoor 2010, Ganesh 2012). Experimental research at the bench scale is also needed to validate the

conclusions made from simulation work. The research presented here is a step toward understanding local capillary trapping at the bench scale. The specific objectives are to establish protocol for laboratory assessment of local capillary trapping and to determine the influence of geologic and petrophysical characteristics on countercurrent buoyancy driven flow of $CO_2$ and brine. Based on these relationships, a particular geologic formation, for which fluid and rock properties (including heterogeneity) are known or can be measured, could be analyzed for suitability as a $CO_2$ storage site. The potential for local capillary trapping to enhance capacity for $CO_2$ storage/sequestration in the formation of interest can also be evaluated.

## 2.2 $CO_2$ and brine properties

### 2.2.1 Wettability

Previous work by Hernandez (2011) has demonstrated that wettability has a significant effect on two phase immiscible fluid buoyancy-driven displacement in a porous medium. A hydrophilic (water wet) porous medium prefers water while a hydrophobic (oil wet) porous medium prefers oil; a porous medium of mixed wettability has both hydrophobic and hydrophilic surfaces. In this research, the assumption is that the deep saline aquifer of interest is originally water wet.

### 2.2.2 Viscosity ratio

Viscosity ratio, *M*, of the two immiscible fluids is crucial in determining their migration pattern in traditional displacements driven by pressure gradients, e.g. between injection and production wells in oil and gas reservoirs. Cinar et al. (2007) and Crowe el al. (2005) have qualitatively proven that as the viscosity ratio, $\mu_{displacing}/\mu_{displaced}$ is decreased, preferential flow paths emerge. Ferer (2011) quantified this phenomenon and developed a model to predict the flow pattern, which has a practical implication for

injection of $CO_2$ at large capillary number into brine saturated porous media. The results are summarized in Figure 2.5 below.

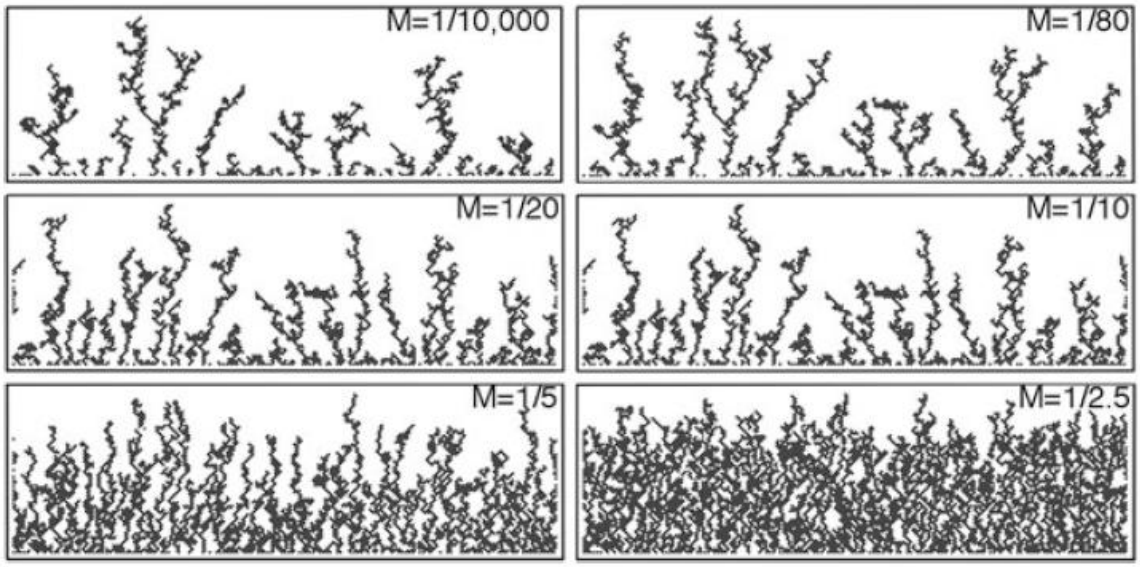


Figure 2.5: Simulated breakthrough patterns for one of five realizations of capillary number $N_c$ = 0.0040 and for viscosity ratios from $M$ = 0.0001 to $M$ = 0.4. A non-wetting less viscous fluid is injected from a line source at the bottom toward a line sink at the top (practical implication to the movement of bulk stored $CO_2$ in saline aquifer). (Ferer et al. 2011).

From the results, increasing viscosity ratio changes migration of invading fluid from a fractal ('fingering') pattern into a more compact pattern. One thing to take note is that the above simulation results have no buoyancy component, which is not completely analogous to the buoyancy driven migration of $CO_2$ and associated experiments presented in this thesis work. The source of 'fingering' in Figure 2.5 above is due to viscous instability but not heterogeneity, since the model assumes a homogeneous porous medium.

Lovoll (2005, 2010) studied the influences of gravity, capillary and viscous forces during drainage in a porous medium made of a single layer of 1 mm glass beads. They concluded that when gravity is stabilizing and larger than the viscous forces, the invasion

of a non-wetting liquid into a wetting liquid is stable. In situations where the magnitudes of viscous-, capillary- and gravity forces are comparable and with decreasing apparent gravity, capillary fingering is gradually transformed to viscous fingering. The combination of displacement structure, pressure, saturation and the capillary number gives a scaling relation linking pressure, saturation, system size and capillary number.

### 2.2.3 Interfacial tension

Interfacial tension is necessary for calculating capillary pressure in a designated liquid-liquid, or liquid-solid system. In order to make accurate prediction and calculation for $CO_2$ storage in deep saline aquifer, the interfacial tension between brine and supercritical $CO_2$ is important, especially in the context of local capillary trapping. Scientists and engineers have made series of experiments and simulations to predict the brine-$CO_2$ interfacial tension under typical geologic storage conditions.

Chalbaud et al. (2009) has indicated that the interfacial tension between brine and $CO_2$ is influenced by salinity of the brine. They found that interfacial tension can also be varied by the density difference of the two liquids. If the density difference between $CO_2$ and brine is less than 0.6 g/cm$^3$, the interfacial tension between the two phases stays relatively constant around 28 mN/m (as shown in Figure 2.6 below).

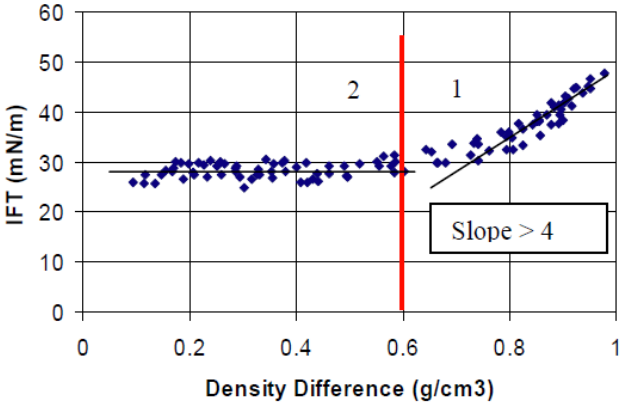


Figure 2.6: Variation of the interfacial tension of brine-$CO_2$ with density difference (Chalbaud et al., 2009).

The interfacial tension between $CO_2$ and brine is also subject to pressure and temperature influences. Neilson et al. (2012) found that the interfacial tension between $CO_2$ and brine at 20 MPa tends to be independent of temperature. It, however, is strongly dependent on pressure at 383 K. These relations are shown in Figure 2.7 below.

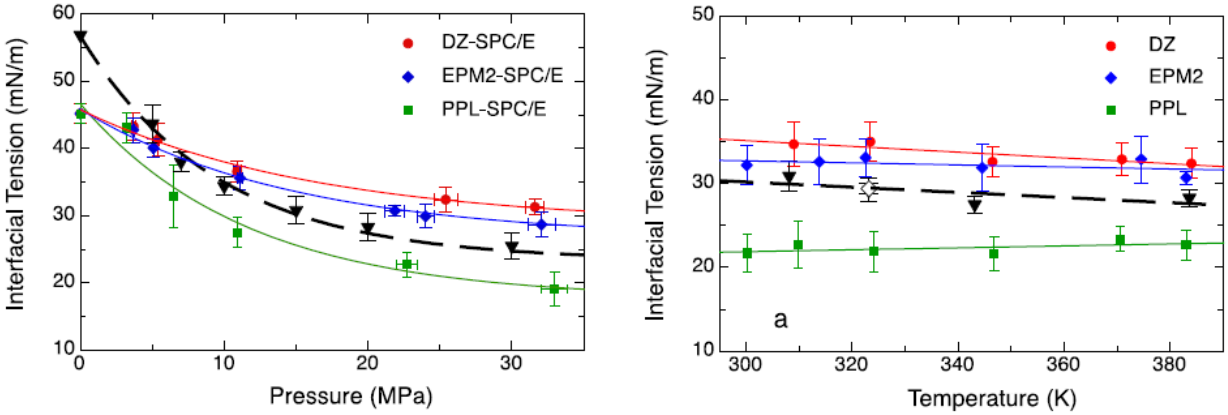


Figure 2.7: (left) Interfacial tension between $CO_2$ and brine is heavily dependent on pressure at 383 K. The value tends to plateau beyond 20 MPa. (right) Interfacial tension between $CO_2$ and brine tends to be independent on temperature at 20 MPa. (Neilson et al. 2012)

### 2.2.4 Heterogeneity

Reservoir heterogeneity and fluid properties are principal factors influencing $CO_2$ migration pathways in the buoyancy/capillary regime. In a porous medium, heterogeneity significantly affects the capillary pressure. For typical field conditions and injection rates, buoyancy and capillary forces grow dominant over viscous forces within tens to hundreds of meters of the injection wells resulting in remarkably different fluid migration patterns. Previous work by Saadatpoor (2009) suggests that in formations with sufficiently heterogeneous capillarity, the structure of the rising $CO_2$ plume reduces the volume of rock invaded. Ganesh (2012) has suggested that, as the degree of heterogeneity in a storage domain increased, $CO_2$ migration patterns exhibited a spectrum of structures,

from ‘dispersed’ capillary fingers with minimal rock contact to back-filled ‘compact’ distributions of saturation with much larger storage efficiency, but still far from “compact”.

Saadatpoor (2012) also revealed the relationship between heterogeneity correlation lengths and total $CO_2$ storage capacity in a particular formation. He suggested that increasing horizontal correlation length increases the total local capillary trapping capacity, while increasing vertical correlation length decreases the total local capillary trapping capacity. The results are summarized in Figure 2.8 below:

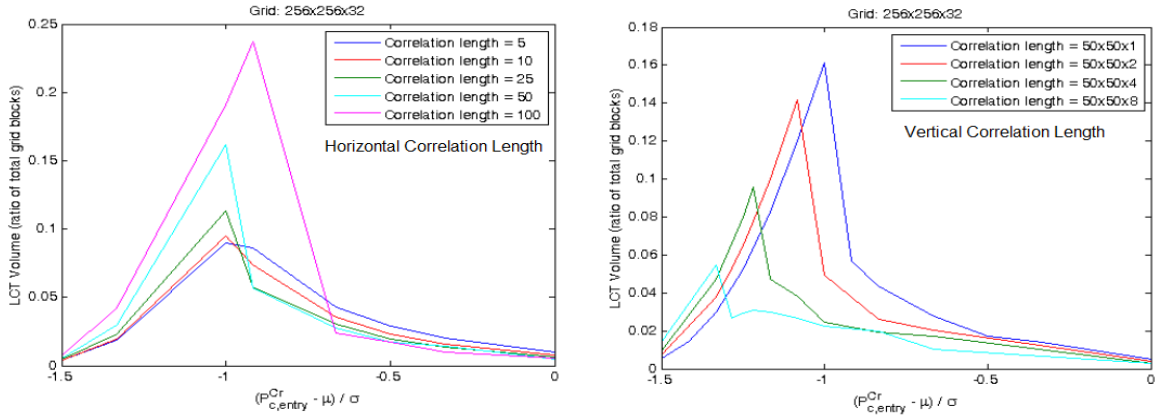


Figure 2.8: (left) Evolution of the local capillary trapping volume with normalized critical capillary entry pressure for base case with different horizontal correlation lengths. (right) Evolution of the local capillary trapping volume with normalized critical capillary entry pressure for base case with different vertical correlation lengths. (Saadatpoor 2012)

Besides Saadatpoor’s numerical model, others (Hesse and Woods 2010; Green and Ennis-King 2010; Mouche et al. 2010) built models to up-scale the impact of small-scale heterogeneities on the buoyant flow and residual trapping of $CO_2$ in a brine-saturated system to the reservoir scale. They conclude that among other factors, saturation buildup beneath intra-reservoir flow barriers is highly dependent on the lateral extent and vertical distribution of heterogeneities, which is in agreement with

Saadatpoor's prediction (2012). It illustrated the equally important role played by depositional structures and diagenetic horizons, as compared to mudrock distribution, in the movement and steady-state distribution of $CO_2$ plume. In addition, $CO_2$ should be considered immobile in the absence of recharge from continued injection, if the buoyant $CO_2$ exists beneath the spill point of intra-reservoir heterogeneities.

## 2.3 Experimental assessments of $CO_2$/brine interactions

While many simulation efforts investigate the migration of stored $CO_2$ in the subsurface, experimental assessments have also been performed to couple the knowledge learnt about $CO_2$/brine interactions.

### 2.3.1 $CO_2$/brine interaction experiment at the core scales

Krevor et al. (2011) injected $CO_2$ and water at typical reservoir conditions (9 MPa pore pressure and 50 ℃) into a sandstone core, which had two regions of distinct capillarity: the upstream 10 cm long region has relatively high permeability and homogeneous sand, and the downstream 3 cm long region has low permeability due to crossbedding and high capillary entry pressure for $CO_2$. $CO_2$ concentration builds up upstream of the capillary barrier during the drainage process displacing water; and the accumulation of $CO_2$ cannot be displaced during 100% water flooding resulting in trapped saturations that are a factor 2–5 times higher than what would be expected from residual trapping alone. They demonstrated that capillary barriers can immobilize $CO_2$ as a continuous phase at saturation higher than would be possible as isolated blobs. In addition, they suggested that the capillary barrier in this case was the sub-core scale sand bedding planes, and not the low permeability mudrock lenses. This is important, because it claims that the heterogeneities sufficient to cause local trapping are more prevalent than would be expected from an estimate of the distribution of tight rocks in the reservoir.

This means there are ample spaces for $CO_2$ geologic storage, and the gas trapped beneath capillary barriers occupy more pore spaces than would expected by residual trapping.

### 2.3.2 $CO_2$/brine interaction experiment at the bench scale

Plug and Bruining (2007) showed that wetting alteration and the abrupt phase changes and accompanying density and viscosity changes may affect the success of $CO_2$ sequestration. They performed capillary pressure measurement on an unconsolidated sand system using $CO_2$ and distilled water up to near critical states. This method could quantify static drainage and imbibition capillary pressure as a function of various temperatures and pressures of practical interest. Small injection rate of $CO_2$ into the sand pack created a near static condition. They obtained capillary pressure curves and found significant capillary pressure fluctuations and negative values during imbibition observed at near critical conditions. The capillary pressure behavior should be considered in $CO_2$ sequestration application, in particular to the caprock integrity and drainage and imbibition events in heterogeneous rocks. Increasing $CO_2$ pressures decrease the interfacial tension between $CO_2$ and water, therefore decreasing the primary drainage capillary pressures. The wettability of quartz sand is altered to intermediate wet in the presence of $CO_2$ under supercritical conditions (Plug and Bruining 2007). The water production and gas injection behavior depends largely on mass transfer rate and diffusion of $CO_2$ in water, but these effects become negligible for the injection of liquid $CO_2$. They claim that $CO_2$/brine interaction near critical condition is immiscible, and the capillary pressure is not influenced by the dissolution of $CO_2$ in water.

## 2.4 Integrity of caprock for $CO_2$ storage

Experiment and simulation have both been done to study the integrity of caprocks for $CO_2$ geologic storage, which is deemed as the key component for such projects to be successful. According to Shukla et al. (2010, 2011), induced changes in pressure and stresses caused by $CO_2$ injection on the behavior of the rock mass, especially the caprock and any major traversing low-permeability geological structures, will impact the integrity of the caprock geomechanically. Injection of $CO_2$ leads to increasing pore pressure and reduced effective stress, increasing the likelihood of exceeding the capillary entry pressure of the caprocks and of caprock fracturing.

Saadatpoor (2009, 2010) simulated $CO_2$ leakage cases with homogeneous and heterogeneous capillary pressure field in a typical saline aquifer. $CO_2$ trapping is quantified based on the results of the leakage. Capillary heterogeneity is introduced via Leverett scaling group. They concluded that ignoring heterogeneity gives the worst case estimate of the risk. Local capillary trapping reduces potential leakage through failed seal, but a range of $CO_2$ leakage amounts can occur depending on heterogeneity and location of leak. The thickness of the sealing layer and the presence of an active open aquifer connected to the leak do not change the leakage volume of $CO_2$. Experimental evidence is still yet to be discovered to visualize and validate the predictions made by simulation.

Busch et al. (2010) proposed a method to estimate the in-situ capillary threshold pressure of a sealing formation based on Young-Laplace Equation, assuming a completely water-wet system, zero degree contact angle and constant interfacial tension. But $CO_2$ interfacial tensions and contact angles change with pressure, temperature and salinity of the brine. Based on this assumption, they calculated the maximum $CO_2$ column heights using different IFT values from literature shown in Figure 2.9 below:

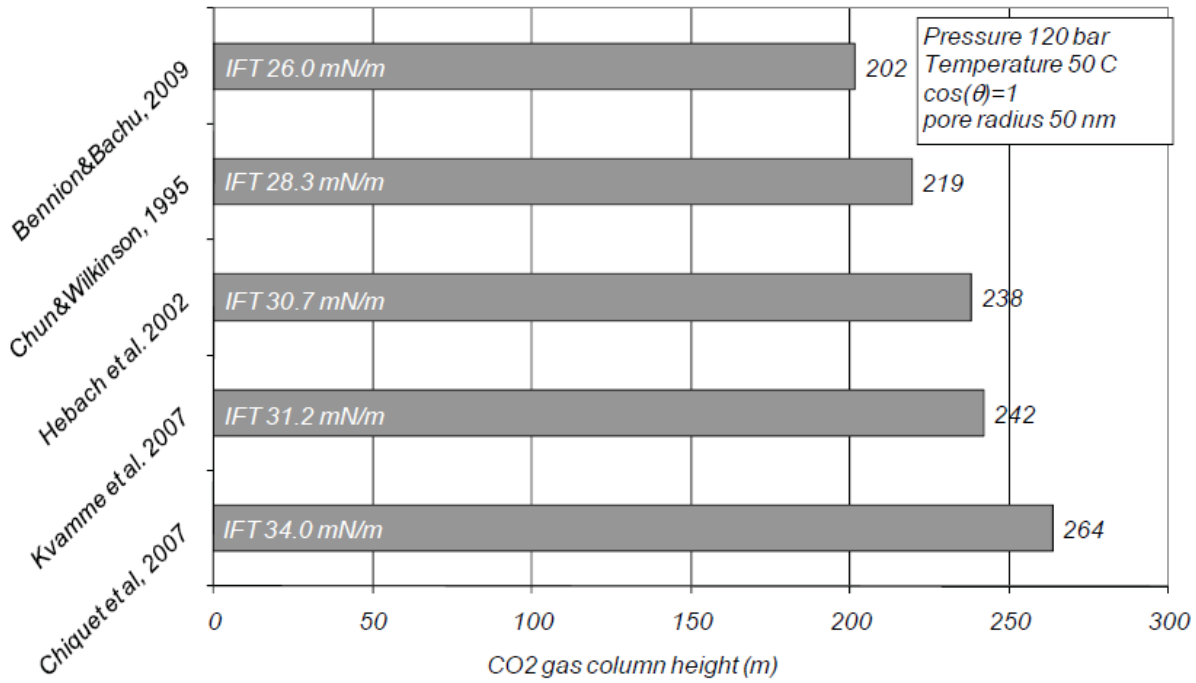


Figure 2.9: Calculated maximum $CO_2$ column heights using different IFT values and constant contact angle and pore radius values for a $CO_2$ storage reservoir at 1200 m depth corresponding to about 12 MPa hydrostatic pressure and 50°C. (Figure from Busch 2010)

Any faults and joints present in the seal are commonly considered as potential leakage pathway with high $CO_2$ flux rate out of the reservoir, thus compromising the storage capacity and integrity. Capillary leakage can be significant in terms of flow rate after capillary entry pressure is exceeded, especially for saline aquifer where formation pressurization after $CO_2$ injection could be higher than the original reservoir pressure.

Edlmann et al. (2013) performed an experiment which exposed 38 mm diameter fractured Kimmeridge Clay caprock samples recovered from 4 km depths to supercritical $CO_2$ under in-situ pressure, temperature and geochemistry. They found that sc$CO_2$ will not flow through tight natural caprock fractures, even with a differential pressure across

the fractured sample in excess of 51 MPa. However, gas phase $CO_2$ flows readily through the fracture. The group suggested that a critical threshold of fracture aperture size will possibly control $CO_2$ flow along the fracture, and recommended pressure and temperature comfortably above the critical point for $CO_2$ storage.

## 2.5 Persistence of local capillary trapping to $CO_2$ storage safety

The work presented in this thesis is a step forward from previous studies on two phase immiscible buoyancy-driven countercurrent migration in porous media in the context of local capillary trapping. Until now, there had been no other experimental protocol established to systematically evaluate the persistence of such trapping mechanism. This work will not only serve to meet the objective of assessing the persistence of local capillary trapping mechanism, but will also serve to fill the void of investigating flow behavior under the influence at the bench scale.

# Chapter 3 Experimental Setup

## 3.1 Experiment concepts

The experiments in this research work arrange for a buoyant nonwetting phase to rise through a heterogeneous domain, displacing wetting phase, mimicking the rise of $CO_2$ in an aquifer with spatially varying capillary entry pressures. Figure 3.1 below presents a simple illustration of this experiment concept.

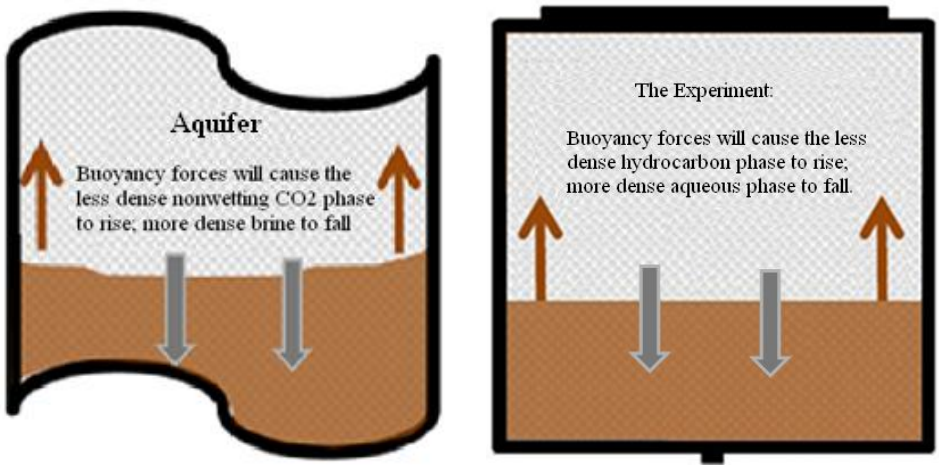


Figure 3.1: The concept for the experiment. The experiment set up enables two phase immiscible buoyancy-driven counter-current displacement. The porous medium is designed to account for heterogeneity of capillary entry pressure at the cm scale.

Far from an injection well, the $CO_2$ being stored in a reservoir will migrate primarily because of buoyancy. As shown in Figure 3.1 above, in a typical storage aquifer, buoyancy forces will drive the less dense non-wetting $CO_2$ phase to rise and the wetting more dense brine phase to fall. Similarly, in the experiments conducted in this research, buoyancy forces will drive the less dense non-wetting hydrocarbon phase to rise and the denser wetting aqueous phase to fall. From the point of view of immiscible displacement, the nonwetting hydrocarbon phase rising in the hydrophilic lab apparatus is

equivalent to nonwetting $CO_2$ rising in the hydrophilic aquifer. This forms a countercurrent buoyancy displacement movement in the laboratory apparatus because of the boundary conditions (closed sides), and in the reservoir when the $CO_2$ plume extends across a wide area; when the area is wide, lateral displacement of brine is slow and the brine instead sinks through the $CO_2$ countercurrently.

The two types of porous media domains relevant to this research work and their wettability properties are summarized in the Table 3.1.

| **Porous Media Domain** | **Non-Wetting Phase** | **Wetting Phase** |
|---|---|---|
| *Nature:*<br>Saline Aquifer (Hydrophilic) | $scCO_2$<br><br>$\rho$ = 500-700 kg/m$^3$<br>$\mu$ = 0.05 cP | brine<br><br>$\rho$ = ~1000 kg/m$^3$<br>$\mu$ = 0.3-0.4 cP |
| *Experiment:*<br>Hydrophilic container walls and hydrophilic glass beads | 90% decane +<br>10% Mineral oil<br><br>$\rho$ = 724 kg/m$^3$<br>$\mu$ = 0.9 cP | 60% $H_2O$ +<br>40% glycerol<br><br>$\rho$ = 1084 kg/m$^3$<br>$\mu$ = 7.0 cP |

Table 3.1: Relevant domain wettability overview

A porous medium made of optically favorable and hydrophilic glass beads was made to represent the storage reservoir. The following section explains the experimental set up in more detail.

## 3.2 Experimental apparatus

When fully assembled, the apparatus forms a transparent quasi two-dimensional domain which enables the observation of the fluids' behaviors within the bead/grain packing. The complete experimental apparatus consists of four separate parts,

1. Pyrex glass containment box ("the envelope")
2. Steel caps (top and bottom)
3. Pivoting steel frame
4. Fluid flow system, and is shown in the following Figure 3.2.

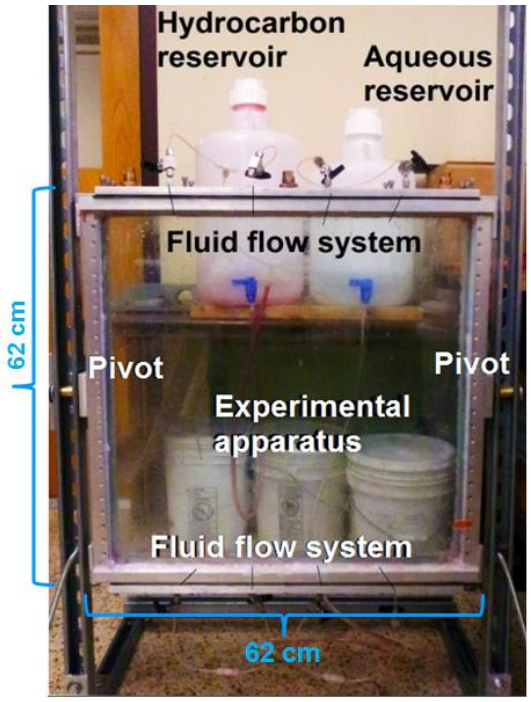


(a)

(b)

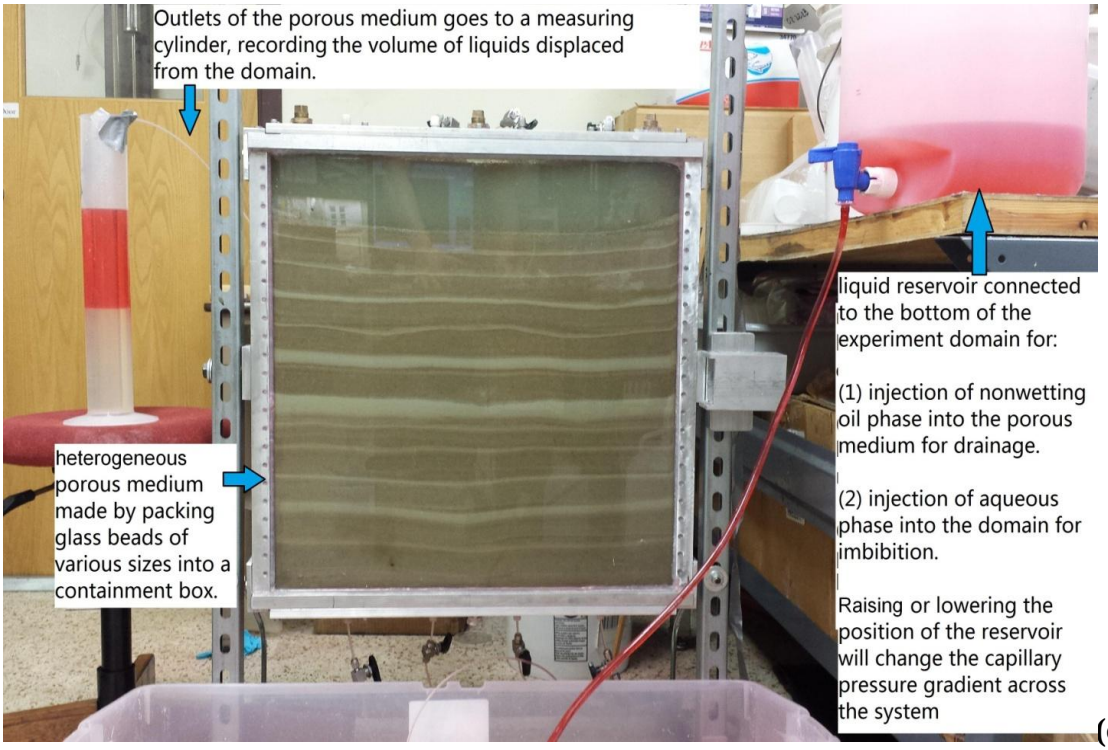


(c)

Figure 3.2 (continues to next page)

Figure 3.2: Experimental apparatus. (**a**) A 2 ft by 2 ft by 0.1 ft Pyrex glass containment box with steel caps tapped with fluid entry/exit ports and valves (top and bottom). Box is mounted on horizontal pivots in a metal support frame. Total inside volume of the containment box is about 700 cubic inches (11.33 liter). The pivots enable the easy flipping of a gravity stable initial condition by 180 degrees to start the experiment. (**b**): Example of packed domain. Various sizes of water-wet silica beads are packed into the glass containment box with desired patterns, to create a porous medium with heterogeneity of interest. Different color corresponds to different sizes of beads, as each type of beads has its own optical characteristic. (**c**): A fully assembled, operating experimental set up. Liquid reservoir attached to the bottom can be replaced either with oil reservoir or aqueous reservoir, serving different purposes of drainage (entry of nonwetting phase into the domain while simultaneously displacing water) or imbibition (entry of water into the system simultaneously displacing oil). The outlet from the domain is not submerged in to the measuring cylinder, but is open to atmosphere and kept at the same height as the top of the domain for maintaining hydrostatic pressure.

The dimensions for the experimental apparatus are 2 ft x 2 ft x 0.1 ft To provide an airtight seal, a gasket custom cut from 1/8” thick neoprene is layered between the glass envelope and its metal caps. Each of the metal caps has twelve (12) 1/2" threaded holes for a total of twenty four (24). All of them are utilized for a secure attachment by means of 1-1/2" tightened bolts. The steel frame allows for seamless pivoting of the experimental apparatus. Attachment of apparatus to frame is by means of two steel plates, both of which are secured on two opposing sides.

To enable fluid flow into the experimental apparatus, there are four (4) two-way valves on each of the top and bottom caps (8 valves in total). The valves serve as the inlets and outlets for oil based nonwetting fluid and aqueous based wetting fluids. All valves and connectors are 1/8” and utilize 1/8” plastic tubing. Those in the fluid flow tubing system are nylon Swagelok and those directly connected to the experimental apparatus are stainless steel Swagelok.

By opening and closing the attached control valves and manipulating the position of attached reservoirs, different types of boundary conditions to the porous media can be achieved. These are shown in the following Figure 3.3 (migration in closed domain after nonwetting phase emplacement) and Figure 3.4 (migration in open domain during nonwetting phase emplacement):

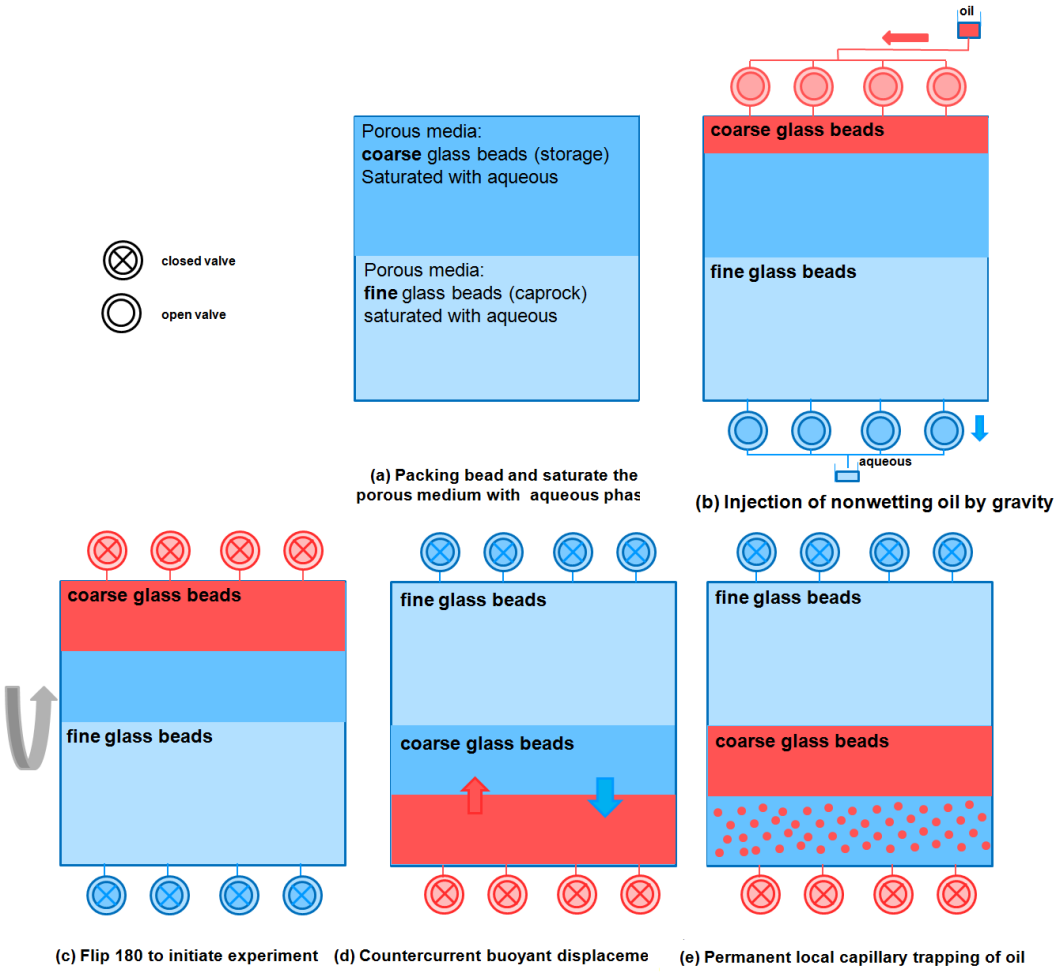


Figure 3.3: Lab arrangement for a two phase, immiscible, closed-boundary, counter-current displacement. (a) Pack beads with different sizes (here: coarse for storage reservoir, fine for the caprock) to achieve desired heterogeneity, and saturate the entire domain with wetting phase (blue). (b) Inject nonwetting oil phase from the top via gravity, displacing wetting phase from the bottom. (c) Close all valves (circles at top and bottom of domain) and rotate the containment box about the horizontal axis through middle of the domain such that the fine beads region is at top of domain to form the caprock (a capillary barrier to the buoyant nonwetting phase in the storage reservoir). (d) Density difference between the wetting and nonwetting phases will drive the buoyant immiscible counter current movement in a closed environment. (e) Mobile nonwetting phase accumulates beneath the capillary barrier, locally trapped. Part of the nonwetting phase are trapped in the original section as residual (red dots).

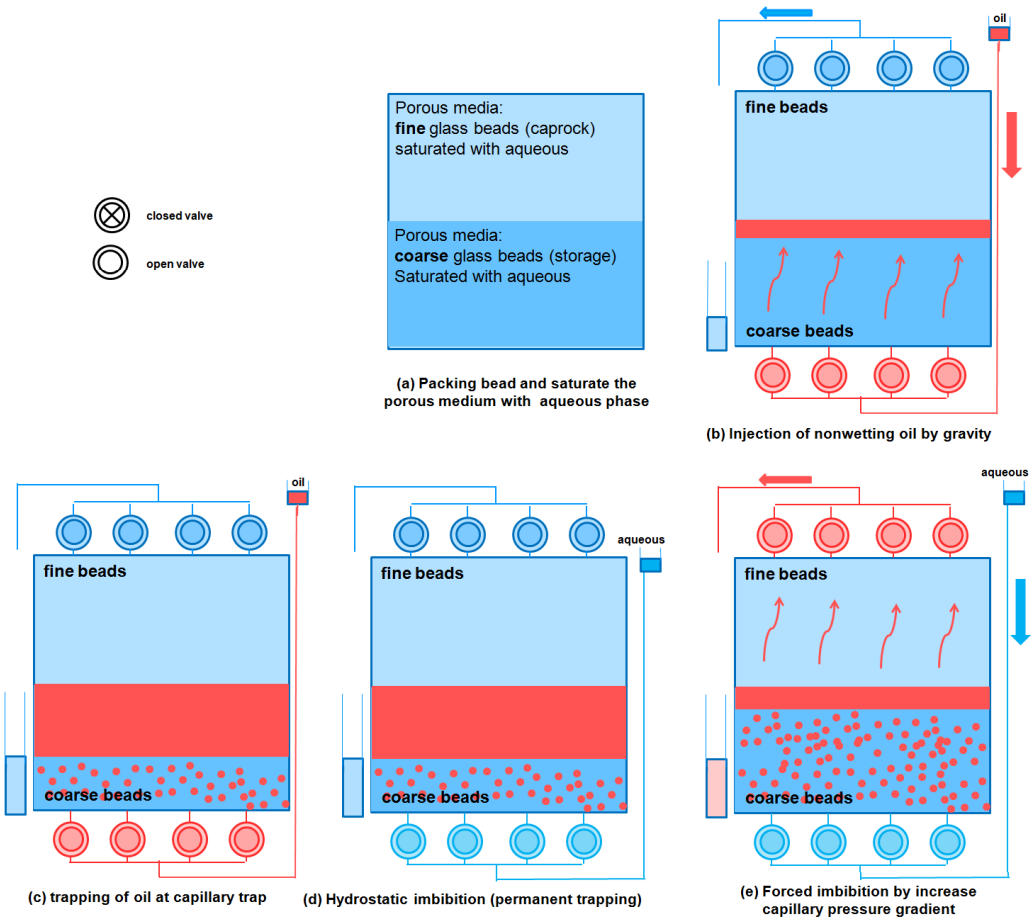


Figure 3.4: Lab arrangement for a two phase, immiscible, open-boundary, counter-current displacement movement. (a) Pack beads with different sizes to achieve heterogeneity, and saturate the entire domain with wetting phase. (b) Inject nonwetting oil phase from the bottom via gravity, displacing wetting phase from the top. (c) Less dense nonwetting phase rises and trapped permanently beneath capillary barriers. (d) Replace the oil reservoir with an aqueous one at the same height as the top of the domain for hydrostatic potential gradient. (e) Raise the aqueous reservoir to increase the capillary pressure gradient across the domain.

Manipulating the open (circle)/close ('X') state of valves, and positions of reservoirs (red = nonwetting oil; blue = wetting aqueous) create various types of boundary conditions and features (hydrostatic potential, forced imbibition, artificial fractures, etc). Different size of beads corresponds to different capillary entry pressure.

## 3.3 Experimental design considerations

Two objectives drove the design of these experiments and each objective involved the assessment of immiscible two-phase buoyancy driven flow in porous media, with practical application to track $CO_2$ migration in a saline aquifer:

1. To determine the influence of geological and petrophysical characteristics (particularly heterogeneity) on the persistence of local capillary trapping;

2. To mimic and demonstrate how leakage, e.g. if the top seal is compromised, could affect the mobile phase in a local capillary trap.

### 3.3.1 $CO_2$ and brine relationship

The relationship of physical properties of supercritical $CO_2$ and brine was discussed in the Introduction section. It is crucial to have an experiment that is as analogous as possible to in situ conditions. Matching the viscosity, density and interfacial tension relationships is of particular importance. As described in Introduction section, the viscosity ratio has an effect on the stability of immiscible displacement. The density difference between $CO_2$ and brine drives the buoyant movement of the $CO_2$ plume in the aquifer. The interfacial tension governs the capillary pressure associated with the fluid flow in such porous media. Therefore the final experimental design should not only match these relationships but also be able to initiate buoyant movement easily and consistently.

### 3.3.2 Saline aquifer environment

Saline aquifers are an aqueous environment in which brine is the wetting fluid and $CO_2$ is the non-wetting fluid. The experimental apparatus used by previous researchers (Hernandez 2011) was made of polycarbonate which is hydrophobic. It proved difficult to obtain reliably hydrophobic granular material to use in that apparatus, so a new apparatus was constructed from Pyrex glass. The glass has an affinity for water and thus is hydrophilic, which mimics the natural environment when filled with a hydrophilic porous medium.

### 3.3.3 Ambient conditions

The experiment is performed at ambient conditions for safe, convenient observation and digital capture (by means of a high definition video camera) of the progress in the open laboratory setting. Experiments run at storage formation temperatures ($T > 300$ K) and pressures ($P > 20$ MPa) are challenging and the imaging reported in this work would not be available. The existing experimental apparatus is not designed to withstand conditions other than ambient.

### 3.3.4 Qualitative analysis

Due to the novelty of this research topic and concept, at this stage observations of local capillary trapping and residual trapping made by this experimental set up are qualitative, based on visual indicators, rather than quantitative. The non-wetting oil phase used in this experiment, which represents the rising stored $CO_2$ in the saline aquifer, is dyed red with trace amount of oleic acid ($C_{26}H_{24}N_4O$). Therefore, when the nonwetting oil phase entered the porous media, more redness means greater saturation. Future work will attempt to quantify the nonwetting phase saturations in the experimental domain.

### 3.3.5 Final experimental design

The final experimental design incorporated the refining of the previous experimental apparatus so that the seal is robust (no fluids leaked out) and the bead packing fills the entire domain without any settling, such that the experiment is convenient and repeatable.

For these experiments, the aqueous phase will act as wetting brine does in the storage aquifer and the hydrocarbon phase will act as the non-wetting $CO_2$ phase does in the aquifer. Mimicking the density relationships of supercritical $CO_2$ and brine in nature with convenient fluids in the lab, the buoyant movement to be observed occurs when the aqueous phase falls while the hydrocarbon phase rises.

## 3.4 Fluids

In order to perform the experiments at ambient conditions, it was necessary to develop a fluid pair that was as analogous as possible to that of $CO_2$ and brine at aquifer conditions. In the temperature and pressure range expected for many storage aquifers (depths of 1 km or more) the density of the $CO_2$ phase will be 500 to 700 kg/m$^3$. Thus the density difference driving $CO_2$ movement will be 300 to 500 kg/m$^3$. For typical storage conditions the $CO_2$ viscosity is about 0.05 cP and the brine viscosity is about 0.3 to 0.4 cP. The ratio of viscosities of nonwetting and wetting phases is therefore about 0.05/0.35 or 1:7. (Hernandez 2011)

The fluids used to match the supercritical $CO_2$-brine viscosity and density relationship are water/glycerol mixture and a light mineral oil/decane mixture; the latter are both Fisher brand chemicals and were bought online from Fisher Scientific. The fluid properties were obtained experimentally.

The density of the water/glycerol mixture was obtained through a simple experiment in which a graduated cylinder was weighed before and after a known fluid volume was poured.

Due to the hydrophilic nature of the experimental apparatus, brine/glycerol mixture serves as the wetting phase and a light mineral oil/decane mixture serves as the non-wetting phase. The density difference between brine/glycerol ($\rho_w$ = 1084 kg/m$^3$) and the light mineral/decane oil mixture ($\rho_o$ = 724 kg/m$^3$) is about the same than that of $CO_2$ and brine at aquifer conditions (Cinar et al. 2009). Of greater concern is matching the viscosity ratio. As explained in Chapter 2, viscosity ratio of the immiscible fluids determines their migration pattern. If the viscosity ratio of the surrogate fluid pairs used in these experiments deviates from the value of 1:7, the flowing pattern of the fluids in the domain will not resemble the true migration pattern of rising $CO_2$ in the actual storage saline aquifer. Therefore the accuracy of estimating the total storage capacity of such storage formation will be compromised, and the assessment of the persistence of trapping mechanism, such as Local Capillary Trapping, will be also influenced adversely.

A Fann 35 model rotational viscometer was used to obtain the final Newtonian viscosity of the mixture. With a R1-B1-F1 rotor, bob and spring combination running at 300 rpm and 600 rpm, the viscosity is the difference between the two values read directly from the dial readings and corrected according to the user manual guide.

Figure 3.5 below depicts the viscosity of a mixture of light mineral oil ($\mu$ = 44 cP) and decane ($\mu$ = 0.92 cP) as a function of decane fraction according to the quarter power mixing rule (Equation 3.1):

$$\mu_{mixture} = \left( x_a {\mu_a}^{-\frac{1}{4}} + x_b {\mu_b}^{-\frac{1}{4}} \right)^{-4} \qquad (3.1)$$

where,

$\mu_i$ is the viscosity of pure component $i$,

$x_j$ is the volume fraction of component $j$ in the mixture.

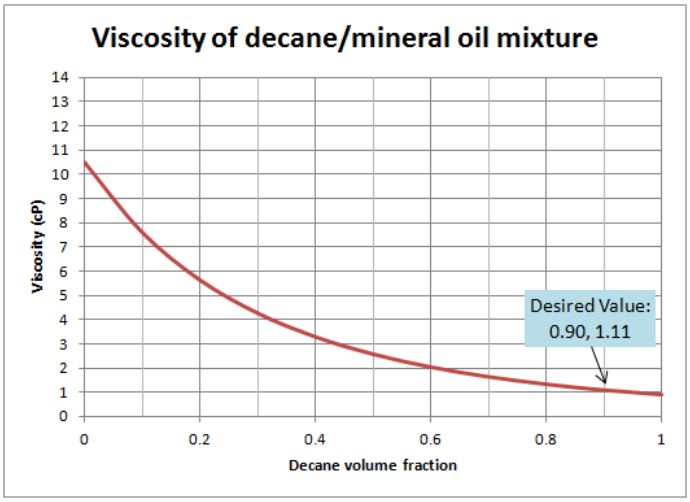


Figure 3.5: Quarter-power mixing rule applied to a decane/mineral oil mixture at ambient conditions. The actual viscosity of the mixture agrees to this prediction well (Hernandez 2011).

Experimentally, the desired viscosity of 1.1 cP was achieved with the addition of a certain amount of decane to the original volume composition. This value is indicated in Figure 3.5 above. In line with the experimental results, for the buoyant displacement experiments we used a mixture of 0.1 light mineral oil/0.9 decane by volume to represent the $CO_2$ phase. The target composition of the brine/glycerol was also determined using the quarter-power mixing rule (Equation 3.1 above). In line with the experimental results, for the buoyant displacement experiments we use a mixture that is 0.591 brine/0.409 glycerol by volume to represent the brine phase in an aquifer. The measured viscosity values and calculated values are summarized in the following Table 3.2.

| Component Fraction | | Experimental (using the Fann 35 viscometer) | | | Calculated |
|---|---|---|---|---|---|
| $H_2O$ | Glycerol | Reading @ 600 rpm | Reading @ 300 rpm | **Viscosity (cP)** | **Viscosity (c)** |
| 1 | 0 | 6 | 4.8 | 1.2 | 1.0 |
| 0.9 | 0.1 | 7.5 | 5 | 2.5 | 1.4 |
| 0.8 | 0.2 | 10 | 6.5 | 3.5 | 2.1 |
| 0.7 | 0.3 | 13 | 7.5 | 5.5 | 3.1 |
| 0.6 | 0.4 | 19 | 12 | **7** | 5.0 |
| 0.5 | 0.5 | 35 | 21 | 14 | 8.5 |
| 0.4 | 0.6 | 59 | 31 | 28 | 15.8 |
| 0.3 | 0.7 | 141 | 81 | 60 | 32.5 |
| 0.2 | 0.8 | Out of Range | Out of Range | N/A | 78.5 |
| 0.1 | 0.9 | Out of Range | Out of Range | N/A | 244.4 |
| 0 | 1 | Out of Range | Out of Range | N/A | 1200.0 |

Table 3.2: Viscosity of water/glycerol mixture at ambient conditions. Pure water and glycerol have viscosities of 1 cP and 1200 cP respectively. The experimental value was obtained by subtracting the 300 rpm reading from the 600 rpm reading and adjusted according to the user guide. The calculated value is based on "quarter power mixing rule".

This information is also plotted in the following Figure 3.6:

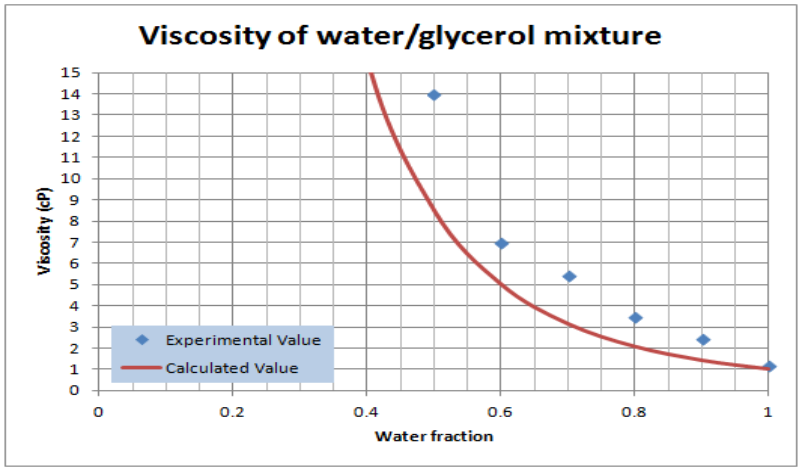


Figure 3.6: Quarter-power mixing rule applied to a brine/glycerol mixture at ambient conditions (red curve) predicts the trend of the measured viscosity of the mixture (blue curve).

Tables 3.3 below provides a summary of the individual fluid properties and the relationships between the fluid pairs respectively.

| Fluid | Viscosity (cP) | Density (kg/m$^3$) |
|---|---|---|
| **Typical Storage Aquifer** | | |
| Supercritical $CO_2$ | 0.05 } 1:7 | 500-700 } Δρ= 300-500 |
| Brine | 0.3-0.4 | ~ 1000 |
| **Ambient conditions:** | | |
| Brine | 1.0 | 1000 |
| Decane | 0.92 | 720 |
| Light Mineral Oil | 44 | 800 |
| **90% Decane + 10% Mineral Oil (non-wetting phase, surrogate for $CO_2$)*** | 1.1 } 1:7 | 724 } Δρ=360 |
| **60% Brine + 40% Glycerol (wetting phase)*** | 7.0 | 1084 |

*Fluids used in the experiment

Table 3.3: Convenient Fluid Pair w/Properties Analogous to $CO_2$/brine

To match the viscosity ratio of $CO_2$ and brine, the mixture compositions were adjusted as indicated in Table 3.3 above.

### 3.5 Wettability and contact angle

It is expected that Pyrex glass used to construct the transparent faces of the containment box is hydrophilic. To verify this, a transparent water tank was filled with the mixed aqueous wetting phase. A pair of rubber pieces of equal height were placed and submerged at the bottom of the tank, with about 5 cm apart. The glass material to be tested was then placed on the two rubber pieces, and submerged.

Hydrocarbon phase droplet (dyed with red food coloring) was then transferred via a transfer pipette to the cavity formed by the glass material and the two rubber blocks. Due to density difference between the two liquid phases, buoyancy drove the hydrocarbon droplet to rise, to which was then trapped at the lower surface of the glass material and formed a contact angle.

A high definition video camera recorded the image from a level parallel to the glass piece and the contact angle was measured. Results from different combinations of fluid pairs are summarized in the following Figure 3.7.

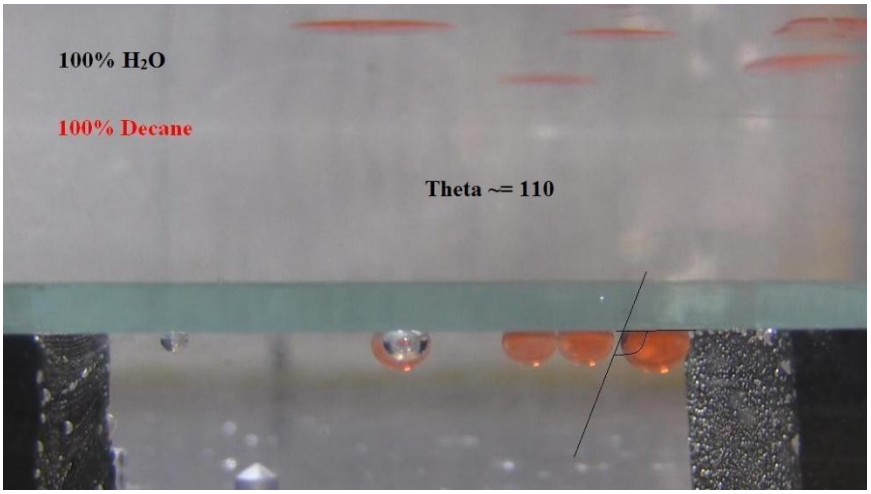


**(a)**

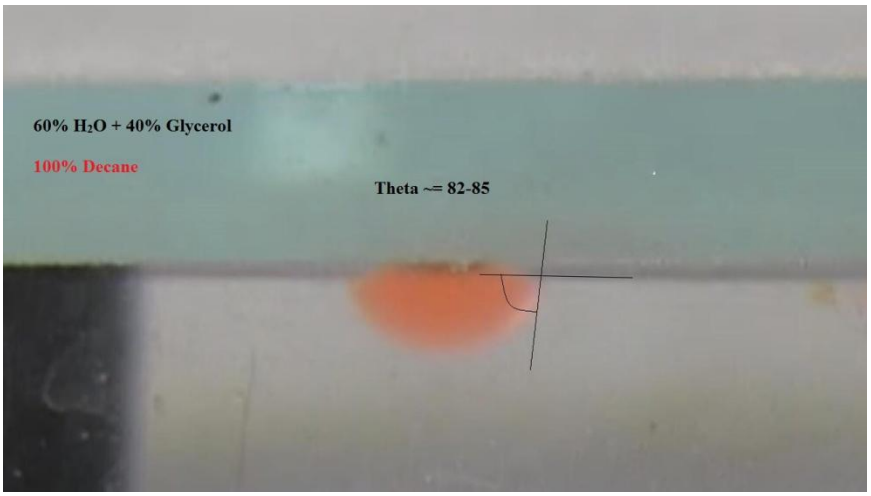


**(b)**

Figure 3.7: (continues to next page)

(Figure 3.7 continued)

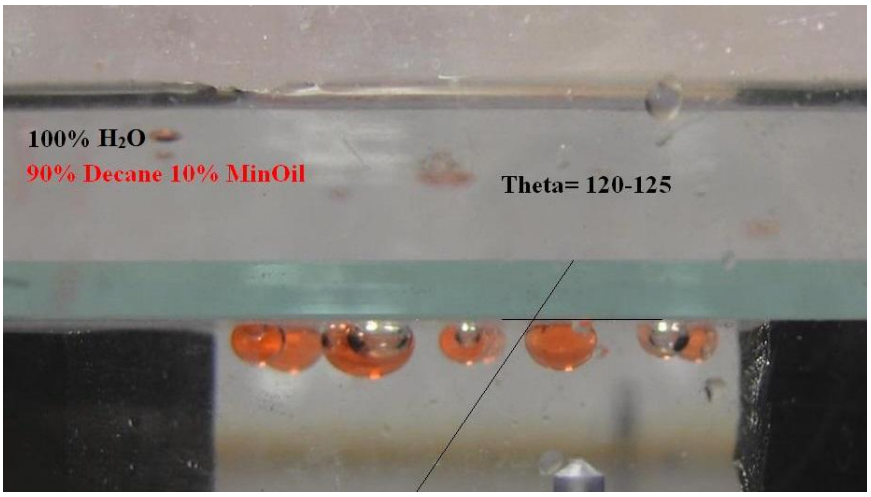


**(c)**

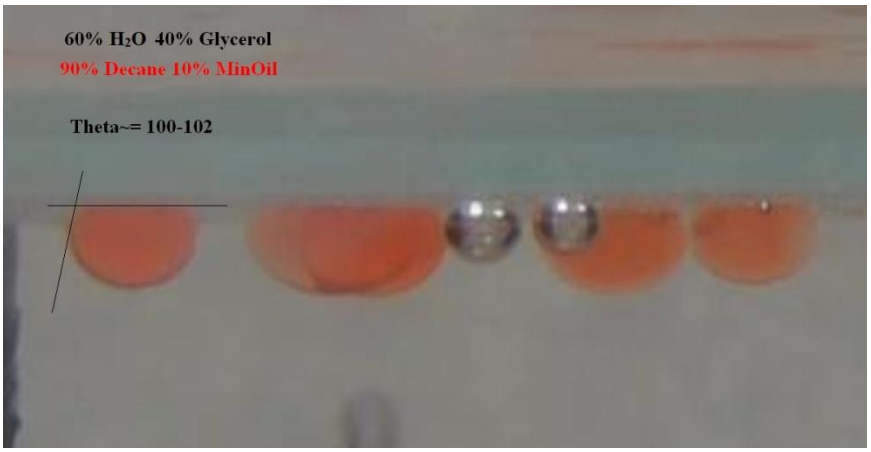


**(d)**

Figure 3.7: Different fluid pair combinations and their contact angles on hydrophilic Pyrex glass surface, non-wetting phase is dyed in red. **(a)** Pure decane droplets (dyed in red) surrounded by pure water form a 110 degree contact angle on Pyrex glass surface. **(b)** Pure decane droplets (dyed in red) surrounded by 60% water 40% glycerol mixture form an 82 degree contact angle on Pyrex glass surface. **(c)** 90% decane 10% mineral oil mixture droplets (dyed in red) surrounded by pure water form a 120-125 degree contact angle on Pyrex glass surface. **(d)** 90% decane 10% mineral oil mixture droplets (dyed in red) surrounded by 60% water 40% glycerol form a 100-102 degree contact angle on Pyrex glass surface.

Adding mineral oil into decane will increase the contact angle. Adding glycerol into water will decrease the contact angle. The larger the contact angle, the more hydrophobic the non-wetting phase is, the better for the objective of achieving largest capillary pressure according to Young Laplace Equation. Taking viscosity, density difference and interfacial tension into consideration, the fluid pair that best suits the experiment is 60% water 40% glycerol (as wetting phase) and 90% Decane 10% mineral oil (as non-wetting phase).

It is also important to note that the two phases are immiscible during the time period range of the experiments (several hours to days).

A ring tensiometer is used to measure the interfacial tension (IFT) between the non-wetting phase (90% Decane + 10% Mineral Oil) and wetting phase (60% Water + 40% Glycerol). Assuming perfect wetting (zero contact angle), the IFT between the two phases is measured to be 30.4 dynes/cm. With a 100 degree contact angle, the IFT is calculated to be 27.8 dynes/cm according to Equation 3.2 below, while the actual interfacial tension of brine-$CO_2$ system under reservoir condition is averaged to be 30-35 dynes/cm (Chalbaud et al. 2006).

$$\sigma = \sigma' \cdot cos\theta \qquad (3.2)$$

where,

$\theta$ is the contact angle between the fluid/fluid interface and the solid surface.

$\sigma$ is the actual interfacial tension between the two fluids with a contact angle $\theta$.

$\sigma'$ is the interfacial tension between the two fluids with perfect contact ($\theta$ = 180°).

### 3.6 Beads

The experimental apparatus is a hydrophilic glass containment box packed with hydrophilic glass beads and/or sand. Glass beads all come freshly from manufacturer, Potters Industries Inc. Average bead size distribution and theoretical capillary entry pressures for a column of packed beads are calculated (using interfacial tension of 27.8 dynes/cm for the brine/glycerol – decane/mineral oil interface and a contact angle of 100 degrees). The beads properties are summarized in following Table 3.4.

| Bead Name | Approximate Bead Diameter Distribution | Average Bead Diameter | Capillary Entry Pressure (Theoretical) | Capillary Entry Pressure (Experimental) | Maximum possible trapped oil column height |
|---|---|---|---|---|---|
| | (mm) | (mm) | (Pa) | (Pa) | (cm) |
| P-5 mm | 4.7 - 5.3 | 5.0 | 67 | 104 | 2.9 |
| P-3 mm | 2.8 - 3.2 | 3.0 | 111 | 143 | 4.0 |
| P-2 mm | 1.8 - 2.2 | 2.0 | 167 | 208 | 5.9 |
| P-0230 | 0.43 - 0.60 | 0.5 | 667 | 887 | 25.1 |
| P-0120A | 0.28 - 0.22 | 0.25 | 1334 | 1735 | 49.1 |

Table 3.4: Properties of beads used in experiments

Shown in Table 3.4, the capillary entry pressure of the bead packs is inversely proportional to the diameter of the beads. This is because for monodisperse beadpacks the characteristic pore throat size $r_{throat}$ (which determines the capillary entry pressure) is proportional to the bead size $R_{bead}$ (typically $r_{throat} \approx 0.3 R_{bead}$). Thus halving the bead size doubles entry pressure, according to Young Laplace Equation (Equation 3.3 below):

$$P_c = \frac{2\sigma \cdot cos\theta}{r} \qquad (3.3)$$

where,

$P_c$ is capillary pressure.

$\sigma$ is the interfacial tension between the two fluids.

$\theta$ is the contact angle between the fluid/fluid interface and the solid surface.

$r$ is the radius of the pore throat.

The detailed calculations for contents of Table 3.4 are shown in the following sections. Notice that all the values in the table are for dense random packing of single bead size.

### 3.6.1 Calculation of capillary entry pressure of bead packs (theoretical values)

The radius of the pore is related to the radius of the beads by a factor of 3 (Bryant 1996), i.e. $r_{pore}=r_{bead}/3$. When viscous and body forces are negligible, the configuration of two fluids is governed by Young-Laplace equations (Equation 3.4 below).

$$P_c = \sigma C \qquad (3.4)$$

Where

$P_c$ is the capillary pressure to the curvature of the interface between the two phases,

$\sigma$ is the interfacial tension between the nonwetting and wetting phases,

$C$ is the sum of the two principal curvatures, or twice the mean curvatures of the interface. $C=1/r_1+1/r_2$.

A sample calculation of capillary entry pressure and maximum possible trapped oil column height of a dense random packing of the 0.5 mm diameter beads is shown in the following section.

***Sample calculation**:*

Diameter of beads = 0.5 mm,

$r_{bead}$ = 0.00025 m,

$r_{pore} = r_{bead}/3 = 8.33 \times 10^{-5}$ m,

$C = 1/r_{pore} + 1/r_{pore} = 24000$ $m^{-1}$,

Measured interfacial tension = 30.4 dynes/cm = 0.0304 N/m

Contact angle of 100 degree,

Product of interfacial tension and cosine of contact angle =

0.0304 N/m × $cos(100°)$ = 0.0278 N/m = 27.8 dynes/cm.

Capillary entry pressure of the random dense bead pack =

$P_c$ = 0.0278 N/m × 24000 $m^{-1}$ = 667 Pa

Maximum possible trapped oil column height =

$P_c / \Delta\rho / g$ = 667 Pa / 360 kg/$m^3$ / 9.81 N/kg = 0.189 m = 18.9 cm

### 3.6.2 Calculation of capillary entry pressure of bead packs (experimental values)

For comparison with the theoretical values, the actual capillary entry pressures of bead packs were also measured experimentally. The following Figure 3.8 illustrates the experiment schematics.

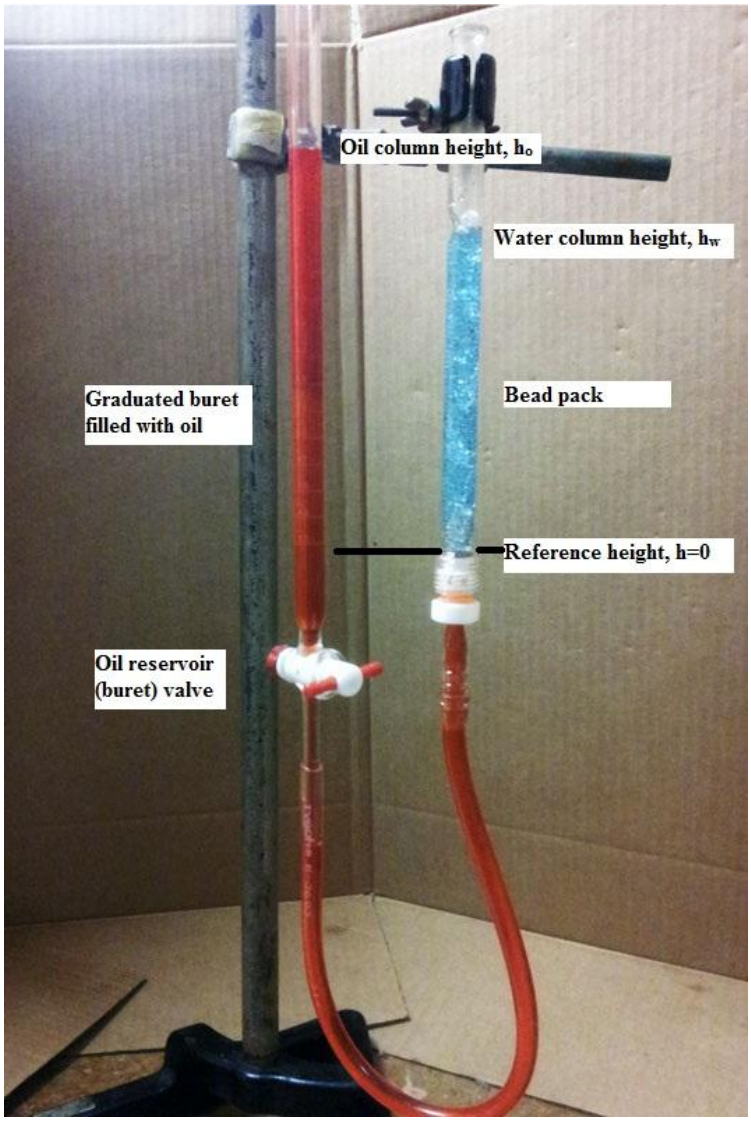


Figure 3.8: A labeled schematic of the wettability experiment. A bead pack (right) is saturated with water (dyed blue) and connected to an oil (dyed red) reservoir. An increase in oil pressure (accomplished by raising the oil reservoir height) is initiated in increments until oil displacement into the bead pack occurs.

The initial step is to set up the bead column in the glass tube; the column is then saturated with blue-dyed water. Bead pack saturated with food coloring (blue) dyed water is connected to an oil reservoir, in this case a graduated burette. Once saturated, the height of the oil column can be measured relative to the reference height indicated in Figure 3.8. This reference height starts at the bottom of the bead pack and marks the water-oil interface; it also aligns with the beginning of the graduations on the burette serving as the oil reservoir. The height of the oil column is then calculated using the equation for capillary pressure, denoted by following Equation 3.5.

$$P_c = g(\rho_o h_o - \rho_w h_w) \qquad (3.5)$$

where,

$g$ is gravity in m/s$^2$.

$\rho_w$ is the density of water in kg/m$^3$.

$\rho_o$ is the density mineral oil in kg/m$^3$.

$h_w$ is the height of the water column relative to the reference height in m.

$h_o$ is the height of the mineral oil column relative to the reference height in m.

Solving the equation for zero capillary pressure, the only unknown is the height of the oil column. The gravity is divided out and the height of the oil is calculated as the density of oil multiplied by the height of the oil column divided by the density of the water. For example, the density of water is 1000 kg/m$^3$ and the density of light mineral oil is 800 kg/m$^3$, thus when the relative height of the water is 80% of the relative height of the oil then the capillary pressure at the oil-water interface at the reference height is zero.

The opening of the valve on the oil reservoir initiates the experiment at this state of zero capillary pressure. Any movement in the water column, oil column or fluid

interface is recorded. If there is no movement, the oil reservoir height is increased by a small increment by raising the burette. Typical increments are 1.2 cm as the major graduations on the burette are 1.2 cm apart and using the graduations as markers aids in keeping the experiment consistent. After the system is allowed to reach equilibrium, any movement in either fluid column heights and/or the fluid interface is recorded. The process is continued until the bead column is entirely saturated with oil and all the water is displaced out and accumulated at top of it. The higher the increase required for initial displacement of oil into the water saturated bead pack, the more water wet the medium (or the smaller the beads) and hence the higher the calculated displacement pressure. The expected displacement pressure can be estimated using the Young Laplace equation for capillary pressure.

The Young Laplace equation for capillary pressure for two immiscible fluids in contact with a solid surface is given by Equation 3.2 in previous section.

A contact angle less than $30^{o}$ indicates a water wet medium. A contact angle greater than $90^{o}$ indicates an oil wet medium; oil will not enter the water saturated water-wet bead pack until the displacement pressure is exceeded.

The results of experiments for different bead sizes are shown in Table 3.4. The agreement with the theoretical expectation is reasonably good.

## 3.7 Experiment procedures

**Preparation of the Experimental Apparatus.** Each experimental sequence begins with the cleaning and drying of the experimental apparatus. A residual-free soap, water and ethanol are all used along with thick paper towels to wipe down all surfaces of the experimental apparatus, including the gasket, caps and containment box. After cleaning, the gasket is then aligned and positioned in place, then followed by the cap. They are tightened by screws afterwards.

### 3.7.1 Closed-boundary experiments:

Figure 3.9 below illustrates the procedures for conducting a closed-boundary experiment.


Figure 3.9: A graphical representation of the closed-boundary experimental design. The design calls for emplacing the nonwetting phase in a gravity-stable manner (filling from the top), closing valves, then flipping the apparatus to start the buoyancy-driven displacement.

**Step 1: Packing the experimental apparatus.** Packing begins with the glass containment box in the vertical position where the bottom cap is tightened, and the top of the box remains open. Dry beads are introduced into the apparatus via a plastic funnel and settled to the bottom by gravity. The use of a hand held vibrator wrapped in soft material is held against the apparatus to initiate more settling and results in a more uniform pack. Beads of different sizes were placed in sequenced layer to achieve desired

patterns of homogeneity or heterogeneity. Once the "envelope" is completely filled with beads, the top cap is then positioned and secured.

**Step 2: Saturate with the aqueous phase.** The experimental apparatus is now rotated to the position that has the oil flow system positioned at the top and aqueous phase flow system positioned at the bottom. The fluid flow system is connected to two reservoirs, two carboys filled with the aqueous phase and the hydrocarbon phase, placed on a small table behind the experimental apparatus. To initiate aqueous phase flow into the bead pack, the aqueous reservoir valve is opened then the valves designated for aqueous phase flow are opened. Flow into the bead pack is gravity driven. Time to reach complete saturation varied from minutes to several hours according to grain size, and the height of the aqueous reservoir. Air is displaced via the ports from the top. Ports at the bottom are closed once the aqueous phase saturates the entire domain.

**Step 3: Displace with the hydrocarbon phase.** Hydrocarbon phase is then introduced into the domain from the top four ports, by gravity feed; at the same time open two valves at the bottom for displaced aqueous phase to leave the system. The hydrocarbon non-wetting phase will build up at the upper portion of the domain till a predetermined volume while aqueous wetting phase has left the system.

**Step 4: The experiment.** All valves and ports are closed, so the buoyant displacement in this step occurs in a closed domain, requiring countercurrent movement of the fluids. Note that Steps 1-3 establish a gravity-stable configuration, as the denser aqueous phase rests below the less dense hydrocarbon phase. To initiate the buoyancy driven displacement, the gravity-stable configuration at the end of Step 3 is reversed by pivoting the apparatus 180 degrees in the frame. The subsequent fluid displacement will be physically analogous to the rise of $CO_2$ non-wetting phase in a saline aquifer as water descends to fill the space vacated by the rising $CO_2$.

For selected experiments, after the migration of oil stops, top and bottom ports are opened and connected to reservoirs to impose a prescribed hydraulic potential across the domain. This enables various boundary conditions, for example, forced imbibition of aqueous phase from the bottom, with accompanying displacement of fluids from the top, or hydrostatic conditions in which no aqueous phase flows into or out of the domain, unless buoyancy-driven outflow of hydrocarbon phase occurs.

**The initial condition**

The initial condition is a packed experimental apparatus which was initially saturated with an aqueous phase that has had a third of that aqueous phase displaced by a hydrocarbon phase. The configuration is gravity stable, as the denser aqueous phase rests below the less dense hydrocarbon phase. Figure 3.10 depicts an example of the initial condition.

Figure 3.10: Initial condition of the closed-state experiment. After packing granular medium of hydrophilic beads in the apparatus, aqueous phase (blue) (the brine/glycerol mixture) was slowly injected from the bottom to fill entire medium, followed by slow injection of light mineral oil/decane mixture (red) from the top to displace aqueous phase through the bottom. To initiate the buoyancy driven displacement, the gravity-stable configuration shown in this photograph is reversed by pivoting the apparatus 180 degrees in the frame (a rotation around a horizontal axis through the middle of the domain in the photograph), thus the denser aqueous phase is placed above the less dense hydrocarbon phase.

### 3.7.2 Open-boundary experiments:

Notice that the initial condition of section 3.7.1 only appears in **closed-boundary** experiments where a 180 degree rotation of the experiment domain is required to set the less dense buoyant oil phase from the top to the bottom, allowing it to rise. **Open-boundary** experiments do not have such initial condition as the buoyant nonwetting oil phase is injected from bottom and rises simultaneously as soon as it enters the domain. Following Figure 3.11 depicts the sequence of an open-boundary experiment.

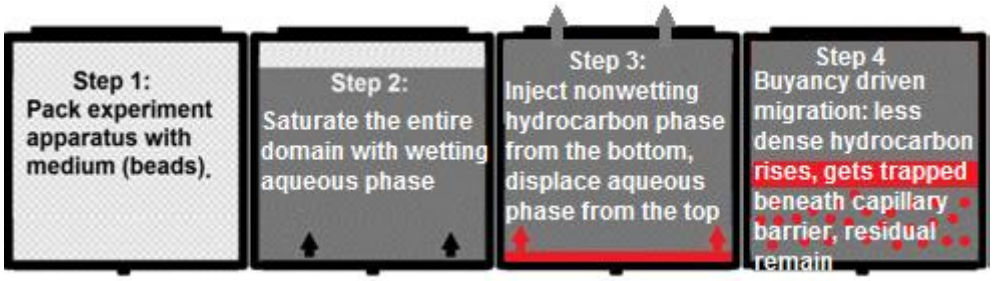


Figure 3.11: A graphical representation of the open boundary experimental design. The design calls for emplacing the nonwetting phase in a gravity-unstable manner (continuously filling from the bottom), open valves, then buoyancy drives the less dense nonwetting phase to move up until it reaches the capillary barrier and gets trapped.

**Step 1: Packing the experimental apparatus.** Packing procedure is similar to the step listed in Section 3.7.1. Beads of different sizes were placed in sequenced layer to achieve desired patterns of homogeneity or heterogeneity. Once the "envelope" is completely filled with beads, the top cap is then positioned and secured.

**Step 2: Saturate with the aqueous phase.** The fluid flow system at the bottom is connected to an aqueous phase reservoir, placed on a small table behind the experimental apparatus. To initiate aqueous phase flow into the bead pack, the aqueous reservoir valve is opened then the valves at the bottom of the envelope are opened. Flow into the bead pack is gravity driven. Time to reach complete saturation varied from minutes to several

hours according to grain size, and the height of the aqueous reservoir. Air is displaced via the ports from the top.

**Step 3: Inject the hydrocarbon phase (drainage).** The aqueous phase reservoir connected to the bottom is replaced by a hydrocarbon phase reservoir. So this red-dyed nonwetting hydrocarbon phase is then introduced into the domain from the bottom four ports, by gravity feed; at the same time the displaced aqueous phase leaves the system through the top valves and gets collected in a measuring cylinder via a tube. The hydrocarbon non-wetting phase will build up beneath the capillary barrier till a predetermined volume. The volume of hydrocarbon injected should equal to the volume of aqueous phase displaced (collected in the measuring cylinder). The subsequent fluid displacement will be physically analogous to the rise of $CO_2$ non-wetting phase in a saline aquifer as water displaced to fill the other spaces.

**Step 4: Maintain / manipulate the pressure boundary conditions.** All valves and ports remained open. The hydrocarbon reservoir connected to the bottom of the domain is then replaced by an aqueous reservoir, whose liquid level is at the same height as the top of the domain to maintain a hydrostatic pressure gradient across the system. Positions of the aqueous reservoir can be raised to increase the hydraulic potential gradient, and consequently the capillary pressure gradient across the system. Depending on the accumulated oil column height, the capillary pressure against the barrier is changing. Once the capillary pressure exerted by the oil column exceeds the entry pressure of the capillary barrier, oil invades the barrier and escaped from the system.

## 3.8 Types of experimental domains

Several types of homogeneous and heterogeneous domains were examined. Theoretically, the rising non-wetting phase should accumulate at a boundary between

regions of different bead sizes (if and only if the smaller beads are in the higher elevation region) until the height of the continuous oil column below the boundary imposes a capillary pressure equal to the entry pressure of the smaller beads in the region above the boundary. If more oil joins this column from below and thus increases the continuous column height, oil will leak through the boundary until the column height decreases to the critical height. The oil that remains below the boundary is an example of the local capillary trapping phenomenon.

Table 3.5 below summarizes the characteristics of the different experimental domains used in this research and their objectives.

| Exp | Beads Diameter (mm) | Domain Description | Objectives | Observation / Summary |
|---|---|---|---|---|
| 1 | 0.5, 2, 3, 5 | Patchy<br>(closed system) | Influence of heterogeneity on LCT (closed system) | Accumulated oil column applies a $P_c$ that cannot exceed the $P_{c\_entry}$ of top seal. LCT trapping is permanent. |
| 2 | 0.045 sand, 0.25, 0.5, 2, 3, 5 | Layered<br>(closed system) | Influence of increased lateral length on LCT (closed system) | Maximum lateral correlation maximizes trapping. All the oil gets trapped in the closed system. Trapped oil column cannot escape the 0.25 mm seal because its applied $P_c$ is less than $P_{c\_entry}$ of seal. |
| 3 | 0.25, 0.5, 2, 3, 5 | Patchy/ Layered<br>(closed system), aqueous resvr raised to 84 cm higher than top of domain (open) | Persistence of LCT, forced imbibition | Increase lateral correlation increases trapping. Bead pack boundaries serve as preferential flow paths for rising fluids. Residual trapping is obvious, some LCT persisted after 10X increase in applied hydraulic gradient. |
| 4 | 0.25, 0.5 | Layered, Syncline seal, aqueous reservoir same level at the top, oil reservoir on floor. | | Syncline seal combined with corner effect allowed some escape of trapped oil. LCT seal hold 90% of oil predicted. Via corner artifact the system lost much of the trapped oil under forced imbibition. |
| **5** | 0.25, 0.5 | Layered, anticline seal,<br>fracture in seal, both reservoirs at the same level as the top. | Persistence of LCT, influence of fracture in seal. | Fracture in the seal serves as the preferential flow paths for rising oil. |

Table 3.5 (continues to next page)

(Table 3.5 continued from previous page)

| | | | | |
|---|---|---|---|---|
| 6 | 0.25, 0.5, 2 | Layered anticline seal, switching at long time from closed state to open state with hydrostatic potential boundary condition | Persistence of LCT, influence of shape of seal. | Long settling time made corner effect obvious. Thick 2 mm layer "stored" much oil which escaped from seal and should have been displaced out. |
| **7** | 0.25, 0.5, 2 | Layered anticline seal, switching at short time from closed state to open state with hydrostatic potential boundary condition | | Short settling time reduces corner effect in the time frame of the experiment. Both reservoirs at the same level as the top. Permanence of LCT. |
| 8 | 0.25, 0.5, 2 | Anticline seal, closed state first, then open state when rising oil reached seal, influence of edge effect obvious | | Corner effect is obvious. Local heterogeneity in the "store" section of the domain. |
| **9** | 0.25, 0.5, 2 | Anticline seal, open state for hydrostatic pressure gradient. Raising the aqueous reservoir gradually. | Persistence of LCT, threshold of breakthrough $P_c$. | Threshold escape pressure of oil from experiment is in agreement with the calculation. Corner effect is reduced. |
| **10** | 0.25, 0.5, 2 | Multiple anticline seal, fill and spill, open state, point source, artificial fracture in the seal | Persistence of LCT when the caprock is fractured. | Locally trapped non-wetting phase remain secure even when there is a fracture induced in close proximity in the caprock. Leakage in one part of the caprock does not affect the adjacent traps. |

Table 3.5: Summary of different experimental domains studied in this work.

## Chapter 4 Results and Discussion

This chapter presents a series of experiments in which porous media heterogeneity is varied. Hydrophilic silica beads with different sizes were used to create different heterogeneous patterns, through which the nonwetting oil phase representing the $scCO_2$ migrates and gets trapped by the capillary barriers.

Main observations from those experiments suggest that, when managed properly, almost all of injected nonwetting phase was immobilized locally by the capillary traps present in the heterogeneous porous media. Results show that the total nonwetting phase immobilized by local capillary trapping (LCT) mechanism in an open domain with hydrostatic pressure boundary condition could remain indefinitely.

Moreover the results demonstrate that local capillary trapping mechanism is persistent when the hydraulic potential is increased for the open boundary condition domain. This has huge and positive impact on the safety and security for storage.

In the following sections, each section header includes bead sizes and qualitative description of heterogeneity and boundary conditions, followed by a brief statement of objective of that particular experiment. For each experiment, the results are shown in time lapse series, to provide the reader a better understanding of the actual migration pathway of the fluids in the heterogeneous porous media.

In the text of this section, “seal” generally implies a continuous lateral region of small (fine) beads and “reservoir” or “store” implies a region of large (coarse) beads below the “seal”.

**Experiment 1**

**(0.5 mm, 2 mm, 3 mm and 5 mm, patchy, closed system)**

**Objective: demonstrate accumulation of buoyant phase in local capillary traps**

Four types of silica beads of different sizes are present in this packing in regions indicated in Figure 4.1 below; the darker colored beads are 0.5 mm in size while the lighter colored beads are 2 mm, 3 mm and 5 mm in diameter. The "patches" of larger-bead regions beneath 0.5 mm beads are expected to act as local capillary traps for the nonwetting phase as it rises from its initial emplacement at the bottom of the domain.

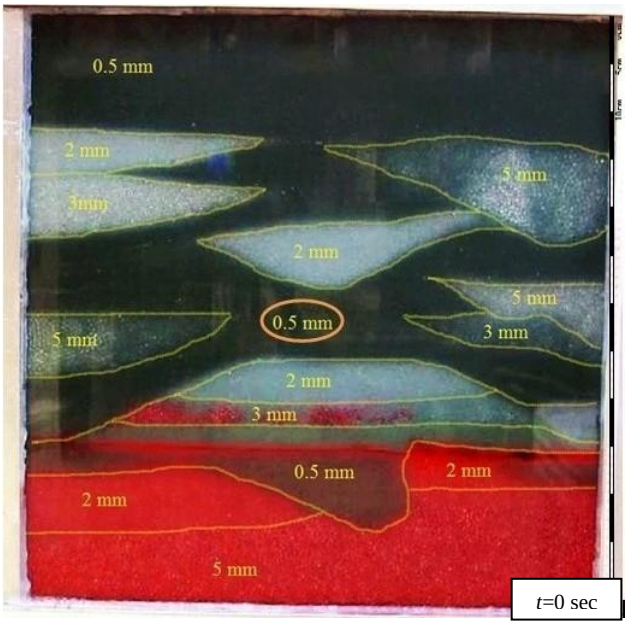


Figure 4.1: Initial condition of experiment in a heterogeneous domain with region boundaries outlined in yellow. Less dense non-wetting hydrocarbon phase (red-dyed) is about to rise and the denser wetting aqueous phase is to fall simultaneously.

Figure 4.2 below shows a timed sequence of the buoyancy-driven countercurrent migration of the two immiscible fluids in a closed-boundary heterogeneous porous medium.

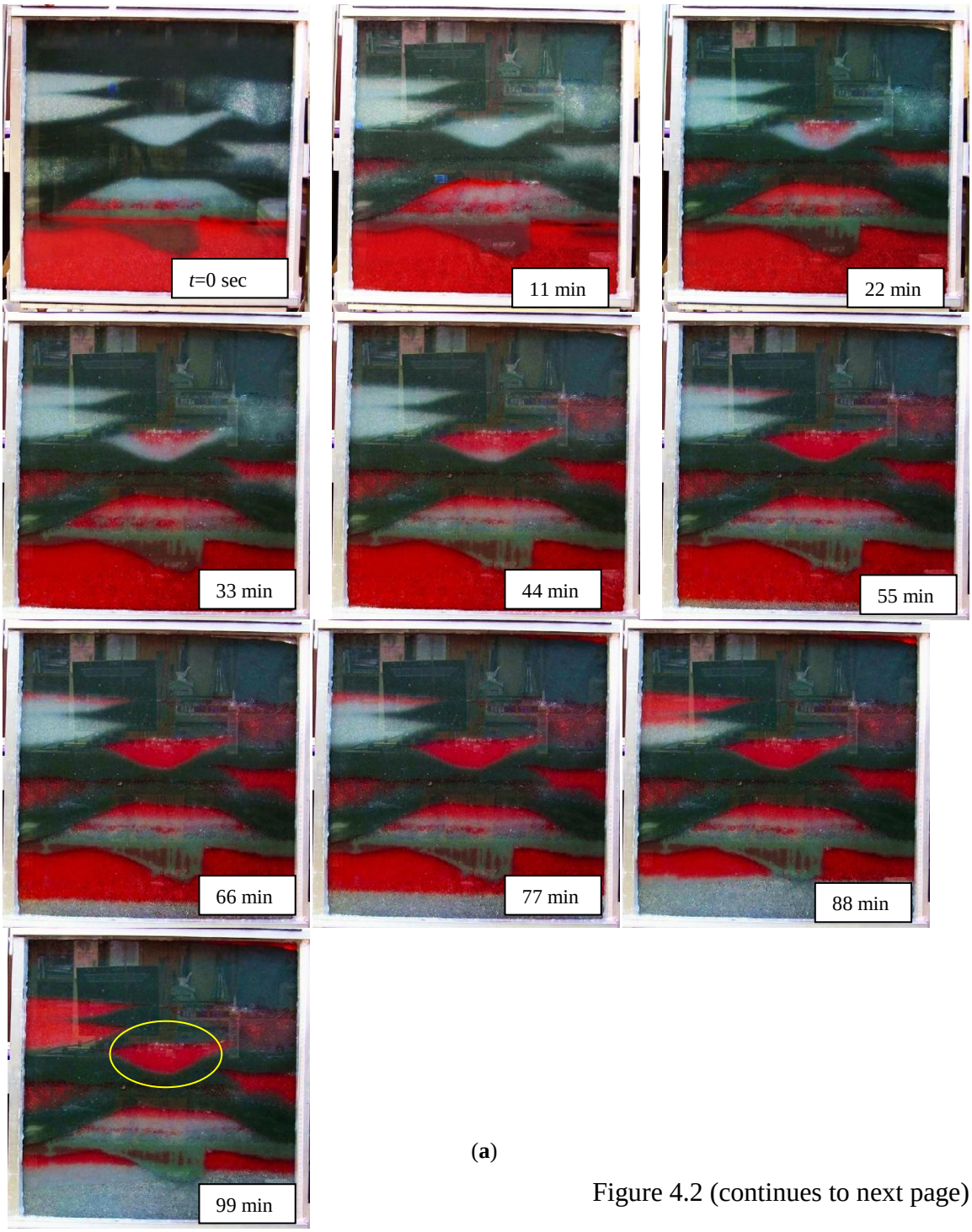


(**a**)

Figure 4.2 (continues to next page)

(Figure 4.2 continued)

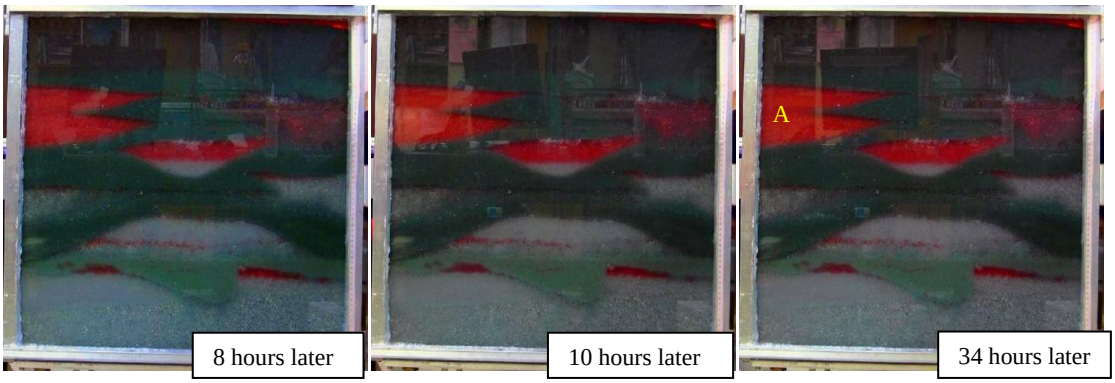


(**b**)

Figure 4.2: The sequence of snapshots chronicling the oil movement over a series of several hours, with 11 minutes interval for each snapshot in (**a**), and hours interval in (**b**). Initially the hydrocarbon movement appears to prefer one preferential flow path (circled section in (a)). The total movement is fast at the beginning, and then slowed down. The most interesting observation is the accumulation of the oil at the boundary of the bead sizes.

In this experiment, the rise of hydrocarbon phase was fast for the first 100 seconds after flipping (the start of the experiment), then the migration slows down as the rising front encounters the region of 0.5 mm beads (circled in Figure 4.1). It took 56 minutes for the hydrocarbon front to pass through entire domain and reach the top. It took about 150 minutes for the migration of fluids to stop.

The corresponding capillary pressures at the top of each oil column are smaller than the entry pressure of the capillary barrier above, as expected. For example, Area A in Figure 4.2 (b) above has an accumulated nonwetting phase column height of about 12 cm beneath the 0.5 mm bead layer. The column will exert $P_c = \Delta\rho gh$ =360 kg/m$^3$ × 9.81 N/kg × 0.12 m = 852 Pa, which is smaller than the entry pressure of the 0.5 mm barrier of 887 Pa (see Table 3.4 from Chapter 3 of this thesis).

After the migration of the red-dyed nonwetting phase stopped completely, the experiment domain was allowed to sit for a long enough period of time to make sure the trapped nonwetting phase stays in the trap permanently. A final snapshot was shown in the following Figure 4.3.

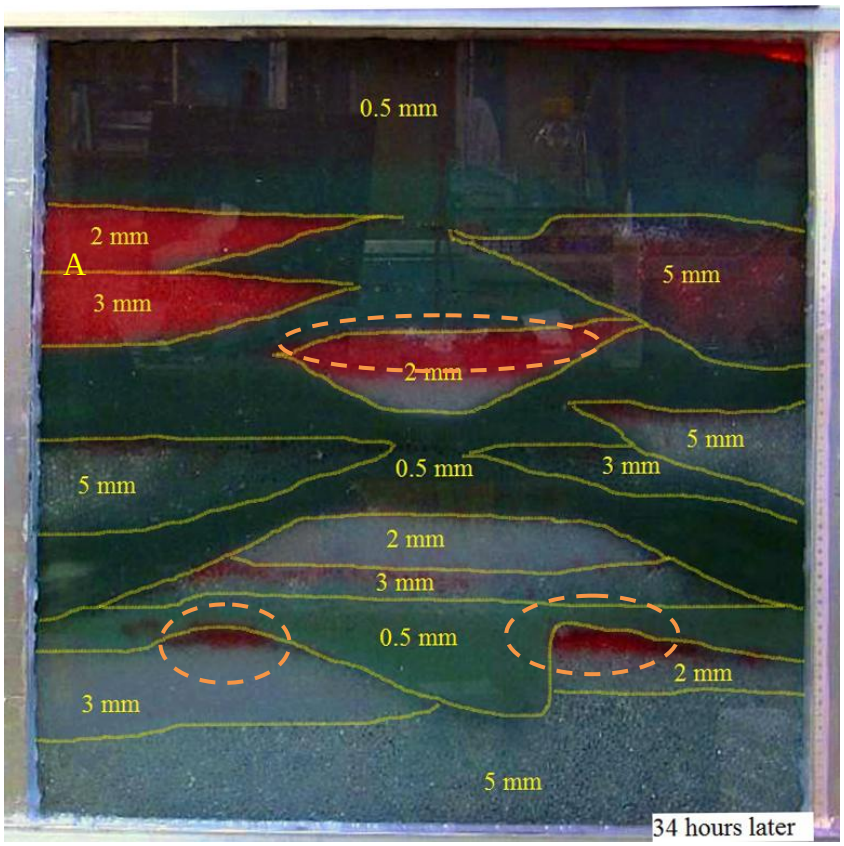


Figure 4.3: Oil migration almost completely stopped 3 hours after the experimental began. Oil has been trapped in coarse bead regions below boundaries with regions of sufficiently smaller beads. The circled sections appear to be where Local Capillary Trapping occurs. The configuration shown here from 34 hour is unchanged from the 3 hour observation. The circled sections illustrate local capillary trapping of nonwetting phase beneath boundaries of regions of smaller beads above larger beads.

Figure 4.3 shows that 34 hours after the flipping, the fluids remained at the same position as they did at the end of 3 hours; this confirmed that the oil accumulated at circled regions was trapped locally and permanently by the capillary barriers.

Previous work (Hernandez 2011) suggested that the 0.5 mm beads may serve as an effective capillary barrier in this experiment. Nonetheless, a significant amount of oil migrated to the top of the domain (darker portion in the topmost section of 0.5 mm beads, Figure 4.3). The 0.5 mm beads can hold, in theory, a 25 cm oil column, if the beads are uniformly and tightly packed. In area A (top left in Figure 4.3), however, the observed oil column height is half the theoretical value. This is because the entry pressure is smaller at the walls of the apparatus. The pores formed between beads and the walls at the left and right sides of the apparatus (where side wall meets front wall and back wall) are about twice the size of pores between beads. The hydrocarbon phase migrated along the side walls into the uppermost portion of the porous medium, establishing sufficient column height to backfill that part of the medium.

The results from this experiment offer promising and interesting insight. A geologic change to a finer grain size serves as a barrier to fluid flow; as explained in previous section, this is a result of capillary entry pressure. Finer grains create smaller pore sizes which result in higher capillary entry pressures. Nonwetting fluid cannot enter into the finer grain medium until the capillary entry pressure is exceeded. Thus a temporary barrier is formed; whether fluid held by this barrier can subsequently escape is an important characteristics of "local capillary trapping" (Saadatpoor 2009).

**Experiment 2**

**(0.045 mm, 0.25 mm, 0.5 mm, 2 mm, 3 mm and 5 mm, layered, closed system)**

**Objective: demonstrate extent of LCT beneath laterally extensive barriers**

This experiment examines LCT beneath laterally extensive barriers. From Figure 4.4 below, when hydrocarbon phase rises from a coarser beads region to a finer beads region, the increasing entry pressure is sufficient to act as an barrier to hinder the flow temporarily, but insufficient to stop the flow. This causes the temporary build up of large saturations beneath each region. The overall migration of the oil phase is fast through the 5 mm, 3 mm and 2 mm region, but slows down in the 0.5 mm region, and completely stopped by the 0.25 mm layer. Figure 4.4 shows the beginning of the experiment.

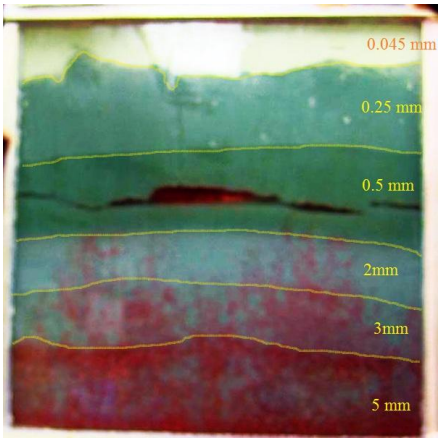


Figure 4.4: 4 seconds after the apparatus is flipped. Channeling of nonwetting phase is evident in the 5 mm, 3 mm and 2 mm regions. The cavities in the 0.5 mm region are artifacts due to the settling of the beads. Hydrocarbon phase (red) rises through a brine/glycerol mixture (1084 kg/m$^3$ and 7 cP) saturated domain of hydrophilic (silica) beads. The beads vary in diameter, packed into a quasi-2D domain (2 ft by 2 ft by 0.04 ft). Several preferential flow paths are observed. The cause is most likely non uniform packing.

Figure 4.5 below shows the timed sequence for the migration of nonwetting phase through the experiment domain.

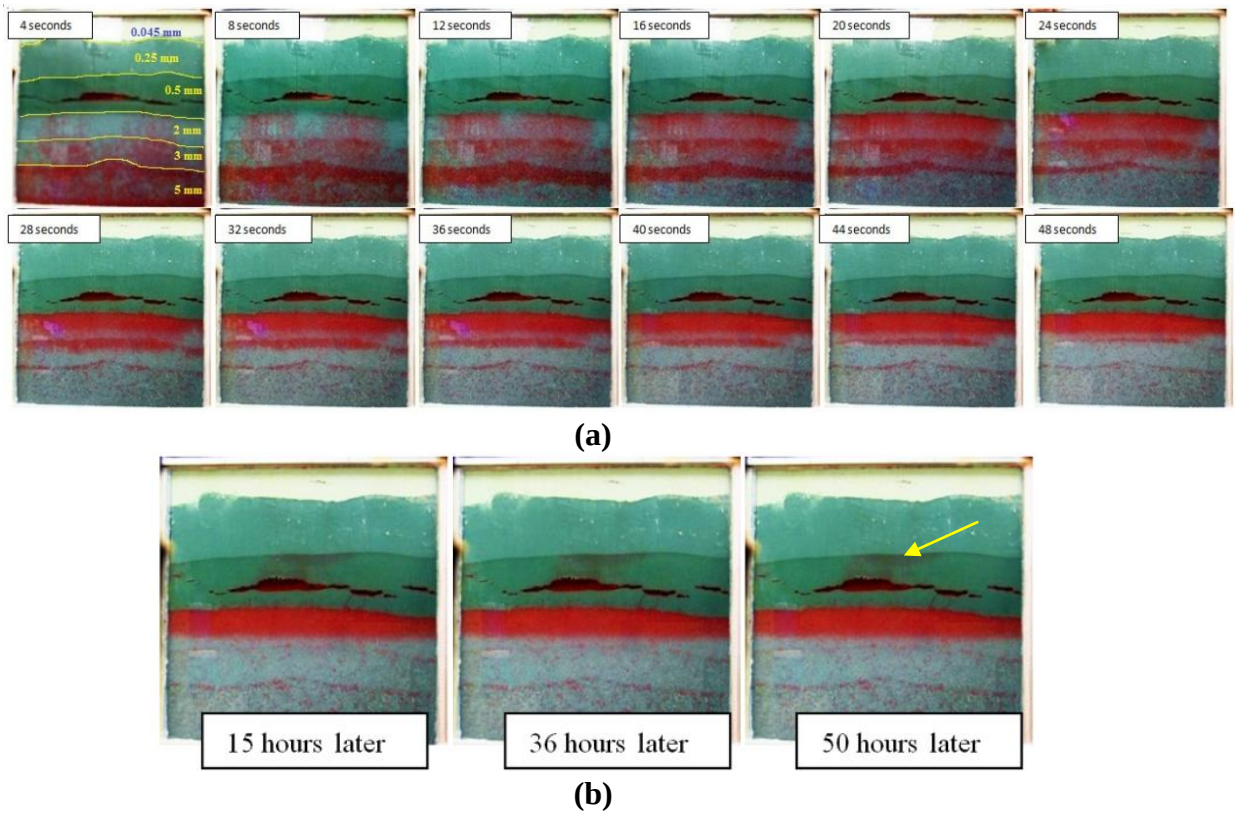


Figure 4.5: Timed sequence of images of Experiment 2. (**a**) First 48 seconds of the experiment. The cavities in the 0.5 mm region are formed by settling of the beads after apparatus was flipped at time zero. Several preferential migration paths are evident, likely due to heterogeneities introduced during settling; (**b**) Long time equilibrium states.

The system was nearly stabilized after 4 hours. Most of the hydrocarbon phase was trapped at the boundary between 2 mm and 0.5 mm layers. Over the course of two days, hydrocarbon migrated through the 0.5 mm beads to the boundary with 0.25 mm beads (see yellow arrow in Figure 4.5(b)).

Accumulation of oil at the boundary between 2 mm and 0.5 mm has an average column height of approximately 6 cm, corresponding to a capillary pressure of 212

Pascal, which is smaller than the entry pressure of 0.5 mm bead pack (667 Pa), as well as the entry pressure of 0.25 mm bead pack (1334 Pa). Oil entered cavities that formed in the 0.5 mm layer after the apparatus was flipped, and stayed there throughout the entire experiment period. The movement of beads that caused the cavities also created defects suggestive of shear bands, which evidently have a smaller entry pressure than the beads, especially where the defects contact the front wall of the apparatus. Oil migrated along these defects to the cavities.

Take a closer look at the last snapshot of the equilibrium state, as shown in the following Figure 4.6.

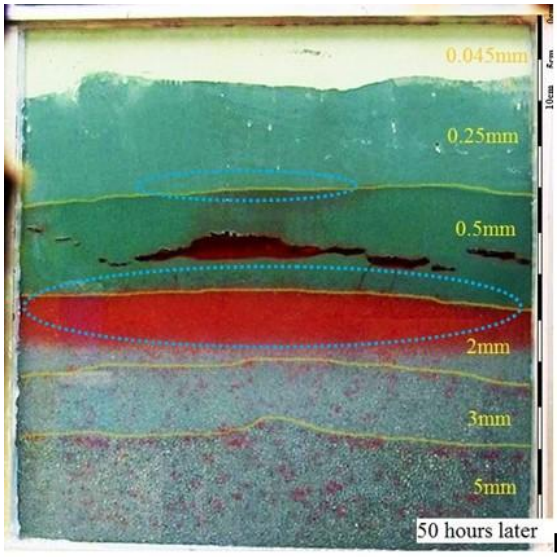


Figure 4.6: The circled sections illustrate local capillary trapping beneath boundaries where smaller beads lie above larger beads. Long lateral extent boundary provides a good trapping capability.

Migration also occurred to the 0.25 mm/0.5 mm boundary, apparently from the cavity in center of layer through the larger pores at the bead/front wall boundary. However, the oil column did not exert a capillary force that is greater than the entry pressure for the 0.25 mm bead pack and its boundaries.

Because 0.25 mm bead pack serves as a seal, the accumulation of oil beneath the 0.5 mm bead layer cannot be unequivocally attributed to local capillary trapping. That is, the oil in the 2 mm bead layer may be there only because the top of the oil column can migrate no further. If the seal at the 0.25 mm layer were compromised, some of the oil currently in the 2 mm layer may leak into the upper layers. The next experiment illustrates a method to test apparent local trapping for permanence, i.e. for being truly trapped locally.

**Experiment 3**

**(0.25 mm, 0.5 mm, 2 mm, 3 mm and 5 mm, patchy and layered heterogeneous domain – closed counter current displacement)**

**Objective: demonstrate persistence of LCT under forced imbibition**

*Part 1 closed system:*

The porous medium in the third experiment was a hybrid of layers and regions of different bead sizes. The counter-current displacement of the two phases was initiated as in the previous experiments. After 30 hours, local capillary trapping is observed at various spots in the system, where buoyancy driven uprising oil has accumulated beneath the region of higher capillary entry pressure (see Figure 4.7 below).

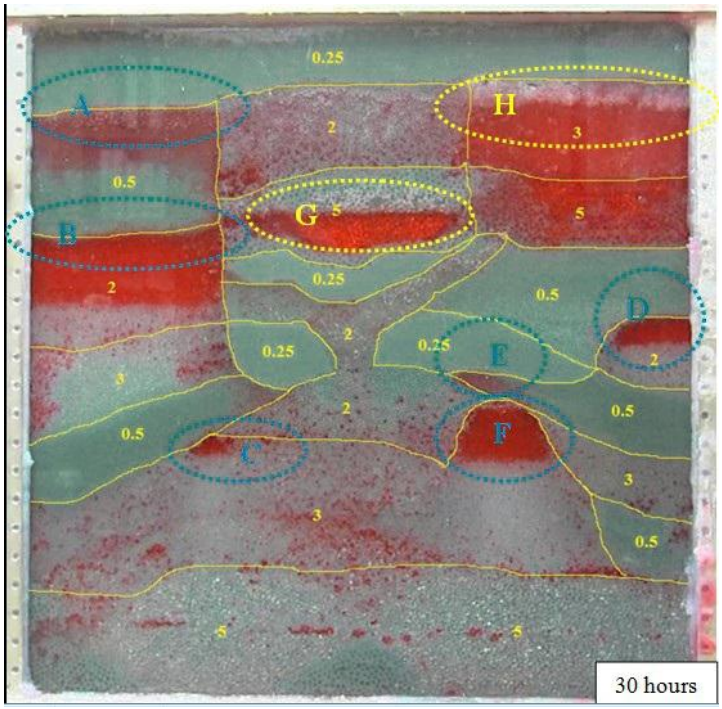


Figure 4.7: Nonwetting phase migration stopped within 30 hours after Experiment 3 began. The circled sections illustrate local capillary trapping of nonwetting phase beneath boundaries of regions of smaller beads above larger beads. Shorter lateral extent boundaries provide less trapping capability, compared to Figure 4.6. Numbers indicate bead sizes in mm.

The aqueous hydrostatic pressure gradient across the domain is $\rho_w g$ = 1084 kg/m$^3$×9.81 N/m = 10.6 kPa/m and oil hydrostatic pressure gradient is $\rho_{nw} g$ = 724 kg/m$^3$×9.81 N/m = 7.1 kPa/m. The system is at a closed state, which has a capillary pressure gradient of 10.6-7.1 = 3.5 kPa/m across the domain, such that the denser aqueous phase falls down and less dense oil phase moves up (counter current displacement) and finally reaches equilibrium. At equilibrium, the capillary pressure at top of an accumulated oil column is less than or equal to capillary entry pressure of beads above the oil column. The capillary pressure exerted by an oil column is equal to $h_{oil\_column}$×3.5 kPa/m. For example, in Figure 4.7 region B, the oil column height is about 2.5 inches (0.0635 m), so the capillary pressure exerted by this oil column at its top is 0.0635 m×3.5 kPa/m = 222 Pa, which is less than the entry pressure of the 0.5 mm beads above (887 Pa, Table 3.4). Therefore accumulation occurs.

Late in this experiment, air entered the porous medium because of a leak on the lower right side of the apparatus. The air migrated to the upper portion of area G and H in Figure 4.7. Thus the trapping in area G and H involved a more complicated 3-phase interaction, not just the intended grain size variation as in Experiments 1 and 2. Nonwetting phase column heights are less than the nominal height that the corresponding bead layer could hold, consistent with edge effects at the walls of the domain controlling upward migration.

*Part 2: Forced imbibition of wetting phase from bottom*

After the migration of non-wetting phase stops (equilibrium was reached, Figure 4.7), top and bottom ports are opened and connected via Teflon tubings to reservoirs to impose a constant hydraulic potential across the domain. This enables, for example, forced imbibition of aqueous phase from the bottom, with accompanying displacement of fluids from the top. This procedure measures the permanence of local capillary traps established during the earlier buoyancy-only displacement. That is, any nonwetting phase held in some region of the beadpack only because of boundary conditions such as closed valves will be able to migrate, whereas nonwetting phase truly trapped by local capillary barriers will not. Figure 4.8 below depicts the schematics of the forced imbibition.

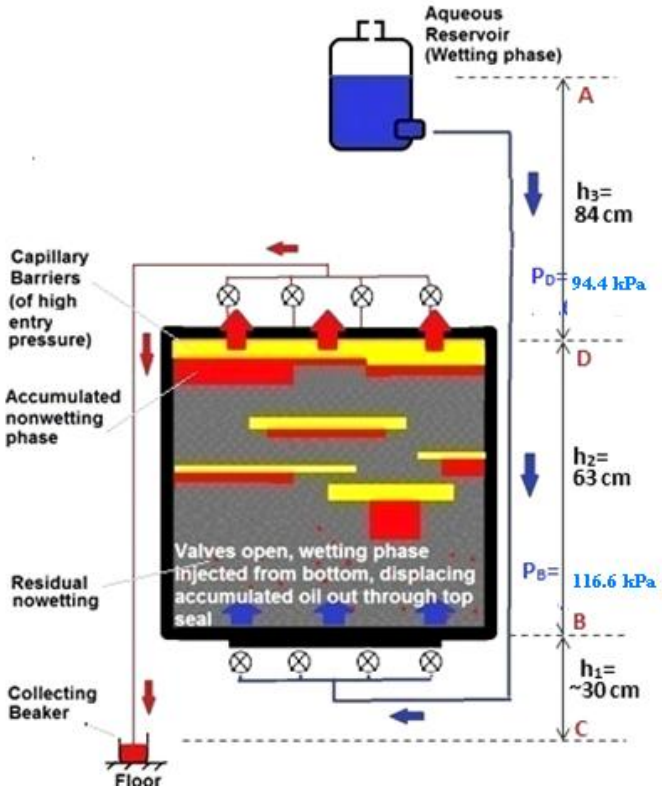


Figure 4.8: Schematics of forced imbibition of wetting phase from bottom. Valves at top and bottom are closed during the countercurrent movement of wetting and nonwetting phase, and after reaching steady state, the valves are opened to impose a prescribed hydraulic gradient across the domain.

After the valves are open, the aqueous reservoir provides a hydraulic potential difference across the domain. If the reservoir is positioned above the top of the domain, this hydraulic potential exceeds the original hydrostatic potential and thereby alters the capillary pressure gradient. For example, in this experiment the aqueous reservoir was positioned 84 cm higher than the top of the domain (Figure 4.8). The domain itself is 63 cm tall and is 30 cm above the floor. So the aqueous reservoir is 84 + 63 + 30 = 177 cm above the floor, and is open to atmosphere so $P_A$ = 101 kPa. Pressure at bottom of the domain, $P_B = P_A+(h_A-h_B)g\rho_w$ = 101 kPa+(177 cm -30 cm) ×9.81 N/m×1084 kg/m$^3$ = 116.6 kPa. The oil reservoir is placed at the floor and open to atmosphere, so $h_C$ = 0 and $P_C$ = 101 kPa. Similarly the pressure at the top of the domain is given by $P_D = P_C-(h_D-h_C)g\rho_{nw}$ = 101 kPa-(93 cm) ×9.81 N/m×724 kg/m$^3$ = 94.4 kPa. Therefore the pressure gradient in the water phase across the domain = (116.6 kPa – 94.4 kPa)/ 0.63 m = 35.3 kPa/m (this will cause upward flow of water through the domain since it exceeds the hydrostatic gradient for the aqueous phase which is 9.81 N/m × 1084 kg/m$^3$ = 10.6 kPa/m). The capillary pressure gradient within oil phase held motionless in a local capillary trap is the water pressure gradient less the oil hydrostatic gradient = 35.3 kPa/m – 7.1 kPa/m = 28.2 kPa/m. The accumulated oil column height multiplied with this capillary pressure gradient will give the capillary pressure exerted by the trapped oil column. For instance, the capillary pressure in a region of trapped oil that is 10 cm in height would be 2.8 kPa in the open system with these reservoir heights, much larger than its original value of 0.35 kPa in the closed system. Thus in addition to driving water through the domain (forced imbibition), this large increment of capillary pressure causes the locally held oil accumulations to exceed the seal capacity for most of local capillary trapping accumulations (see Table 3.4: capillary entry pressure of bead columns), and

most of local traps got disrupted and only short columns survived (except where the presence of air helped block the advance of the oil phase).

Fluids were displaced through the ports of the top fluid flow system. In the following 22 hours, 1000 ml aqueous phase and 375 ml of hydrocarbon phase were displaced. No more oil was displaced after 22 h. The local capillary trapping of oil phase stabilized, as shown in Figure 4.9. Despite the much larger capillary pressure gradient, some oil remained trapped; this is consistent with the basic principle of local capillary trapping, namely that it occurs when $P_c$ at top of oil column is less that $P_{c,entry}$ of porous medium above oil column. Figure 4.9 below shows the equilibrium state for open boundary forced imbibition.

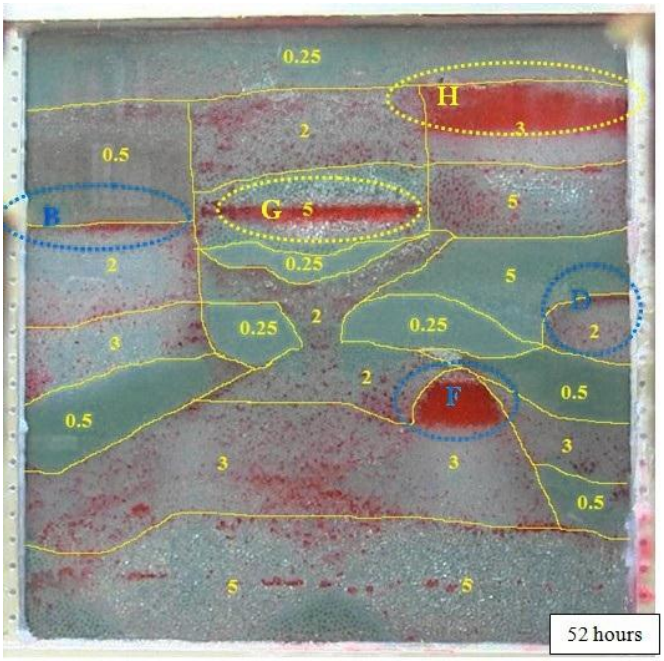


Figure 4.9: Oil migration stopped within 22 hours after boundaries were opened and a hydraulic pressure was applied to the stabilized configuration at 30 hours. The circled sections illustrate local capillary trapping that persists even during forced imbibition, which induces a larger capillary pressure in the oil phase. Inset gives elapsed time since start of buoyancy-driven displacement in closed system.

As explained before, the amount of oil held beneath the capillary barrier depends on the relationship between oil column height and $P_c$. The increased capillary pressure of most oil columns during forced imbibition causes most of the oil trapped at closed, hydrostatic conditions to flow out of the domain (Figure 4.9 compare to Figure 4.8). However, about 2 inches of accumulated oil still survived in Region H of Figure 4.9. The capillary pressure exerted by this remaining oil column = 5.08 cm × 28.2 kPa/m = 1432 Pa, which is still less than the entry pressure of 0.25 mm beads (1735 Pa, Table 3.4). This is consistent to the expectation and demonstrates that LCT can persist after a large increment of capillary pressure, though the mass of buoyant phase trapped necessarily decreases.

Local capillary trapping holds buoyant phase below a capillary barrier, so theoretically it should be possible to move a large amount of nonwetting fluid from local capillary traps if the $P_c$ is large enough (exactly what happened here). But even at the much larger $P_c$ gradient, short columns of oil are still held in region B, D, F, G, and H, proving the persistence of local capillary trapping even with a significant amount of external force. It is also possible that the vertical boundaries between bead patches of different sizes served as preferential flow paths for the migration of rising liquids. In region B of Figure 4.8 and Figure 4.9, accumulated oil in the 2 mm bead layer did not penetrate the 0.5 mm bead layer when the forced imbibition was applied. Instead the oil migrated upwards along the vertical boundary of the two bead patches. The entry pressure of the vertical boundary between different bead patches is smaller than the bead patch itself, due to non-uniform contact of different sized beads, leaving larger inter-granular spaces. Therefore the rising nonwetting phase finds it easier to enter those spaces and flow along the vertical boundary with assistance from buoyancy.

**Findings from experiment 1, 2 and 3**

The buoyancy driven migration path of the non-wetting phase is significantly influenced by the heterogeneity of the domain. Experiments show that the uprising oil plume will selectively fill up the regions with smaller capillary entry pressure (coarser bead patches) first, and accumulate beneath the capillary barrier formed by a region of smaller beads. Migration of buoyant phase through the barrier occurs when the phase column height times the capillary pressure gradient exceeds the entry pressure of the smaller beads, or the entry pressure of defects within the packing (e.g. caused when regions of beads settle after rotating the apparatus). Migration past a barrier can occur when the phase column height exceeds the entry pressure of the boundary between porous medium and wall of apparatus, which is smaller than the entry pressure of a region filled with beads (no edge effect).

Orientation of boundaries between regions affects the local trapping behavior (compare Figure 4.6 and Figure 4.7). Lateral boundaries serve as good barriers, while vertical bead boundaries serve as a connection between trapped regions and became the preferential paths for migrating flows. The observations validate predictions (Saadatpoor 2012) that increasing lateral correlation will yield more local trapping, while increasing vertical correlation will cause less local trapping. Experiment 2 (Figure 4.6) has the longest correlation length, and therefore the capillary barrier trapped most of the nonwetting phase. Experiment 1 (Figure 4.3) and Experiment 3 (Figure 4.7) have longer vertical correlation length than Experiment 2, and thus less nonwetting phase was trapped.

Because continuity of the non-wetting phase column along defects and walls can be difficult to discern, some observed accumulations of non-wetting phase cannot be unequivocally attributed to local capillary trapping. It could be the case that oil formed a

continuous path all the way to the top of the domain and stopped flowing only because the ports at the top of the domain were closed. In other words, the valves at the top of the domain were acting as a “sealing formation” rather than regions of smaller beads in the domain. To test this idea, the boundaries of the apparatus were opened after reaching steady state and a constant hydraulic gradient much larger than hydrostatic was imposed. A significant fraction of the hydrocarbon was displaced, but a substantial amount remained in the accumulations. This indicates that this trapping mechanism is indeed a capillary phenomenon.

**Experiment 4**

**(0.25 mm and 0.5 mm, layered heterogeneous domain)**

**Objective: demonstrate extent of LCT under a syncline-shaped seal with hydrostatic potential gradient followed by forced imbibition**

*Part 1 closed system:*

The porous medium in the fourth experiment simply consists of only 2 types of beads: 0.25 mm and 0.5 mm. The 0.25 mm beads at the top of the domain form an effective seal. Dry packing was used in which the upper portion of the domain was initially dry when nonwetting phase was injected (compared to previous experiments where the entire domain was saturated with aqueous wetting phase first, injected nonwetting phase then displaces the wetting phase out), so that the entry of non-wetting phase into the top of the domain required air to be displaced simultaneously from valves at the top. This may facilitate trapping of air in the domain, and the clustering of beads at packing flaws. After the initial saturation, the closed boundary experiment started and is shown in the following Figure 4.10.

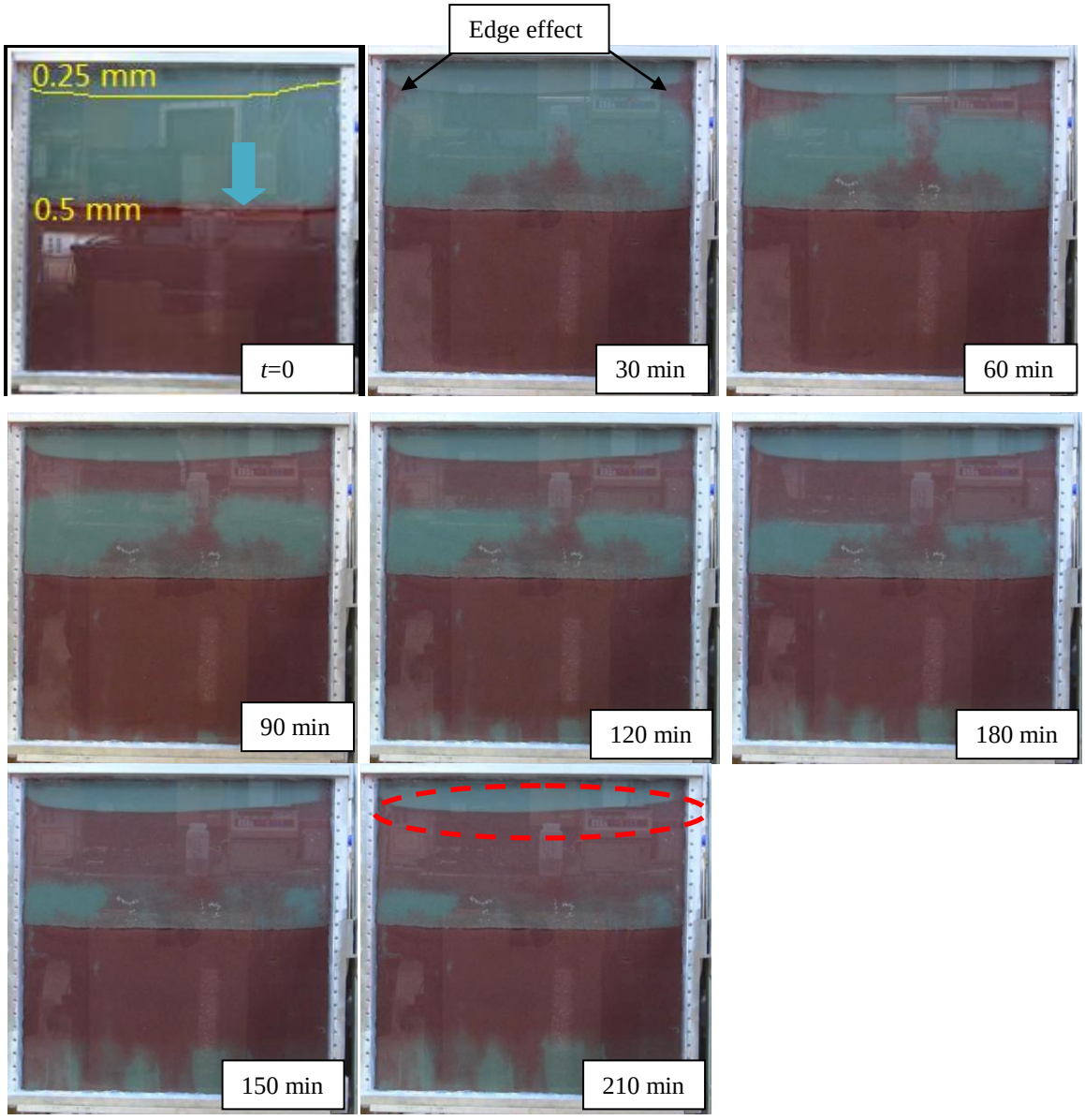


Figure 4.10: Photographs of first 3.5 hours of Experiment 4 (30 min interval). Oil was emplaced in bottom half of the domain, with initial oil phase/aqueous phase boundary (blue arrow pointing) within the 0.5 mm beads ($t$ = 0). Subsequent oil migration driven by buoyancy stopped within 24 hours. Most oil was trapped beneath the boundary of 0.25 mm beads. Additional migration through these beads occurred because of packing artifacts (edge effect, see text above). The red dashed circle indicates local capillary trapping phenomenon in a closed domain.

As shown in Figure 4.10 above, the oil migration in finer bead pack (0.5 mm) in this experiment exhibits less fingering than in previous experiments 1, 2 and 3, in which coarser beads (2 mm and 5 mm) were used. The plume rises in a relatively smooth front. The edge effect along the side wall, where beads meet the flat surfaces and the corner between them to form relatively large pores, is significant. Some oil "slipped" through the corners/edges of the apparatus which has smaller capillary entry pressure than the bead pack. This oil reaches the seal from the sides first (see frame at 30 min, arrows in Figure 4.10) and starts accumulating there. This is interesting because it means that the "edge effect" pores for the small beads, though larger than pores in the matrix of small beads, are still small enough to form a capillary barrier to the rising oil.

The boundary in the middle of the domain (blue arrow in Figure 4.10) was due to packing artifact, where the bottom half of the beads was saturated with oil (from dry fresh beads), and top half was saturated with water/glycerol (from dry fresh beads), resulting in a well-defined boundary (blue arrow in Figure 4.10, first frame). But the two distinct layers of oil are uniformly packed and considered connected, because there is no capillary barrier in the 0.5 mm layer.

The nonwetting fluid rests below the capillary barriers for over 10 days (245 hours) and migrates no farther (refer to Figure 4.11 below), suggesting that this configuration is stable, which proves that the 0.25 mm bead pack served as an effective capillary barrier (seal). No oil migrated through this capillary barrier, which is a strong evidence of local capillary trapping. $P_c$ exerted by the total 50 cm of oil column in the closed system = 0.5 m × 3.5 kPa/m = 1700 Pa, which is less than the entry pressure of 0.25 mm beads (1734 Pa, from Table 3.4).

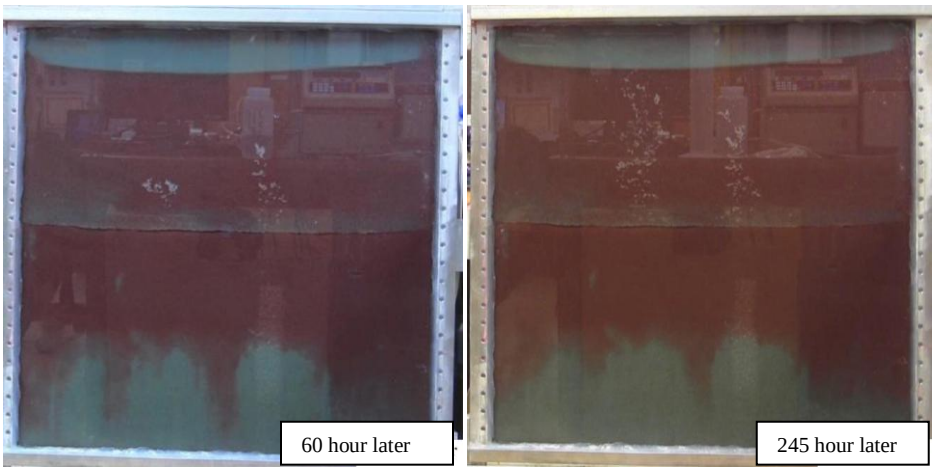


Figure 4.11: late time / final fluid distribution of experiment 4. No oil entered the 0.25 mm beads, consistent with predictions of local capillary trapping.

*Part 2 open boundary imbibition*

At the end of the 245 hours, the top and bottom boundary were opened, and wetting phase is allowed to flow into the system from the bottom ports. The aqueous reservoir liquid surface was kept at the same height as the top level of the domain, such that the hydraulic potential provided by the aqueous reservoir is zero, i.e. no change from the hydrostatic state in the closed domain. The oil reservoir is at floor level and connected to the top ports, therefore the pressure at the top of the domain (outlet) is lower than the aqueous phase hydrostatic pressure. The oil phase in the outlet tube is continuous to oil phase inside the domain, therefore by analysis similar to previous experiment, there is driving force for aqueous phase to enter bottom and flow out from top, along with any mobile not trapped oil. Figure 4.12 below shows the schematics and results for the open boundary imbibition, which proves the driving force for aqueous phase to enter bottom and flow out from top exits.

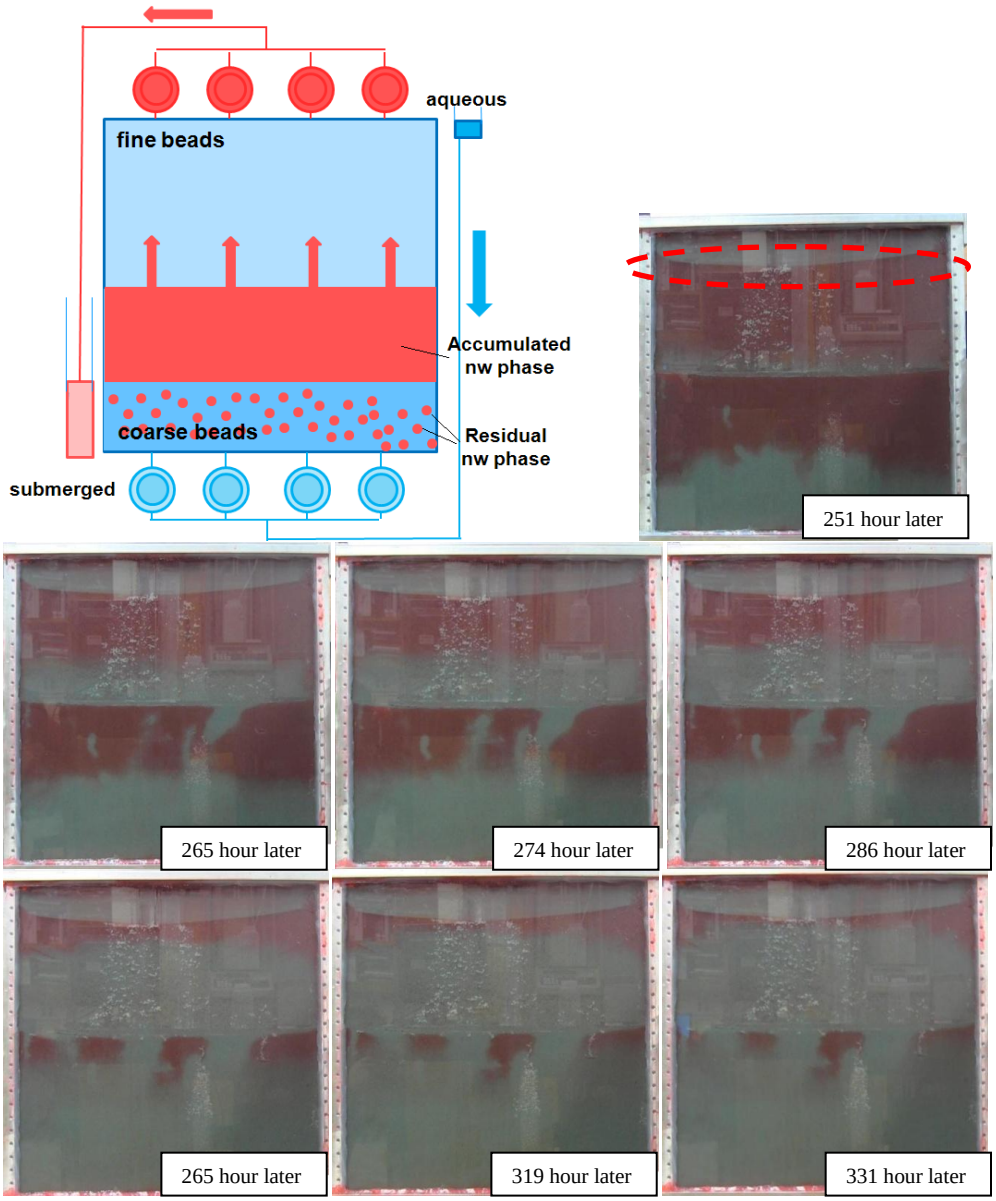


Figure 4.12: Snapshots of the open boundary imbibition of experiment 4. Insets give elapsed time since start of buoyancy-driven displacement in closed system.

Due to the density difference between oil phase in the system and aqueous phase in the aqueous reservoir, oil still got displaced out of the system from the top of the domain, until equilibrium was reached. The exit line was filled with oil. The entering

pressure at the bottom of the domain = 101 kPa + (93 cm – 30 cm) × 9.81 N/m × 1084 kg/$m^3$ = 107.7 kPa. The exit pressure at the top of the domain = 101 kPa – (93 cm) × 9.81 N/m × 724 kg/$m^3$ = 94.4 kPa. Capillary pressure gradient across the domain = (107.7 kPa – 94.4 kPa)/0.63 m – 7.1 kPa/m = 14.0 kPa/m (7.1 kPa/m is the oil hydrostatic pressure gradient).

In the next 80 hours of open boundary imbibition, most of oil escaped the trapped region (see Figure 4.12). Capillary pressure exerted by the 50 cm oil column at the new capillary pressure gradient = 0.5 m × 14 kPa/m = 7000 Pa, which is much greater than the entry pressure of 0.25 mm beads (1735 Pa). Therefore capillary barrier is no longer effective to hold a 50 cm column of oil. With the aid from edge effect and the syncline shape of the barrier, oil was continuously leaving the domain until the 331$^{st}$ hour, when the configuration became stable. However, a considerable amount of oil still gets trapped at the boundary at the top; this again demonstrates that local capillary trapping has a certain level of persistence even when capillary pressure gradients change from initial emplacement conditions. The much shorter oil column compared to the closed state is consistent with the much larger capillary pressure gradient.

**Experiment 5**

**(0.25 mm and 0.5 mm, layered, anticline-shaped seal, with fracture in the seal)**

**Objective: demonstrate persistence of LCT under influence of a fracture in the seal**

Experiment 5 is very similar to experiment 4. The major difference is the shape of the seal, an anticline, as opposed to the syncline-shape in experiment 4. A snapshot of the initial condition of experiment 5 was shown in Figure 4.13 below.

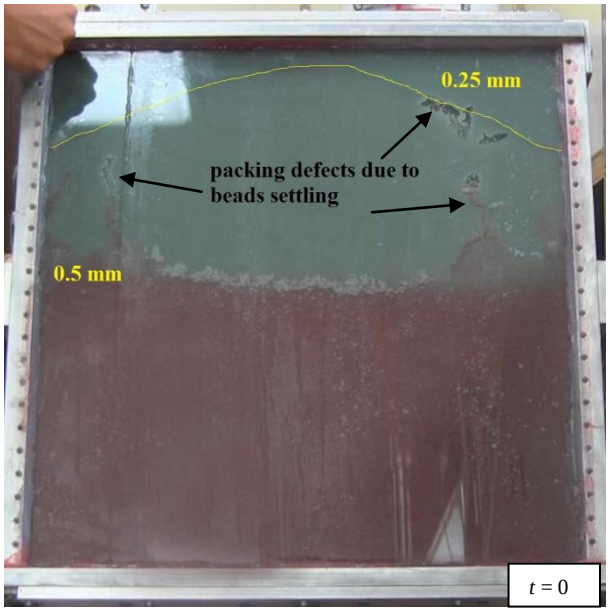


Figure 4.13: Initial condition of experiment 5.

The seal is a layer of fine beads (0.25 mm diameter) above the 0.5 mm beads which act as the storage formation. This time, instead of injecting oil into dry fresh beads, the entire domain was saturated with wetting phase first, such that the oil injected later will displace some aqueous wetting phase. Half of the domain was then filled with nonwetting hydrocarbon phase, displacing out equal volume of wetting phase. The beads settled during emplacement of initial wetting phase saturation. Upon flipping the apparatus 180 degrees (when Figure 4.13 was generated), a crack developed in the porous

media on the left hand side and cavities developed on the right hand side (indicated by arrows in the Figure 4.13), as the result of beads settlement. Upon flipping, less dense nonwetting phase quickly fills into the packing defects, as soon as the crack and cavities developed. Remaining nonwetting phase then starts to rise ($t$ = 0). In the photograph the apparatus is in a closed state.

*Part 1: Closed system.*

*Preparing initial condition*

After packing, two valves at the bottom were opened allow wetting phase to drain while non-wetting phase is directed via gravity into the domain through all 4 valves at the top. This creates a similar saturation and displacement environment as the actual storage aquifer where initially the entire formation is water-saturated and water wet, and then a nonwetting phase enters a portion of the formation, establishing its saturation by displacing wetting phase. This is an improvement to the previous experiment in reducing trapped air in the domain upon injection of wetting phase.

*Countercurrent buoyancy-driven displacement*

After establishing the initial state in Figure 4.13, the domain is flipped so that the less dense oil phase rises in the porous medium. All valves are closed, so that water descends in the medium as oil rises. As shown in Figure 4.14, the oil migration stops at the boundary between fine beads and coarse beads about 12 hours after beginning the experiments. The apparatus was left unaltered for another 10 days (240 hours), during which time no movement of oil was seen.


Figure 4.14: After the apparatus (Figure 4.13) is flipped, buoyancy-driven oil migration continued until oil gets trapped completely by the seal near the top of the domain. Yellow arrow (left panel) indicates the packing defect that is analogous to a fracture that would compromise the ability of the seal to contain buoyant fluid. Red arrow (right panel) indicates column height of oil phase held by the capillary entry pressure of the fine beads.

Almost all the oil gets trapped beneath the anticline shaped seal, even with a "crack" extending into the seal. The crack is visible in Figure 4.13 and Figure 4.14 as a dark streak within the fine-bead layer towards the top left part of the domain. It resulted from the settling of the saturated beads when the domain was flipped. Oil filled up the crack but could not enter the fine beads bounding the crack. The height of the accumulated oil column (as indicated by the double-headed arrow in right panel) is 28 cm, which corresponds to a capillary pressure of 824 Pa, which is smaller than 1334 Pa, the entry pressure of a matrix of 0.25 mm beads for these fluids.

This is a good indication that even if a defect developed in the seal, the storage is still safe, as long as the defect did not extend all the way through the seal, which in this experiment is the continuous lateral region of small beads.

Very little amount of oil "slipped" past the sealing formation via edge effects (smaller entry pressure where beads meet the side walls) to the top of the apparatus.

*Part 2: open boundary imbibition.*

At the 252$^{nd}$ hour, the valves connected to external fluid reservoirs were opened, such that the aqueous wetting phase reservoir is connected to the bottom of the domain while the nonwetting oil phase reservoir is connected with the top. Both reservoirs are open to atmosphere, and their liquid surfaces were at the same height as the system's top. Thus the gradient in potential in the aqueous phase within the domain remained unchanged from hydrostatic when the valves were opened. As shown in Figure 4.15 below, the position of the aqueous phase reservoir is chosen so that the aqueous phase potential at the bottom of the domain is the same whether measured through the aqueous phase domain or through the tubing connected to the reservoir. Though the gradient in potential in the aqueous phase does not change, the open valves now enable any immobilized oil due to boundary conditions (i.e. closed valves) from Part 1 to move. Oil that was immobilized during Part 1 because of local capillary trapping, on the other hand, should not move simply because the valves are open.

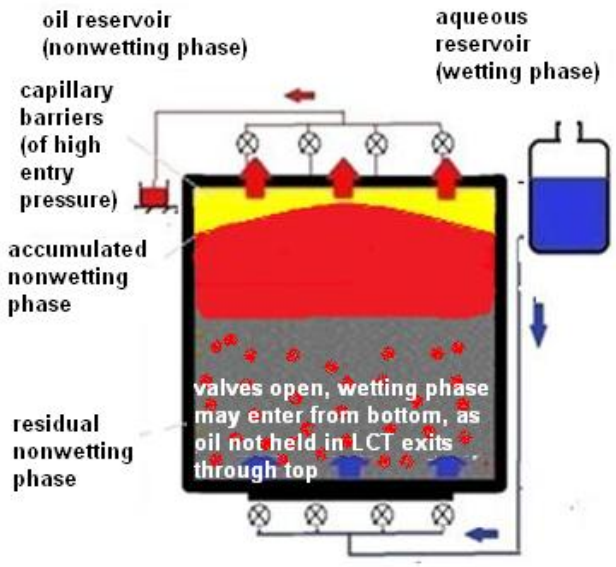


Figure 4.15: Open boundary portion of Experiment 5. The top and bottom valves are opened after buoyant migration ends in Part 1 of the experiment (see Figure 4.14). The liquid surfaces from both reservoirs are kept as the same height as the top of the system so that the hydraulic potential gradient in the domain does not change when the valves are opened. Any oil that was not immobilized by local capillary trapping during Part 1 can leave the domain through the open top valves.

The objective of this part of the experiment is to verify what would happen if the entire system becomes open. In Nature, the actual storage aquifer and the layers above and below it constitute an open system. The results are summarized in the following Figure 4.16.

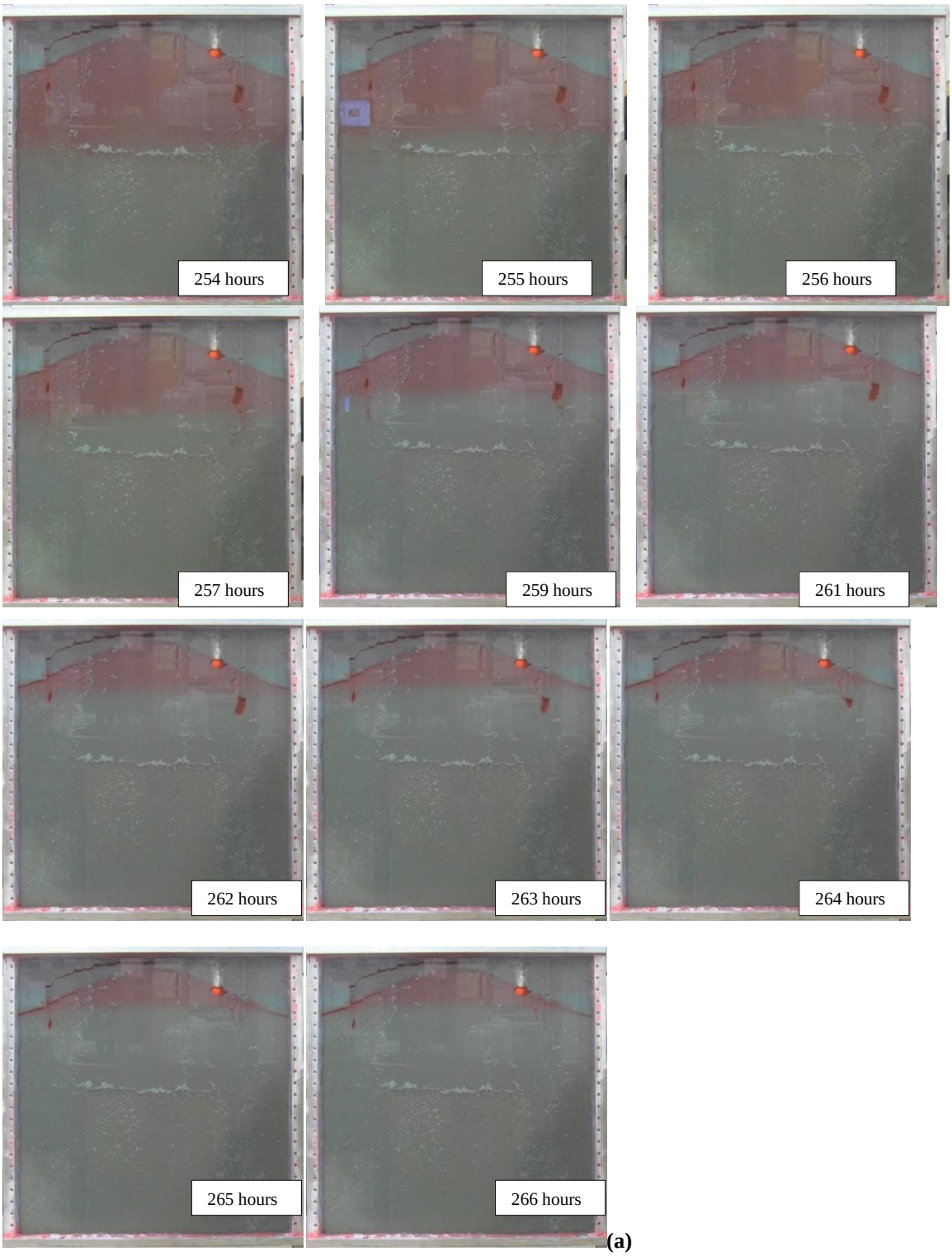


**(a)**

Figure 4.16 (continues to next page)

(Figure 4.16 continued)

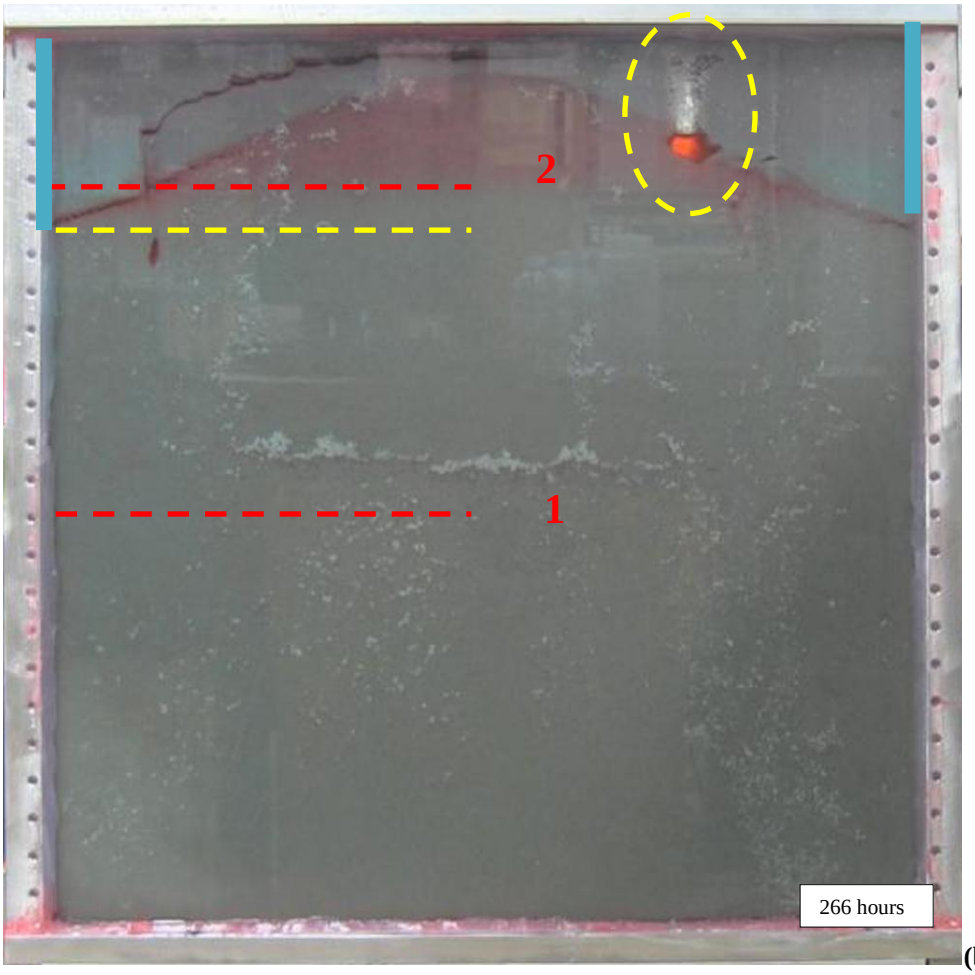


**(b)**

Figure 4.16: **(a)** snapshots of the open boundary imbibition of heterogeneous experiment with the anticline-shaped seal (experiment 5). **(b)** A closer look at the final stage of the open boundary imbibition when the system again reached equilibrium. Insets give elapsed time since start of buoyancy-driven displacement in closed system.

It took 12 hours for the system to re-equilibrate when it is switched from closed to open. Much of the oil phase that was immobile when boundaries were closed (Figure 4.14) leaves the domain through the open valves at the top. However the layer of fine beads was not invaded by any of this mobile oil (the region remains a translucent blue

throughout the experiment), and some of the oil held beneath the sealing layer remains in place.

Two factors contributed to the movement of the oil phase when the valves were opened. One is the artifact of the "corner effect", the second is the presence of a crack in the seal filled with fluid.

1. Corner effect. Beads pack much less tightly in the corners at the left and right sides of the domain (two vertical blue lines in Figure 4.16(b)). Consequently the capillary entry pressure into the upper part of the domain is significantly smaller at the corners. Thus the oil phase likely formed a connected path to the top of the domain along these corners during the closed-boundary buoyant migration (Part 1 of the experiment), though the oil was not able to drain into the layer of fine beads from the corners. When the system becomes open, oil can flow out the top along the corners. As long as oil in the 'storage formation' spans the width of the domain, that oil is connected to the corners, and leakage by this pathway can continue until the oil/water boundary reaches the level marked by the yellow dashed line in Figure 4.16. This is the level at which the coarse bead layer no longer extends across the entire width of the domain. The fact that some oil migration continues is discussed next in item (2).

We note that the connected path of oil in the corners effectively 'short-circuits' the capillary barrier of fine beads, and the fluid motion is controlled by basic hydrostatics. Due to density difference of the oil and aqueous phases, there should be spontaneous adjustment of liquids level to reestablish the equilibrium. This concept is summarized below in Figure 4.17.

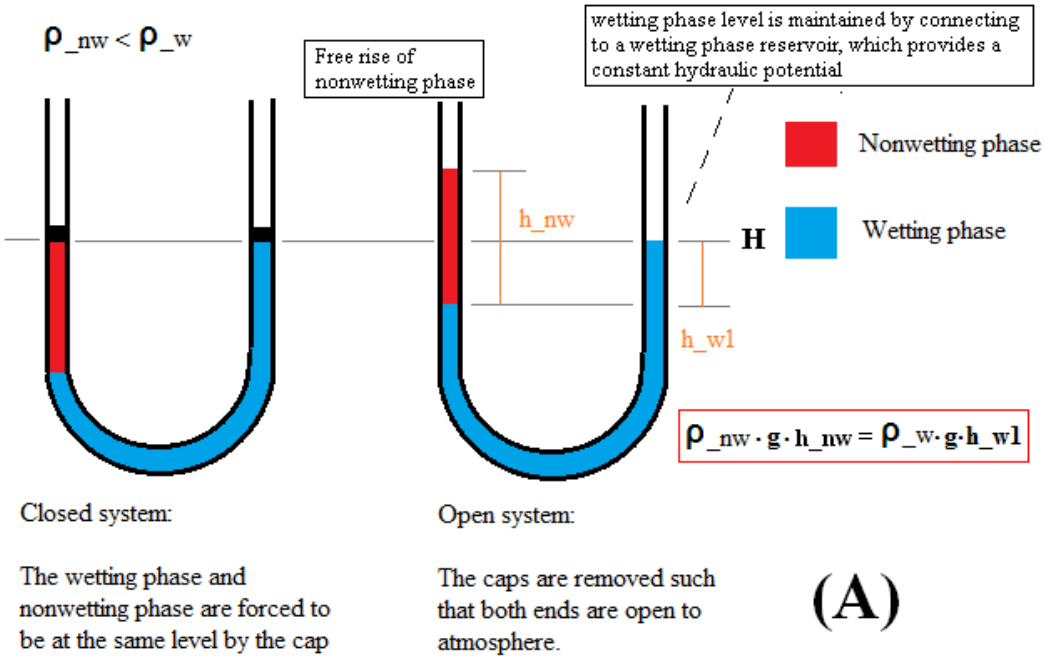


Closed system:

The wetting phase and nonwetting phase are forced to be at the same level by the cap

Open system:

The caps are removed such that both ends are open to atmosphere.

**(A)**

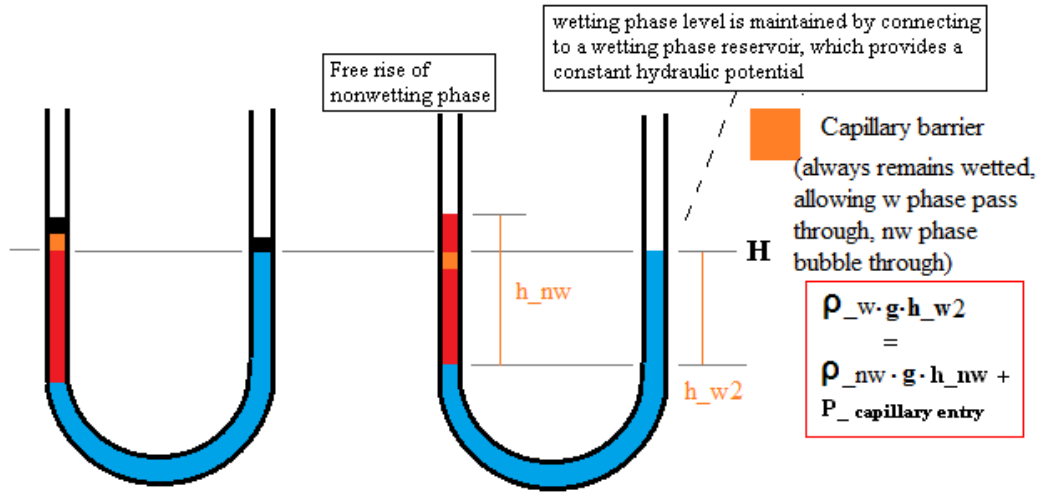


Closed system:

The wetting phase and nonwetting phase are forced to be at the same level by the cap

Open system (with capillary barrier) **(B)**

Caps are removed and each phases are open to atmosphere. The capillary barrier exerts a resistant force against the rising of the non-wetting phase, such that less non-wetting phase is displaced out above the reference height H.

Figure 4.17 (continues to next page)

Figure 4.17: **(A)** Re-equilibration of liquid columns in a U-tube when the system is switched from closed to open. The tube radius is large so capillarity is negligible. Due to density difference ($\rho_{nonwet}<\rho_{wet}$), in the open system, $\frac{\rho_{wet}}{\rho_{nonwet}} = \frac{h_{nonwet}}{h_{wet}}$. **(B)** With a porous medium inserted to act as a capillary barrier in one arm of the tube (orange), the nonwetting phase in the open system does not rise as high above its level in the closed system as in (A). The principle of the porous medium is that it remains wetted and only allow nonwetting phase to bubble through (when the capillary pressure just below the porous medium exceeds the entry pressure $P_{c,entry}$. If wetting phase remains in the capillary barrier, then the nonwetting phase above the barrier won't be connected to nonwetting phase below. The example works only if the initial height of oil in the closed system gives a $P_c$ in the closed system larger than the $P_{c\_entry}$ of the barrier.

The final extent of oil into the corners of the domain will depend on the level of oil held in the external reservoir. If the connected path of oil in the corners effectively 'short-circuits' the capillary barrier of fine beads, the situation is analogous to Figure 4.17 (A), where the level of oil in the corner in the domain, $h_{nw} = \rho_w h_{w1}/\rho_{nw}$. If the oil in the corner doesn't "short circuit" the capillary barrier, accumulated oil column is disconnected by the capillary seal, and the oil level above the barrier should be lower than that without the barrier, because hydrostatic pressure at the bottom of the barrier decreases by an amount equal to the capillary entry pressure of the barrier. In Figure 4.17, the corner effects and the crack both 'short circuit' the capillary seal, therefore readjustment of the liquid in the system assisted the escape of nonwetting oil phase out of the domain.

2. The crack through the seal on the upper left part of the domain. After the valves are opened the oil/water interface keeps rising from its initial location (red dotted line 1 in Figure 4.16) until it reaches the level marked by red dotted line 2. The level corresponds to the intersection of the crack with the 'storage formation' of coarse beads. This suggests that some portion of the nonwetting phase flowed through the crack to the top of the domain (between the top cap and seal) as the experiment progresses, and was able to leave the domain when the valves at the top were opened. The cavity circled in yellow on the right proves this as well since no nonwetting phase flowed from this cavity out of the system. Nonwetting oil remains in the crack because the crack doesn't extend through the 0.25 mm beads all the way to the top of the apparatus. If the crack connected to the port at the top, oil should have kept flowing out of the crack because the entry pressure of the crack is smaller than the seal bead pack. There must be seal grains present between the top of the crack and the top of the apparatus, cutting off the crack.

This experiment shows the principles of local capillary trapping work in practice as well as in theory. Oil phase was held beneath the layer of fine beads in the open system. Oil phase that was originally located in the storage formation below the level where the crack intersects the storage formation escaped when the system was opened. The escape pathways were the relatively open (small entry pressure) regions at the corners of the domain and the crack (very small entry pressure) within the sealing layer. Though the seal integrity was compromised by these pathways, not all the oil escaped. Some oil remained trapped in the region below the undisturbed sealing formation even as water imbibed into the storage formation from below to replace the oil migrating out the top of the domain. This simple observation is representative of a region that would correspond to a single local capillary trap in a storage formation. Once $CO_2$ was held in such a region, it would not escape, regardless of what happens elsewhere in the domain.

The amount of nonwetting phase trapped beneath the seal varies from the closed system to the open boundary system. It is possible that in the closed system, when the oil gets trapped beneath the seal (Figure 4.14), the aqueous phase at the top of the domain (between top cap and seal) did not have flow paths available for counter-current displacement movement and thus remained held above the nonwetting phase; while in the open system, the aqueous phase at the top doesn't have to fall down (it can flow out the top), and the amount of oil trapped beneath the seal in open system may reflect the more accurate storage capacity by local capillary trapping of the particular formation. Therefore it is very important to apply the hydrostatic open boundary condition when estimating the total storage capacity and extent of persistence of the trapping mechanism. A confined closed-state storage space is seldom seen in Nature, while it is possible in the quasi-2D experimental apparatus. Therefore in the subsequent experiments, results obtained with open boundary hydrostatic condition applied are of primary importance for studying LCT.

**Findings from experiment 4 and 5**

1. Compared to Experiment 1, 2 and 3 where bead sizes range from 5 mm to 0.25 mm and degree of heterogeneity is high, Experiment 4 and 5 used less bead variety (only 0.5 mm and 0.25 mm, and degree of heterogeneity is low). Reducing the bead size resulted in a smoother rising front of the non-wetting phase in the storage reservoir (Figure 4.10), instead of fingering through domains with large bead sizes observed previously (Figure 4.5). The smoother front increases storage efficiency, as reducing the preferential flow will increase the total amount of non-wetting phase stored beneath the capillary barrier.

2. The small beads (0.25 mm) are very effective seal for the dimensions of this apparatus (which limit the height and therefore the maximum capillary pressure in an oil-saturated region). Almost all the non-wetting phase is trapped beneath regions formed by these beads.

3. The local trapping mechanism is still stable even when there is a crack in the seal, as long as the crack doesn't extend all the way through the seal to top of the domain to provide a preferential flow for the rising fluid (Experiment 5).

**Experiment 6**

**(0.25 mm, 0.5 mm and thin 2 mm region, layered, anticline-shaped seal, switching at long time from closed state to open state with hydrostatic potential boundary condition applied)**

**Objective: demonstrate influence of open hydrostatic potential on LCT**

*Part 1: Closed system.*

The configuration of seal/reservoir heterogeneity examined in Experiment 5 was also used in experiment 6: anticline-shaped capillary seal made of 0.25 mm beads. In Experiment 6 an additional layer of 2 mm beads (larger and transparent) was put at the top of the domain above the 0.25 mm beads to provide visual aid if there is any accumulation of nonwetting phase at the top.

In the closed system, rising nonwetting phase was locally trapped by the seal, and no visible nonwetting phase accumulated in the 2 mm region at the top of the domain in the early stage (first two hours). The results are summarized in following Figure 4.18.

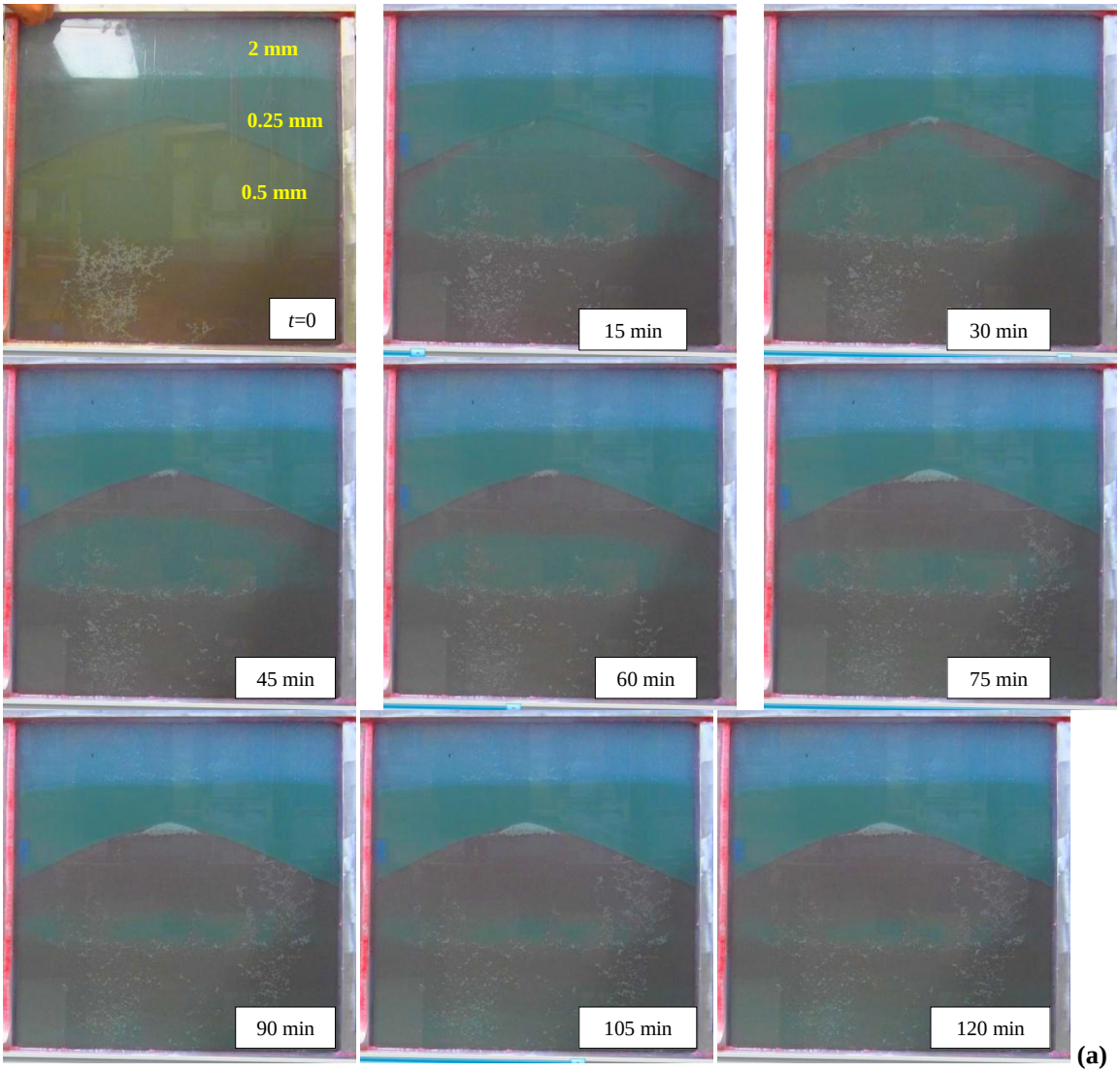


**(a)**

Figure 4.18 (continues to next page)

(Figure 4.18 continued)

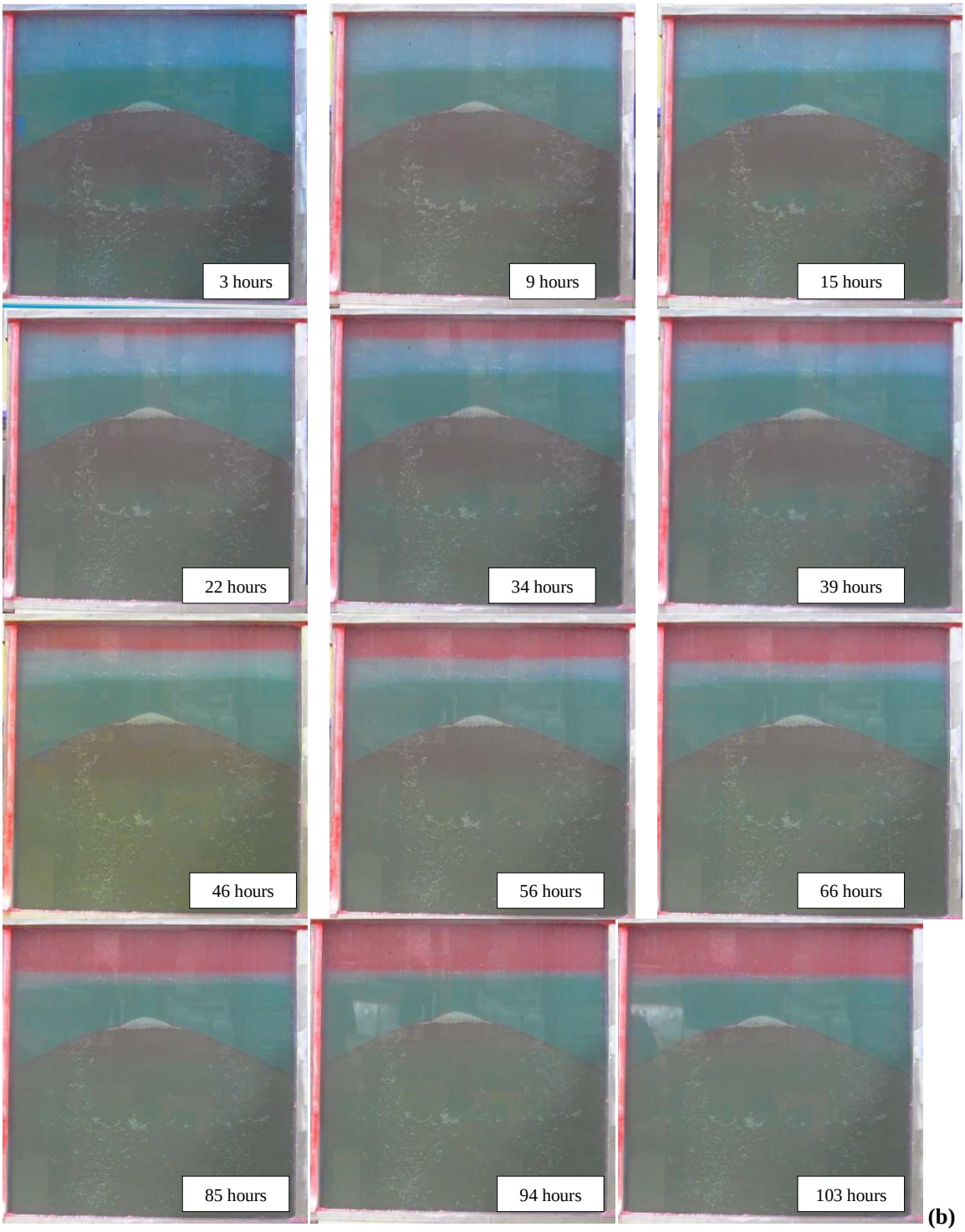


**(b)**

Figure 4.18 (continues to next page)

Figure 4.18: (a) First two hours of experiment 6 (closed system). Rising nonwetting phase plumes were trapped by the capillary seal (0.25 mm beads) and accumulation beneath the seal happens. No escape of nonwetting phase to the 2 mm layer at the top occurred during this time frame. (b) Late time of experiment 6 (closed system). System still remained closed, but between 9 and 15 hours accumulation in the 2 mm layer increases, suggesting migration of the nonwetting phase along the corners of the domain. Insets give elapsed time since start of buoyancy-driven displacement in closed system.

The accumulation of nonwetting phase in the top layer in the late time period of this experiment (Figure 4.18(b)) indicates there must be flow paths from the storage formation (beads below the fine-bead layer) to the top 2 mm layer. However there is no visible crack/fracture found in the fine-bead layer, therefore a reasonable deduction would be the corner effect discussed above for Experiment 5, which enables the slow migration of the nonwetting phase through channels of smaller capillary entry pressure in the corners of the apparatus where the front glass plate, the aluminum side and the beads meet. The oil in the top layer is not held by local capillary trapping, but by the closed ports at the top of the apparatus. Note that oil within the storage formation remains held beneath the fine bead layer and does not invade the fine bead layer from the corners neither from below nor from above via backfilling as oil accumulates in top layer of 2 mm beads. Moreover oil remains held in the ‘storage formation’ layer of beads beneath the fine-bead sealing layer.

*Part 2: open boundary imbibition.*

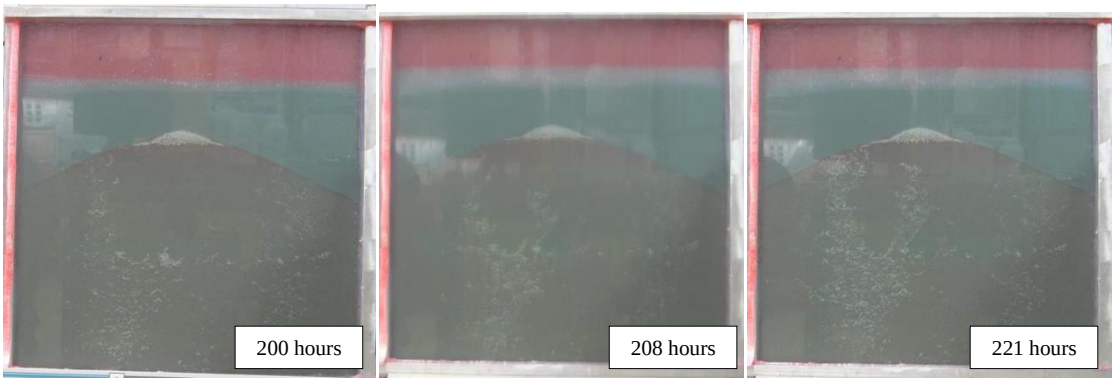


Figure 4.19: Open boundary imbibition of Experiment 6. Insets give elapsed time since start of buoyancy-driven displacement in closed system.

At the 200$^{th}$ hour, the valves connected to the reservoirs opened so that potentially mobile nonwetting phase (i.e. not held in local capillary traps) can migrate or escape. As shown in Figure 4.19 above, a small amount of nonwetting phase in the top 2 mm layer left the system and entered the reservoir connected to the top ports. In the following 8 hours (until 208$^{th}$ hour), the system re-equilibrates with no more nonwetting phase leaving the system. The cessation of movement of oil out of the domain in this experiment is striking compared to the much greater movement in Experiment 5. The reason is that the 2 mm layer enabled all the oil connected to the corners in the storage formation to rise along the corners while the domain was closed. Thus there was no potentially mobile oil in the 'storage formation' layer of beads when the valves were opened. In this sense this experiment also confirms the local capillary trapping phenomenon. The oil held beneath the capillary seal of the fine-bead layer remained there even when oil held above migrated out of the system and water migrated into the system from below to replace that oil. The trapping is local: as long as the capillary pressure remains below the capillary entry pressure for the local barrier, the movement of fluid(s) elsewhere in the domain does not affect the trapped nonwetting phase.

**Experiment 7**

**(0.25 mm, 0.5 mm and thin 2 mm region, layered, anticline-shaped seal, switching after short elapsed time from closed state to open state with hydrostatic potential boundary condition applied)**

**Objective: demonstrate persistence of LCT under open hydrostatic boundary conditions**

Experiment 7 was conducted with the same beads arrangement as previous experiment: the 0.5 mm beads comprises the 'store', 0.25 mm beads comprises the 'seal', and the large 2 mm beads formed a top layer above the seal to visualize any un-trapped nonwetting phase bypassing the seal. The only difference is that this top 2 mm bead layer is thinner compared to Experiment 6, which would "store" less amount of escaped nonwetting phase while still providing visual aid to accumulation.

The entire domain was first saturated with wetting phase, and then non-wetting phase was injected from the top, displacing about half of the wetting phase. After nonwetting phase injection finished, all valves are closed. And the domain is in its initial condition, for which a 180 degree rotation will start the experiment.

*Part 1: Closed system.*

In the first hour, rising plumes of nonwetting phase hit the seal layer and accumulated beneath it. See Figure 4.20(a) below.

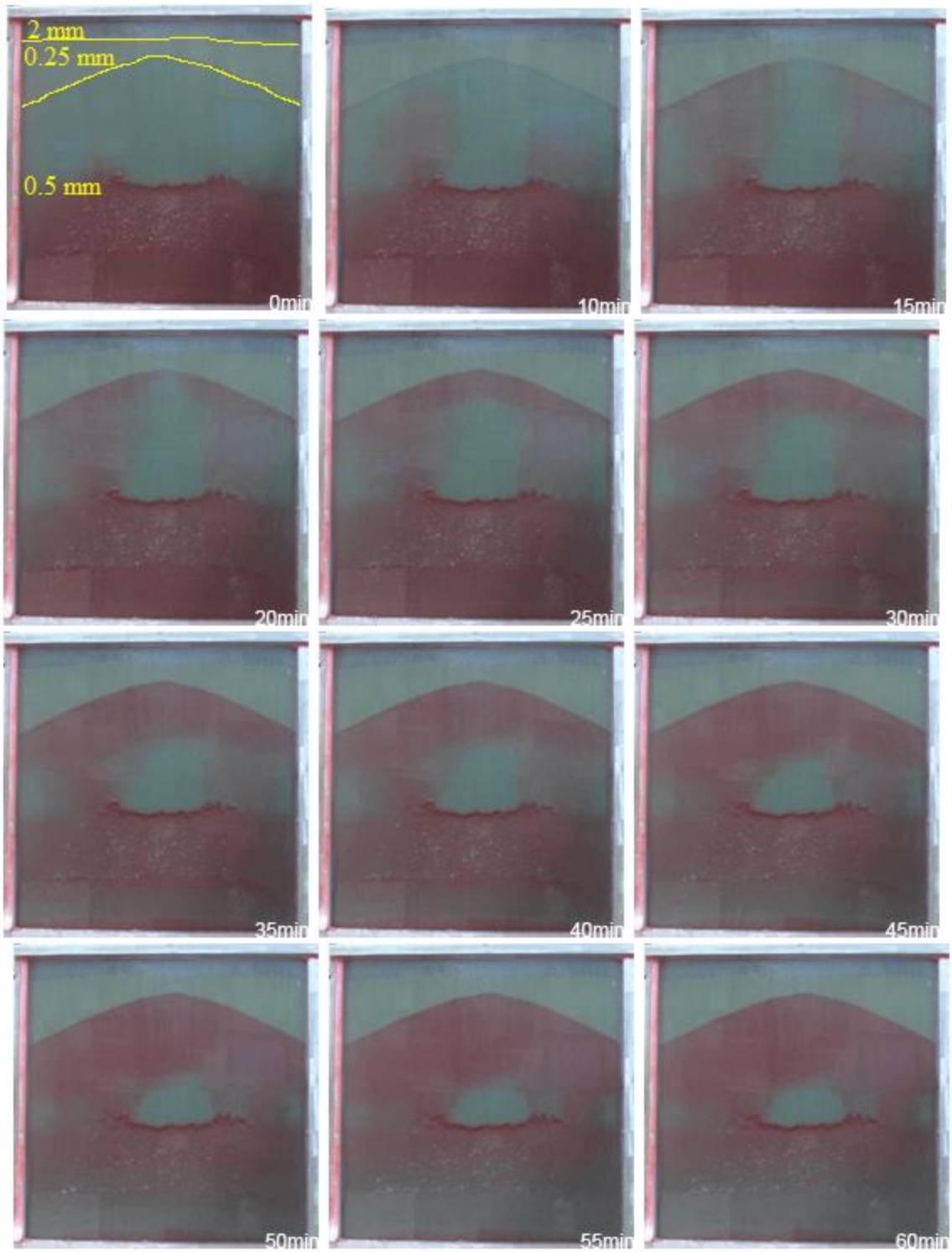


**(a)**

Figure 4.20 (continues to next page)

(Figure 4.20 continued)

**(b)**

Figure 4.20: (a) First one hour of experiment 7 (closed system). (b) Equilibrium state of the closed system. System reached equilibrium in 3 hours. Insets give elapsed time since start of buoyancy-driven displacement in closed system.

The closed system reached equilibrium in about 3 hours, meaning no more liquid movement. Countercurrent displacement of wetting and nonwetting phases stopped. As shown in Figure 4.20(b) almost all nonwetting phase was trapped in the coarse-bead region beneath the capillary barrier formed by the fine-bead region. In addition, a fair amount of nonwetting phases remained trapped as a residual saturation in the lower portion of the initially saturated region of 0.5 mm beads.

*Part 2: open boundary imbibition.*

From Experiment 6, the corner effect became apparent at about 9 hour. To reduce this artifact, the open boundary imbibition stage of experiment 7 was conducted starting from the 9$^{th}$ hour. Hydrostatic pressure boundary condition was applied by connecting the

aqueous reservoir to the bottom of the domain and keeping its liquid level the same as the top of the domain. Results are summarized below in Figure 4.21.

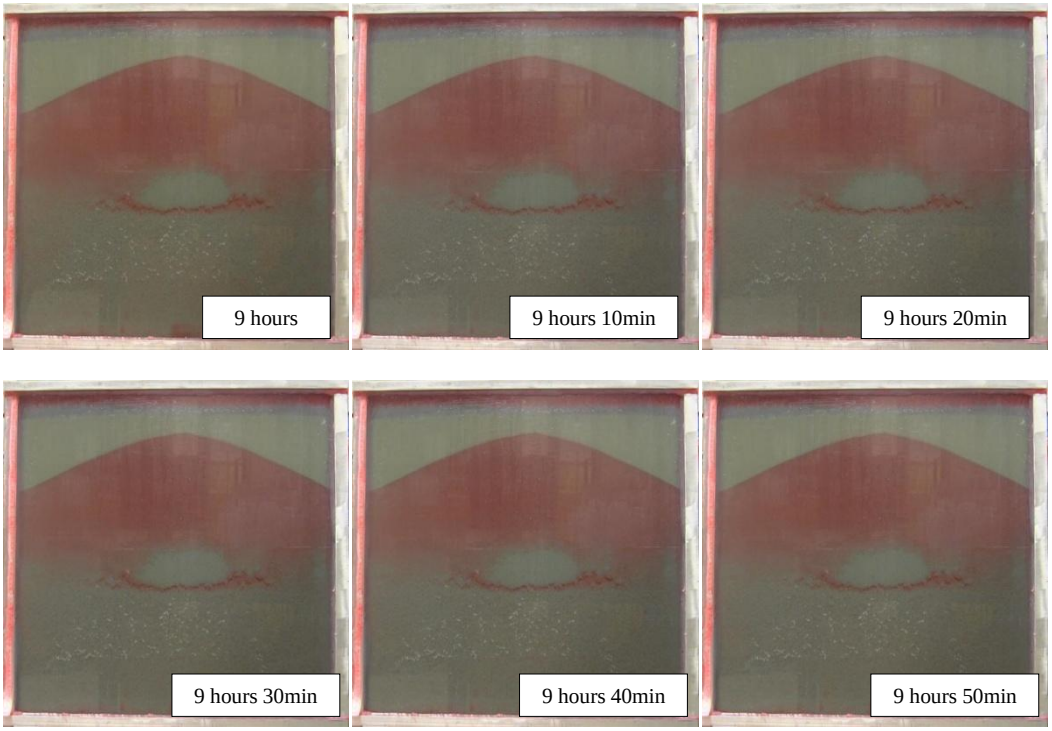


**(a)**

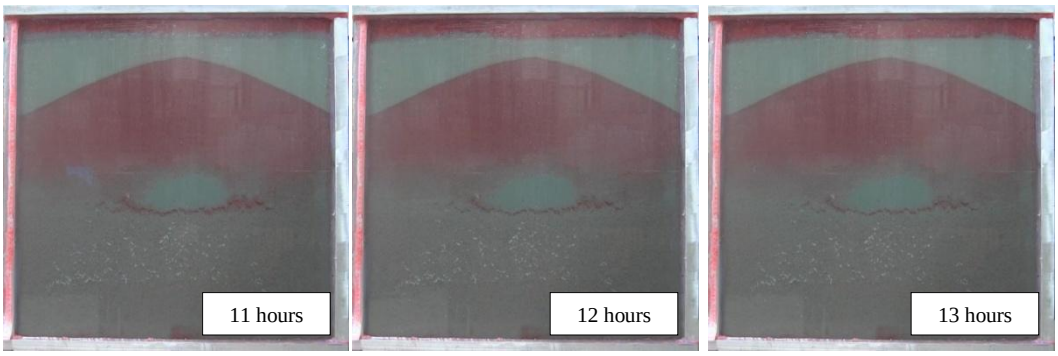


**(b)**

Figure 4.21: **(a)** First hour of the open boundary imbibition. **(b)** Stabilized open system under hydrostatic potential. Insets give elapsed time since start of buoyancy-driven displacement in closed system.

Although migration of oil from the ‘storage formation’ to the topmost layer of 2 mm beads was facilitated by the opening of the valves, very little amount of nonwetting phase was displaced out of the apparatus. No migration of oil from the storage layer through the interior of the sealing layer occurred. This confirms that 0.25 mm bead layer served as a good capillary barrier, and local capillary trapping is persistent even in open systems in which the fluids are at hydrostatic potential gradient, i.e. buoyancy-driven displacement is possible but no pressure-driven flow of either phase is imposed.

**Experiment 8**

**(0.25 mm, 0.5 mm and thin 2 mm region, layered, anticline-shaped seal, closed state at first, then open state when rising oil reached seal, corner effect obvious)**

**Objective: demonstrate extent of LCT in a direct open boundary domain**

As shown in previous experiments, interpretation of the extent and the durability of local capillary trapping in these experiments has been complicated by the ability of the nonwetting phase to rise through packing defects (larger than average pore throats) at the corners of the container holding the beads. In an effort to reduce this effect, the apparatus (the Pyrex glass containment box) was sent for modification. Two quarter-inch-wide two-feet-long hydrophilic metal (aluminum) bars with square cross section were cut diagonally and glued to the inner corners of the glass containment box using silicone gel. Figure 4.22 below shows the modification. The idea is that the oblique angle between the aluminum piece and the glass wall will enable the glass beads to pack more tightly than in the right-angle corners of the earlier version of the containment box.

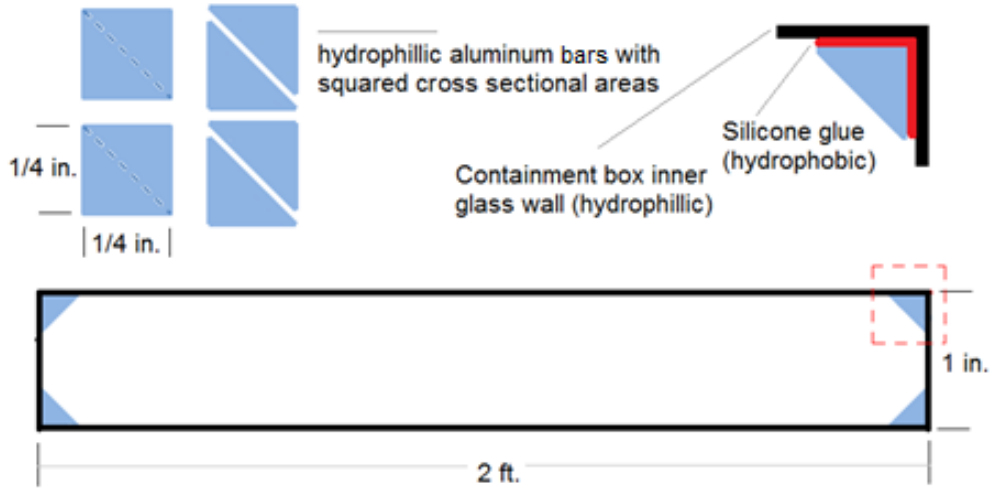


Figure 4.22 (continues to next page)

Figure 4.22: Modification to the experimental apparatus for reducing corner effects. Square corners in original apparatus allow beads to pack loosely and thus introduce regions with relatively large pore throats, through which nonwetting phase can migrate even when it is being held by beads acting as capillary barrier elsewhere in the apparatus. Reducing the angle between flat boundary faces at the corners should reduce the size of pore throats between beads and those faces, making nonwetting phase migration less likely.

Experiment 8 was then conducted with the same beads arrangement as previous experiments: the 0.5 mm beads comprises the 'store', 0.25 mm beads comprises the 'seal', and the large 2 mm beads formed a top layer above the seal to visualize any un-trapped nonwetting phase bypassing the seal. Difference is that the apparatus now has been modified, intended to reduce the edge/corner effect,

The entire domain was first saturated with wetting phase, and then non-wetting phase was injected from the top, displacing about half of the wetting phase. After nonwetting phase injection finished, all valves are closed. And the domain is in its initial condition, for which a 180 degree rotation will start the experiment.

*Part 1: Closed system.*

Experiment 8 was conducted with a thin top 2 mm beads layer, a 0.25 mm beads seal and a 0.5 mm beads store. The anticline store is proven to be effective for trapping. The following Figure 4.23 presents a series of photographs of the closed boundary buoyant counter-current movement.

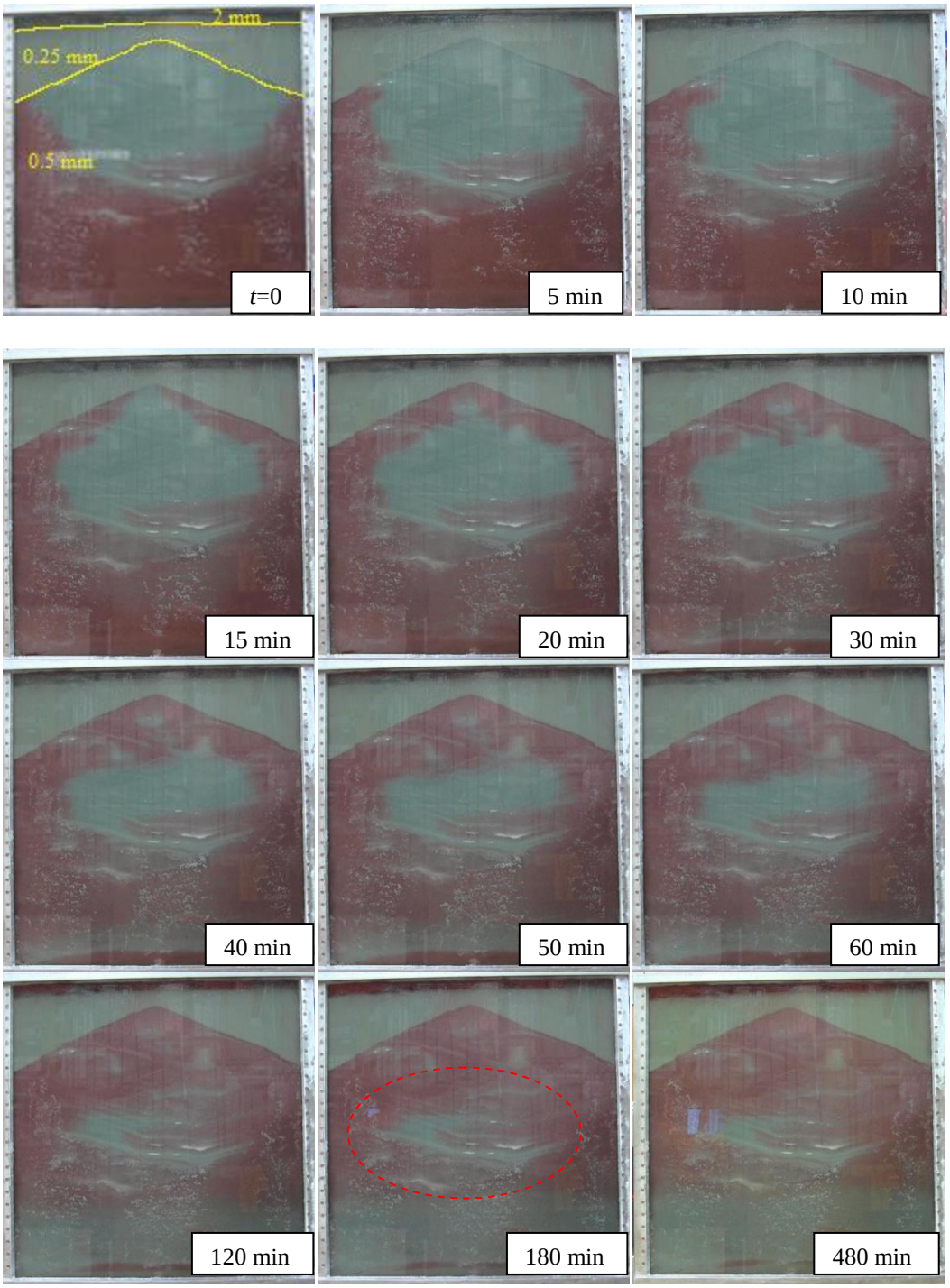


Figure 4.23 (continues to next page)

Figure 4.23: Progress of buoyant migration of nonwetting phase (red) during Experiment 8. Insets give elapsed time since start of buoyancy-driven displacement in closed system. The system was closed throughout the period of migration shown here. The "seal" of fine beads successfully held back the mobile nonwetting phase and caused it to backfill the pore space in the anticline of coarse beads. Though the capillary entry pressure along the corners was larger than in previous experiments, the nonwetting phase nevertheless migrated along the corners of the apparatus and backfilled a small portion of the top of the domain.

The silicone used to glue the aluminum pieces in the corners swells with prolonged direct contact with hydrocarbon phases. This creates a greater surface area of hydrophobic material, creating easy migration pathways for the red-dyed nonwetting phase. This was observed even at the initial backfilling stage; hence corner effect was, in fact, enhanced in this situation, which contradicted the intention of the modification.

Figure 4.23 above shows the first 8 hours of the experiment at closed state. Despite the corner effect at the two sides, the system still reached equilibrium in about 3 hours, which is consistent with previous results.

The beads came fresh from the manufacturer and contained some dust (even finer particle) which contributed some heterogeneity within the 0.5 mm bead pack region (circled region in Figure 4.23 above). The rising nonwetting phase could not reach those regions due to high capillary entry pressure of such bead/dust packs, and accumulated beneath them. This is another manifestation of local capillary trapping, and is a possible direction to proceed when we seek to study finer particle heterogeneity.

*Part 2: Open system*

At the end of the 8th hour, the system was opened; constant potential equal to hydrostatic (i.e. $\Psi = P - \rho_w gz$) was applied to both the top and bottom of the domain by positioning the reservoirs (one connected to top ports, one connected to bottom ports) such that the liquid surfaces are at the same level as the top of the domain. Since the nonwetting phase reached equilibrium in the closed system with hydrostatic potential within the aqueous phase, no movement of fluid is expected when the system is opened, since the hydraulic potential does not change. Indeed, the system reached equilibrium in a short time. Mobile nonwetting phase migrated from the lowest portion of the domain along the corners and increased the saturation in the top portion of the domain. In this experiment the nonwetting phase backfilled into the seal, as becomes clear at 18 hr and 31 hr in Figure 4.24. The reason for this is unclear as the seal formation has never been invaded in other experiments, but the silicone may have facilitated the invasion. The nonwetting phase at the very top of the domain can flow out ports at the top of the apparatus when opened, and it did so. However the nonwetting phase within the coarse beads in the anticline was held by capillary forces and did not migrate, as shown in Figure 4.24 below.

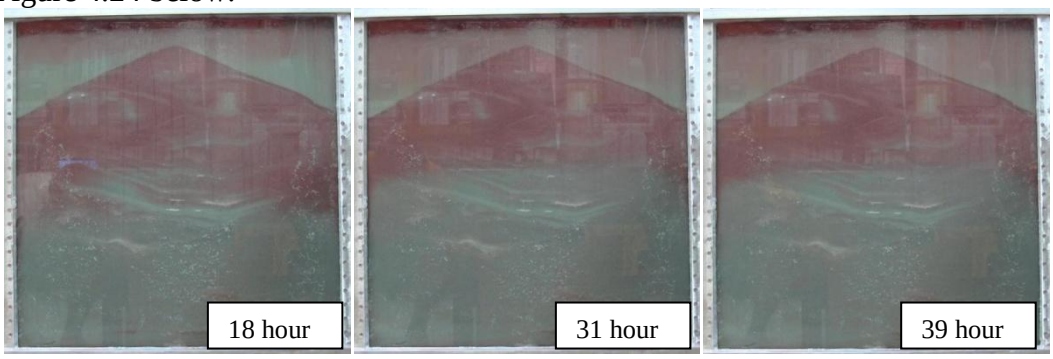


Figure 4.24: Late time equilibrium state (insets give elapsed time since start of buoyancy-driven displacement in closed system) of the open system of experiment 8. Constant hydraulic potential equal to hydrostatic was applied at top and bottom ports at the 8th hour elapsed time.

The open hydrostatic imbibition was followed by a forced imbibition, and results are summarized in the following Figure 4.25. Notice that the time has been reset.

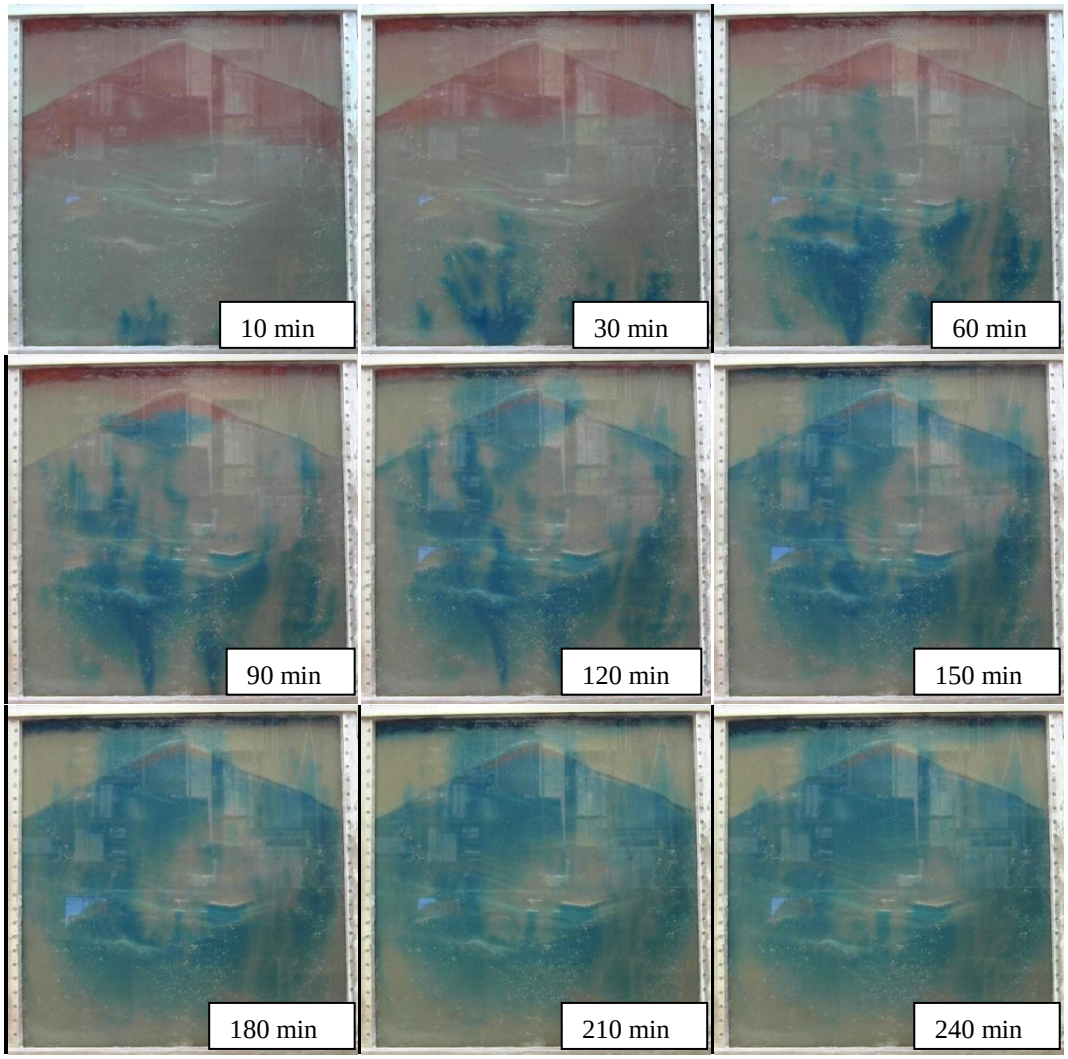


Figure 4.25: Forced imbibition of the wetting phase (blue) displaces non-wetting phase (red) through the capillary sealing layer. The aqueous reservoir liquid surface connected to the bottom ports was raised 14 inches higher than the top of the domain, causing the capillary pressure at the top of the oil column to exceed the capillary entry pressure of the sealing layer. Insets give elapsed time since start of forced imbibition (the clock has been reset at the beginning of the forced imbibition, when the aqueous reservoir is raised).

At the 85$^{th}$ hour, the system remained open, the reservoir connected to the top of the apparatus was not moved, and the aqueous phase reservoir connected to the bottom of the apparatus was raised 14 inches (35.6 cm). The entering pressure at the bottom of the domain = 101 Pa + (35.6 cm + 63 cm + 30 cm – 30 cm) × 9.81 N/m × 1084 kg/m$^3$ = 111.5 kPa. The exiting pressure at the top of the domain, assuming oil phase fills up the exiting line, = 101 Pa - (93 cm – 93 cm) × 9.81 N/m × 724 kg/m$^3$ = 101 Pa. This imposed a pressure gradient of (111.5 kPa – 101 kPa)/0.63 m = 16.6 kPa/m across the aqueous phase in the apparatus, and therefore a 16.6 – 7.1 = 9.5 kPa/m capillary pressure gradient within the oil phase. Consequently the effective capillary pressure at the top of the accumulation of nonwetting phase beneath the "seal" layer increased considerably; recall the capillary pressure gradient the first stage of migration was 3.5 kPa/m. At the increased gradient, the remaining 9 inches (0.227 m) continuous oil column beneath the "seal" at the beginning of the 85$^{th}$ hour (see rightmost panel in Figure 4.24) corresponds to 0.227 m × 9.5 kPa/m = 2156 Pa of capillary pressure, compared to its original (open system at hydrostatic pressure) values of 10 inch × 3.5 kPa/m = 889 Pa (at closed system). This value is much greater than the entry pressure of the 0.25 mm seal (1334 Pa theoretical and 1735 Pa experimental). Therefore blue-dyed aqueous wetting phase came into the domain (Figure 4.25) and displaced the trapped oil through the "seal" beads, then out of the apparatus.

This experiment confirms that local capillary trapping does hold nonwetting phase at saturations above residual, as described in the seminal work by Saadatpoor et al (2009). Since the trapping is exclusively due to the capillary pressure at the top of the nonwetting phase accumulation being smaller than (or equal to) the capillary entry pressure of the porous medium above the accumulation, it should be possible to displace the locally trapped phase if its capillary pressure increases. This is precisely what

happened in the forced imbibition stage of this experiment. The nonwetting phase was trapped at a capillary pressure gradient of 3.5 kPa/m, the value corresponding to buoyancy (density difference between phases) in an otherwise static (no gradients in potential) system and illustrated in Figure 4.23. Raising the aqueous phase reservoir connected to the bottom of the domain by 35.6 cm increased the capillary pressure gradient three-fold, overcoming the entry pressure of the fine beads and allowing the above-residual oil saturation to enter the fine beads.

To calculate the capillary pressure gradient, $P_c$ *gradient*, across the system at open boundary conditions (assuming the outlet is directly open to air and at the same level as the top of the domain):

For <u>hydrostatic potential gradient</u>:

$$P_c \text{ gradient} = (P_{\text{bottom of domain}} - P_{\text{top of domain}})/h_{\text{domain vertical}} - P_{\text{oil hydrostatic}}\text{gradient}$$

$$= (P_{atm}+\rho_{inlet\_tube\_fluid}gh_{domain\_vertical} - P_{atm})/\ h_{\text{domain vertical}} - \rho_{oil}g$$

$$= (\rho_{inlet\_tube\_fluid} - \rho_{oil})g$$

For <u>greater than hydrostatic gradient</u> imposed in the aqueous phase:

$$P_c \text{ gradient} = (P_{\text{bottom of domain}} - P_{\text{top of domain}})/h_{\text{domain vertical}} - P_{\text{oil hydrostatic}}\text{gradient}$$

$$= [P_{atm}+\rho_{inlet\_tube\_fluid}g(h_{domain\_vertical}+h_{w\_reservoir\_elevated}) - P_{atm}]/\ h_{\text{domain vertical}} - \rho_{oil}g$$

$$= \rho_{inlet\_tube\_fluid}g(1+h_{w\_reservoir\_elevated}/h_{domain\_vertical}) - \rho_{oil}g$$

$$= [\rho_{inlet\_tube\_fluid}\ (1+h_{w\_reservoir\_elevated}/h_{domain\_vertical}) - \rho_{oil}]g$$

where,

$h_{w\_reservoir\_elevated}$ is the level of aqueous reservoir being elevated

$h_{domain\_vertical}$ is the vertical length of the domain (in this case, 2 ft).

**Experiment 9**

**(0.25 mm, 0.5 mm and 2 mm, layered, anticline-shaped seal, <u>open state</u> when oil starts to rise)**

**Objective: demonstrate persistence of LCT while determining the threshold $P_{c\_entry}$ for the seal**

Due to apparent corner effect in experiment 8, the experimental apparatus was thoroughly examined before proceeding to the next experiment. It was found that the silicone gel attaching the corner metal slats to the large containment box was swollen due to prolonged exposure to the hydrocarbon organic non-wetting phase. This created a preferential vertical pathway along the corner for the rising nonwetting phase. Therefore, the swollen silicone gel was carefully scraped and removed from the system before carrying on the next experiment, in the hope to reduce the corner artifact.

In Experiment 9, the same heterogeneous configuration of beads as Experiment 8 was used: layer of fine beads above anticline-shaped layer of coarse beads, all beads relatively small (0.25 mm and 0.5 mm). The entire domain was first saturated with aqueous phase, and then the nonwetting phase was injected from top, displacing about half of the aqueous phase initially in place. When the injection of nonwetting phase is complete, the domain was then rotated 180 degree to start the experiment.

To fully mimic the actual storage condition, we switched to open system (top ports open and connected to one fluid reservoir, bottom ports open and connected to second fluid reservoir) as the nonwetting phase begins to rise, i.e. well before it reached the seal. The wetting aqueous phase reservoir was placed at the same height as the top of the domain, and was connected to the bottom of the domain. Nonwetting phase reservoir was connected to the top of the domain. By setting the reservoirs at the appropriate

relative levels, constant hydraulic pressure is applied to the open system. The initial levels are chosen so that the potential gradient corresponds to hydrostatic, and the system reached equilibrium in 3 hours (similar to Experiment 8). Figure 4.26 below shows the first four hours of open state system results.

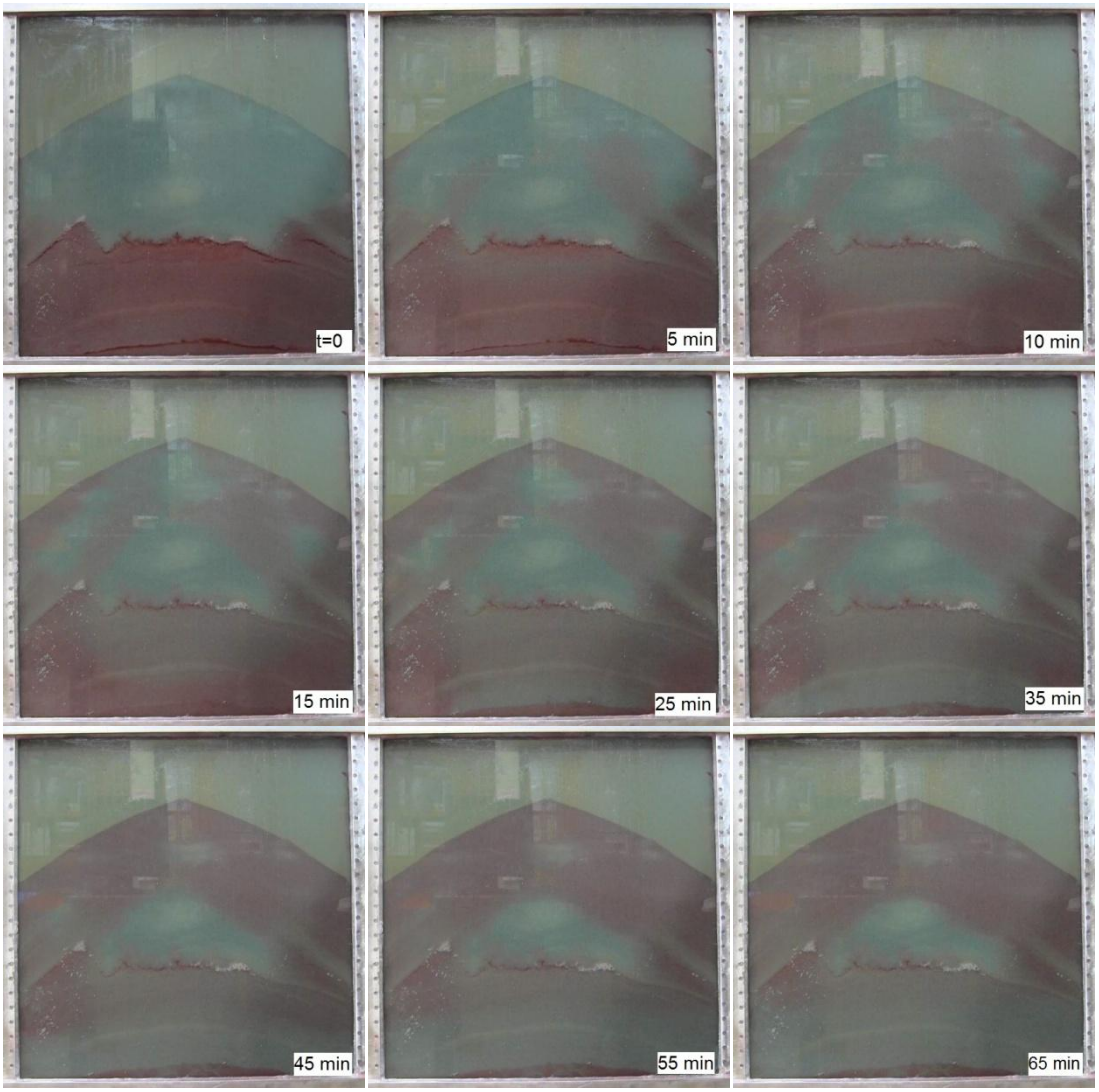


Figure 4.26 (continues to next page)

(Figure 4.26 continued)

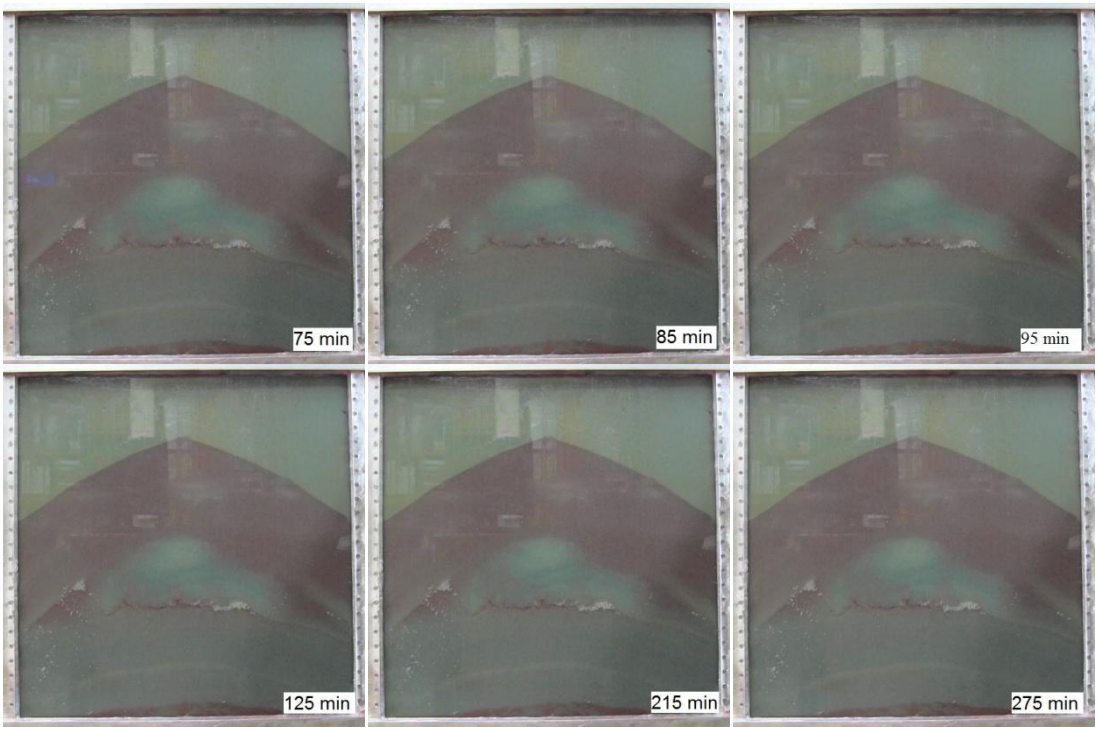


Figure 4.26: First 275 minutes of Experiment 9. Open state was imposed from the beginning when the red-dyed nonwetting phase was rising from its initial emplacement in the bottom half of the domain. Constant pressure gradient corresponding to hydrostatic was applied across the open apparatus. The system reached equilibrium in 3 hours, and nonwetting phase remained secure below the layer of fine beads.

At 430$^{th}$ minute after starting the experiment, the aqueous reservoir was raised 1 inch higher such that the capillary pressure gradient in the accumulated oil column is about 3.7 kPa/m. (Recall that under hydrostatic conditions the capillary pressure gradient corresponds to density difference between the phases and is 3.5 kPa/m for the fluids used in these experiments.) This gradient created a total capillary pressure of 838 Pa at the top of the oil column. No fluid movement was evident anywhere in the system, as shown in Figure 4.27. This is consistent with expectation; the original oil column height was less

than the value needed to reach the capillary entry pressure of the fine beads, and thus a small increase in the capillary pressure at the top of the column was insufficient to exceed the capillary entry pressure.

The aqueous reservoir was then raised to a series of different levels; after each increment in height, a period of time was allowed to pass in order to determine whether the system was at equilibrium, or to allow it to reach equilibrium if any fluid movement was observed. Each new aqueous reservoir height creates a larger pressure gradient in the continuous aqueous phase within the apparatus. This correspondingly induces a larger capillary pressure gradient, and hence increases the capillary pressure at the top of the accumulated oil column. As long as the capillary pressure remains below the threshold pressure, no fluid movement is expected. Once the threshold is exceeded, as shown in the last two frames of Figure 4.27 below, the displacement of red dyed nonwetting phase out of the system by blue dyed wetting phase into the system from the bottom commences.

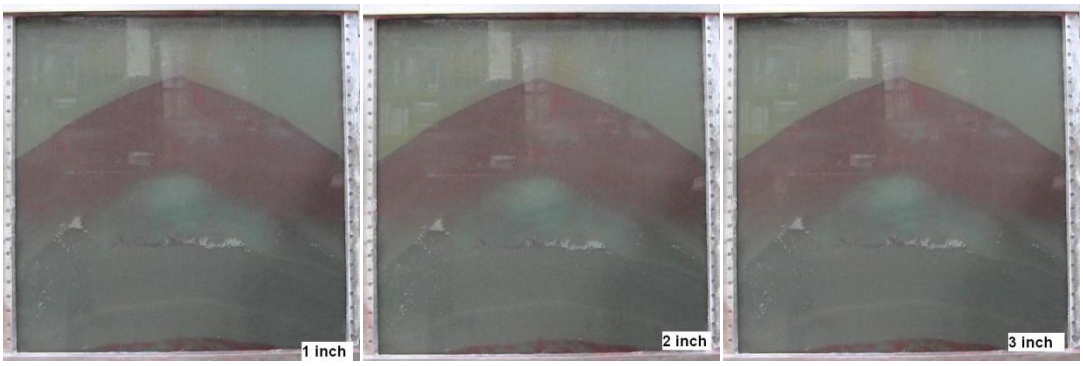


Figure 4.27 (continues to next page)

(Figure 4.27 continued)

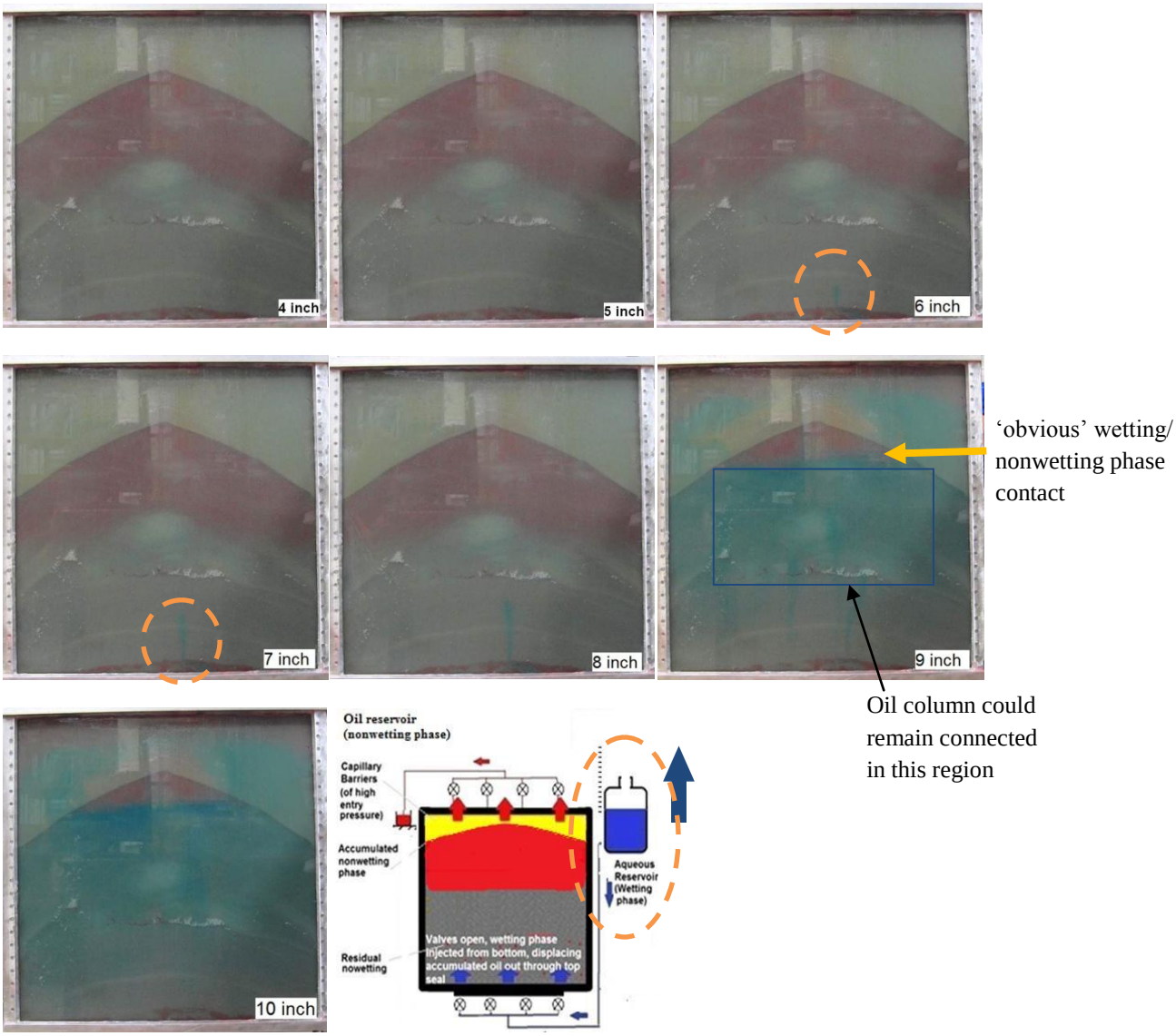


Figure 4.27: The aqueous reservoir connected to the bottom of the domain (schematic at bottom) was raised in small increments above the top of the domain (height indicated at the bottom right corner of each photograph). Until the increments totaled 5 inches, no fluid movement occurred in the system. That is, the red-dyed nonwetting phase remained trapped by capillary forces beneath the fine beads at the top of the domain, even though its saturation was much greater than residual. The blue dyed aqueous wetting phase starts entering the system (indicated by orange circle) when the aqueous reservoir was raised 6 inches above the system, and becomes more apparent during subsequent increments.

While blue dyed aqueous phase enters the system, it displaces out the original fluids (both oil and water) in the system though the top ports and tubing. The major displacement of oil occurs when the reservoir is raised from 8 inches to 9 inches, suggesting that at this point the total capillary pressure due to the trapped oil column height and externally applied hydraulic pressure has exceeded the entry pressure of the capillary barrier, therefore the oil escaped through the seal. Therefore the effective threshold pressure of the capillary seal is determined empirically. Table 4.1 summarizes the observations.

| Aqueous reservoir liquid surface above the top of the apparatus | | Corresponding Hydraulic potential | Capillary Pressure Gradient | Measured Oil Column Height | | $P_c$ Top of the oil column | Oil displaced out |
|---|---|---|---|---|---|---|---|
| (inch) | (cm) | (Pa) | (kPa/m) | (inch) | (m) | (Pa) | (ml) |
| 0 | 0 | 0 | | | | | 0 |
| 1 | 2.54 | 270 | 3.3 | 10 | 0.254 | 838 | 0 |
| 2 | 5.08 | 540 | 3.8 | 10 | 0.254 | 965 | 0 |
| 3 | 7.62 | 810 | 4.2 | 10 | 0.254 | 1067 | 0 |
| 4 | 10.2 | 1080 | 4.6 | 10 | 0.254 | 1168 | 0 |
| **5** | 12.7 | 1351 | 5.0 | 10 | 0.254 | 1270 | 0 |
| 6 | 15.2 | 1621 | 5.4 | 10 | 0.254 | 1372 | 0 |
| **7** | 17.8 | 1891 | 5.8 | 10 | 0.254 | 1473 | 0 |
| 8 | 20.3 | 2161 | 6.2 | 10 | 0.254 | 1575 | 20 |
| 9 | 22.9 | 2431 | 6.6 | 3 | 0.0762 | 503* | 370 |
| 10 | 25.4 | 2701 | 7.0 | 2 | 0.0508 | 356* | 450 |
| 11 | 27.9 | 2971 | 7.4 | 1.5 | 0.0381 | 282* | 490 |

Table 4.1: Determination of the breakthrough capillary pressure of the seal in Experiment 9. Values with * indicate the apparent $P_c$ estimated subject to limitations in the quantification process; refer to assumption (2) below.

Three key assumptions are made when analyzing the image.

1) The entry pressure for the storage formation beads is ignored. When the fluids come from the reservoir connected to the bottom of the domain, they will encounter the beads in the store region first. Those beads also have entry pressure to overcome. Since the beads in the store are twice the size of those in the seal, $P_{c\_entry\_store} = 0.5\ P_{c\_entry\_seal}$. A certain amount of capillary pressure would be required to overcome this $P_{c\_entry\_store}$ value so that oil can enter the domain. However, since the backfilling of the store occurs at the same time that oil rises through the store and water imbibes into the initial (before flipping the apparatus) oil accumulation, it may not be the case that the capillary pressure at the base of the equilibrium (after flipping) oil accumulation is equal to the store entry pressure. The capillary pressure could be close to zero if imbibition were occurring at the base of the accumulation. The calculations in Table 4.1 assumed that imbibition did occur, and thus that the capillary pressure at the base of the equilibrium oil accumulation was zero. If the base of the equilibrium accumulation were at $P_c = P_{c\_entry\_store}$ then the values of $P_{c\_entry\_seal}$ would be larger than the values reported in Table 4.1.

2) The oil column is assumed to be disconnected below the level of obvious large oil saturation. This is potentially problematic as the oil approaches the equilibrium accumulation from the initial accumulation, because the imbibition process in the lower parts of the initial accumulation need not continue all the way to residual oil saturation. That is, oil could still be present at saturations large enough to maintain a connected column but small enough to not be as obviously red (and therefore connected). Accounting for this would require explicitly modeling the capillary imbibition process at the bottom of the initial accumulation. The lower portion of the nonwetting phase will be following imbibition $P_c$-$S_w$ curve, not drainage curve. So the oil column could remain

connected some distance below (blue rectangle in Figure 4.27) the 'obvious' (to the eye) wetting/nonwetting phase contact line (yellow arrow in Figure 4.27), making the effective oil column height larger. In this case the $P_c$ at top of oil column would be larger in the first row (1 inch elevation) of Table 4.1. More importantly, the same considerations apply to the displacement that occurs once the threshold capillary pressure is reached (9 inches elevation). The implication is that the oil column could be considerably longer than the 3 inches of obvious column height in the equilibrium state with 9 inches elevation. In fact it is plausible that the column height would be sufficient to provide 1575 Pa capillary pressure at the top of the column. If this were the case it would be consistent with the principle of local capillary trapping. But being able to see and distinguish residual oil from 'not quite residual' oil in the imbibed region is impossible in this experiment. Proper quantification is not achieved.

3) The resistance against the liquid flow is due only to the bead packs. Permeability and capillary force from the porous media are assumed to be the only factors countering the flow of fluids. The apparatus itself (for example, the top cap, the size of the flow lines/valves, etc) does not provide any resistance to counter the applied pressure. This could potentially make the measured $P_{c\_entry}$ larger than the true value.

Figure 4.28 below is a graphical presentation of the same information as Table 4.1.

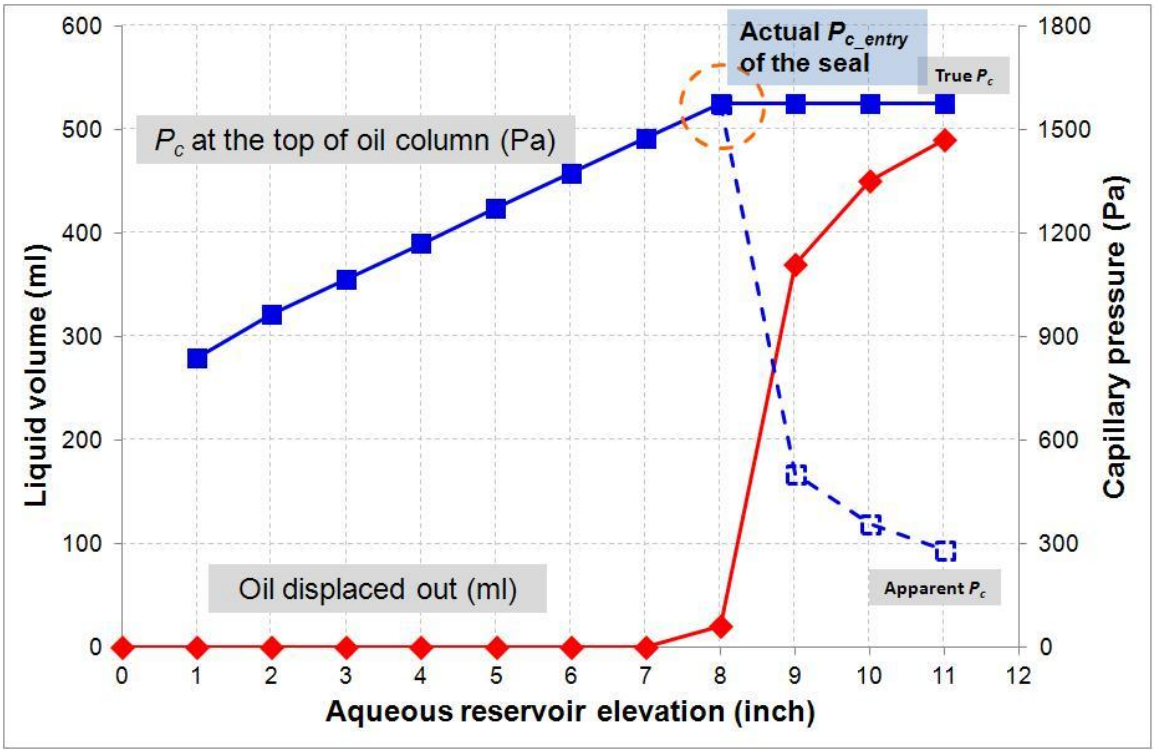


Figure 4.28: Response of a column of nonwetting phase, originally held within a local capillary trap with only buoyancy forces active (aqueous reservoir elevation = 0), as the effective capillary pressure is incremented by raising an aqueous reservoir connected to bottom of the apparatus. The capillary pressure at the top of the oil column (blue line) increases with each increment in reservoir elevation until the total elevation reaches 9 in, at which point some oil drains through the overlying fine beads, gets displaced out (red line) and reduces the column height remaining in the coarse beads. This provides an empirical estimate of the effective entry pressure of the "seal" (the layer of 0.25 mm beads) of about 1750 Pa (orange dashed circle), somewhat greater than the theoretical estimate based on bead size (1334 Pa, from Table 3.4).

As mentioned above, the capillary pressure on top of the accumulated oil column continues to rise as the aqueous reservoir is raised gradually. At 8 inches, the capillary

pressure reached its peak at 1575 Pa, which falls in between the theoretical and empirically determined (refer to Table 3.4) effective capillary entry pressure of the sealing layer of fine beads. The theoretical entry pressure of the fine beads is smaller than the empirical estimate. The theoretical value assumed mono-disperse bead size and a dense, perfectly disordered packing, which are unlikely to exist in the apparatus. The theoretical estimate also assumes the contact angle and interfacial tension are the same as inferred from experiments using these fluids and similar beads, discussed in previous reports. Deviations from these values have proportional effects on the capillary entry pressure.

When the capillary pressure at the top of the oil column exceeded the entry pressure of the fine beads, the accumulated oil column beneath the fine beads started entering the fine bead layer and escaping through the top of the apparatus. Because the system is open, the applied gradient in potential also caused blue dyed aqueous phase to enter the system continuously, and the escaped oil gets displaced out of the system and collected separately. This explains the jump in oil displaced out between 8 inches and 9 inches in Figure 4.28.

The peak capillary pressure of 1575 Pa is a good estimate of the effective value of the threshold capillary pressure of the fine bead layer. After this pressure is exceeded, oil column trapped beneath decreased in height; hence the apparent exerted capillary pressure decreased. Based on the apparent oil column height, the capillary pressure decreased to a value considerably smaller than the entry pressure value (1575 Pa). A possible explanation for this is that the imbibition process at the bottom of the oil column was ignored (refer to assumption (2) about Table 4.1).

The remaining oil in the trap stayed secure for a long time at this particular hydraulic potential / capillary pressure gradient (Figure 4.29).

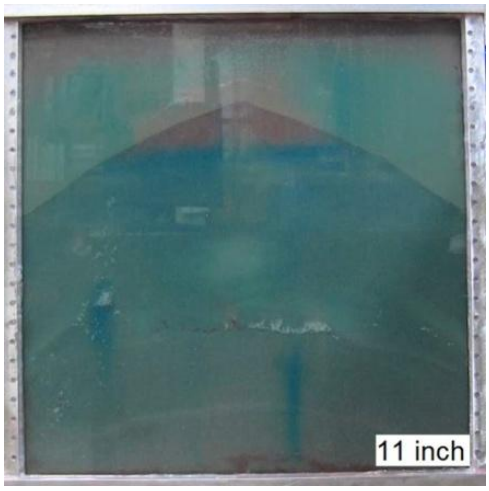


Figure 4.29: The remaining oil in the capillary trap stayed secure for another 33 hours, while the aqueous reservoir was kept 11 inches above the top of the domain.

To further test whether the persistence of the oil beneath the sealing layer of beads is truly dependent on capillarity, the aqueous reservoir is lowered to the original position (the same level as the top of the domain); the collecting reservoir was raised 5 inches higher and a flow line was established from the base of the collecting reservoir to the top ports of the experiment apparatus (replacing the initial outlet line). If any liquid were to flow from the reservoir back into the system at such low height, it would have indicated that the capillary seal was being bypassed and there must have been a connected column for liquids (oil + aqueous phase) backflowing. The results showed that no back flow occurred (Figure 4.30 below), which indicated that the persistence and flow of liquid in the domain are solely controlled by capillarity. In other words, the fine beads act like a check valve, allowing the displacement of oil from the coarse beads into the fine beads only when the capillary pressure exceeds a threshold. The imposition of gradients in hydraulic potential caused viscous flow of connected volumes of fluid, but the viscous

flow is not the cause of the oil displacement from the coarse beads. Rather, the viscous flow is one manifestation of the imposed gradient in hydraulic potential, and the increased capillary pressure gradient is another manifestation of the same imposed gradient. Only the latter affects the oil displacement in this experiment. Figure 4.30 below explains this.

Figure 4.30: The aqueous reservoir connected to the bottom was brought back to the original position (the same level as top of the domain) while the oil collecting reservoir was raised 5 inches higher to drive backflow of oil along connected pathways into the apparatus and into the accumulation remaining in the coarse beads beneath the fine beads. In the absence of such a pathway, no change in the oil accumulation is expected. No back flow occurred, confirming that the oil displacement from the coarse beads into the fine beads is controlled by capillary pressure, not by viscous fluid gradients.

**Key learnings from Experiment 9:**

1. Systematically proved the persistence of local capillary trapping.

2. Initiated quantification process of experimental parameters, such as volume of oil displaced out and capillary pressure exerted by the oil column, for which more accurate experimental results could be obtained and explained in future experiments.

3. Established experimental protocol to measure the actual entry pressure of any given capillary barrier / seal. This protocol, if studied and improved further, could be potentially developed into a method that could possibly measure and test the limit of any given capillary seal, which is very important in actual $CO_2$ sequestration and storage processes since the total capacity of the storage could be estimated by better understanding about the seal/caprock.

**Experiment 10**

**(0.25 mm, 0.5 mm and 2 mm, multiple anticline-shaped seal, fill and spill, <u>open state</u> when rising oil was injected from a point source, artificial fracture in the seal)**

**Objective: demonstrate persistence of LCT when a fracture is developed in the seal**

The objective of experiment 10 was to demonstrate how a fracture, or leakage pathway, in the caprock could affect the locally trapped $CO_2$ beneath adjacent capillary barriers. To mimic the storage condition in nature, Experiment 10 was designed to show the injection and post-injection during storage in an open system, whose hydraulic potential was always kept constant. The following Figure 4.31 and Figure 4.32 show the schematics of the experiment.

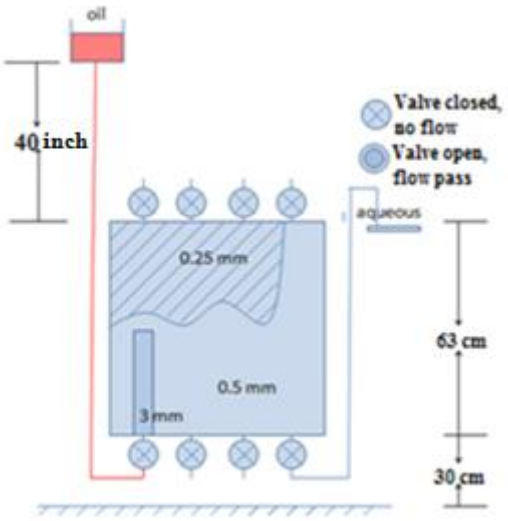


*These lengths are not to scale

**(a)**

Figure 4.31 (continues to next page)

(Figure 4.31 continued)

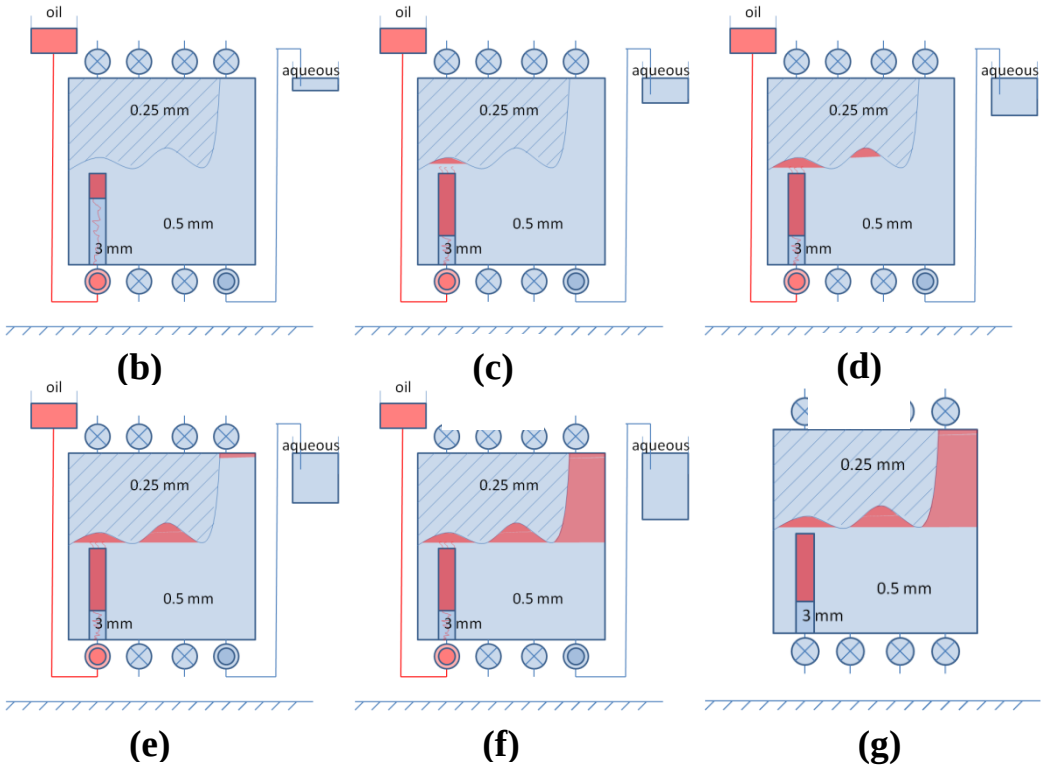


Figure 4.31: Experiment 10 schematics, part 1 – drainage, fill and spill. **(a)** Initial setup of the experimental apparatus. Oil reservoir is elevated to provide positive potential to force entry into system when valve is opened. **(b)** Oil enters the bottom left ports, and first fills up the 3 mm bead column whose capillary entry pressure is least. Aqueous phase leaves the system through the bottom right port. **(c)** Oil continuously fills up the 3 mm column until the accumulated oil column exerted a higher capillary pressure than the 0.5 mm beads entry pressure; oil started filling up the first trap beneath the seal formation. **(d)(e)(f)** "Fill and spill". After the first trap was completely filled, oil continues to enter the domain, driven by buoyancy, migrates to the adjacent traps and fills them. **(g)** When all the traps are completely filled, all valves are closed.

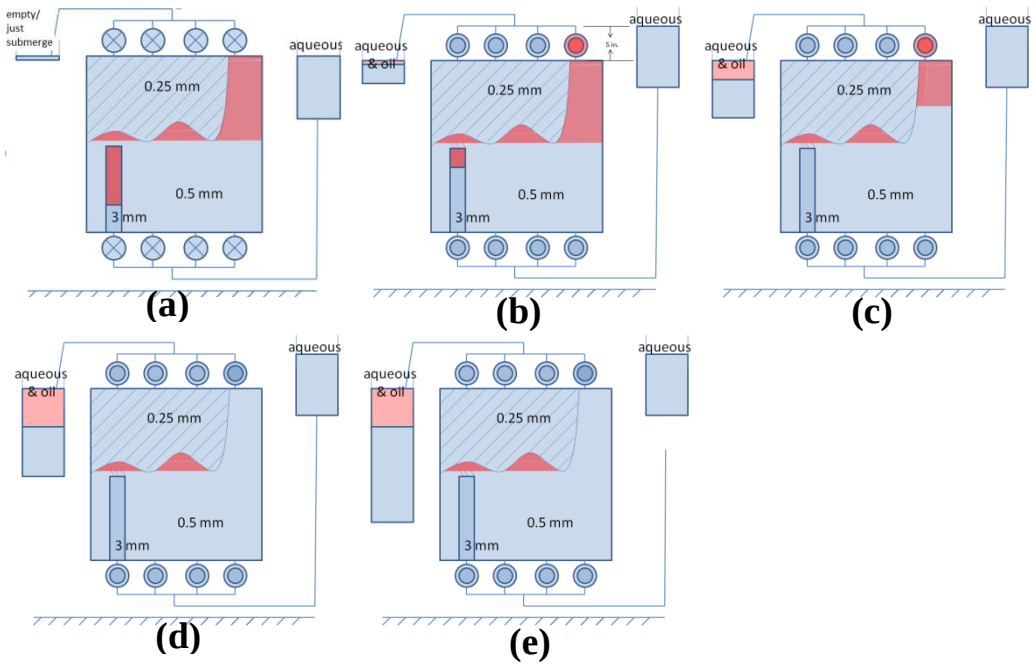


Figure 4.32: Experiment 10 schematics, part 2 – imbibition when a model fracture induced in the caprock. **(a)** System was connected to two reservoir kept at the same height as the top of the domain to maintain a constant hydraulic potential. **(b)** Open all valves, so the aqueous phase could go into the system from the bottom. The reservoir connected to the bottom was raised 5 inches higher to facilitate flow. **(c)(d)(e):** The accumulated oil in the uppermost "trap" is held back only by the closed valve of the top right port, so opening the valve mimics creation of a fracture through the "seal". Oil is displaced out completely, while the oil in the adjacent traps is expected to remain intact. Aqueous phase continuously enters the system from the bottom as oil and aqueous phase leave through top ports to the collecting reservoir.

The actual experiment was conducted by following the schematics. The 0.25 mm beads serve as the seal formation, 0.5 mm beads serve as the store, and the 3 mm coarse bead column is to direct flow of the nonwetting phase into the capillary trap. After

packing, the entire domain was saturated with aqueous phase. 180 degree rotation is not needed, as the nonwetting phase is directly injected from the bottom of the domain from the beginning.

The 1st attempt proved the experiment set up successful, but the results were complicated by edge effects due to prolonged experiment time. So the experiment was repeated to mitigate the adverse impact. Results from both attempts are summarized in the following sections.

***Experiment 10, 1st attempt***

The actual experiment result resembles the expectation of Figures 4.10.1 and 4.10.2. The following Figure 4.33 shows the results in the first stage of the experiment.

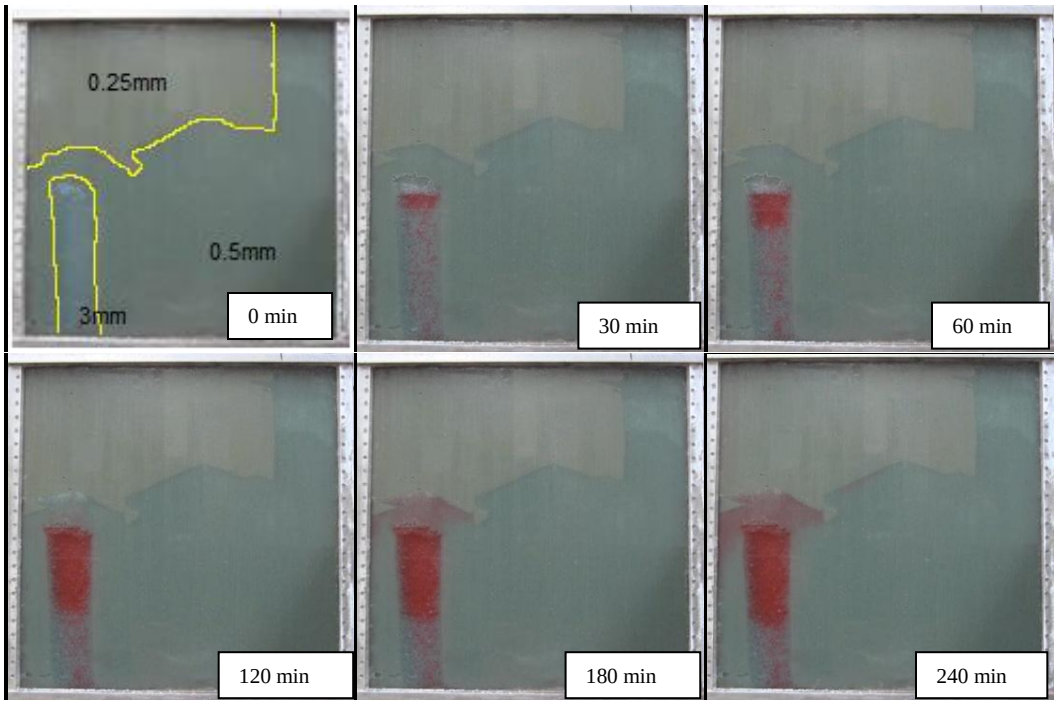


Figure 4.33 (continues to next page)

(Figure 4.33 continued)

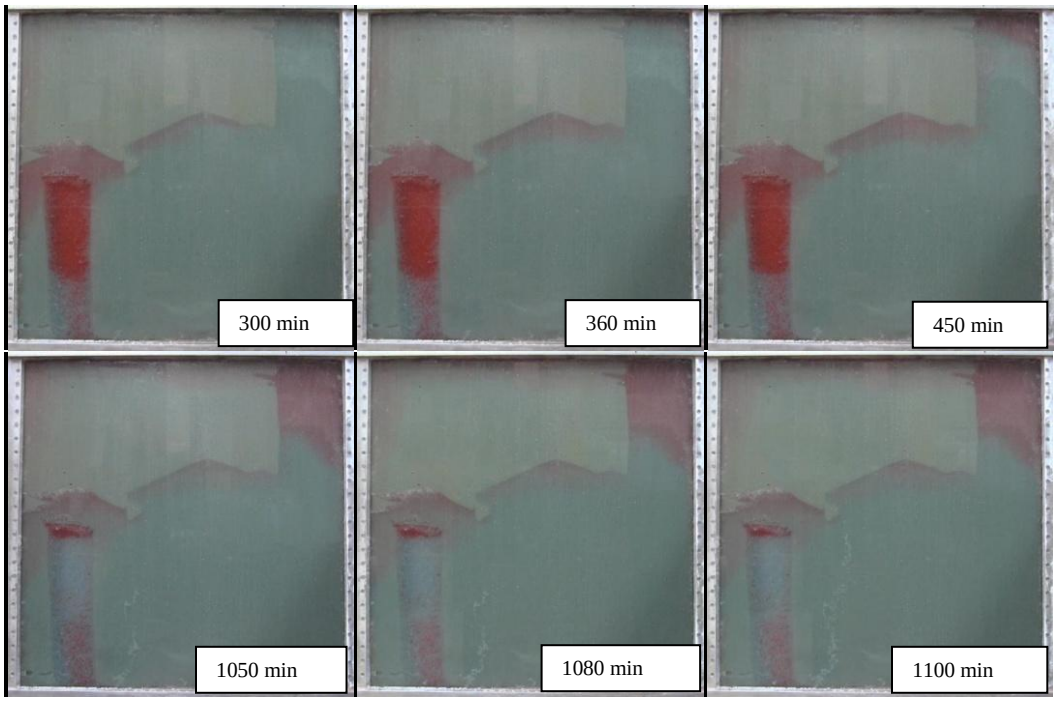


Figure 4.33: Experiment 10, 1st attempt results, part 1 – drainage, fill and spill. Only the bottom left most and bottom right most valves are open to oil and to aqueous phase, respectively (cf Fig. 4.10.1).

The red dyed oil enters the system from the bottom left ports, displacing aqueous phase through the bottom right most port. The rising oil fills the 3 mm column, followed by the first trap in 0.5 mm region, then second, then the last trap which connected to the top right port (serving as an artificial fracture). Between 450 minutes and 1050 minutes, edge effect becomes apparent, such that the oil in the 3 mm column escaped and flowed along the left side of the domain all the way to the top of the system. But the oil in the traps remained relatively intact.

At 1100th minute after starting the experiment, injection of oil stopped since the trap on the top right corner has been mostly filled. The next phase of the experiment, imbibition of aqueous phase, was then initiated. All valves opened, and blue dyed

aqueous phase entered from the bottom, displacing liquids (oil and aqueous phase) out of the system through the top. Results are shown in the following Figure 4.34.

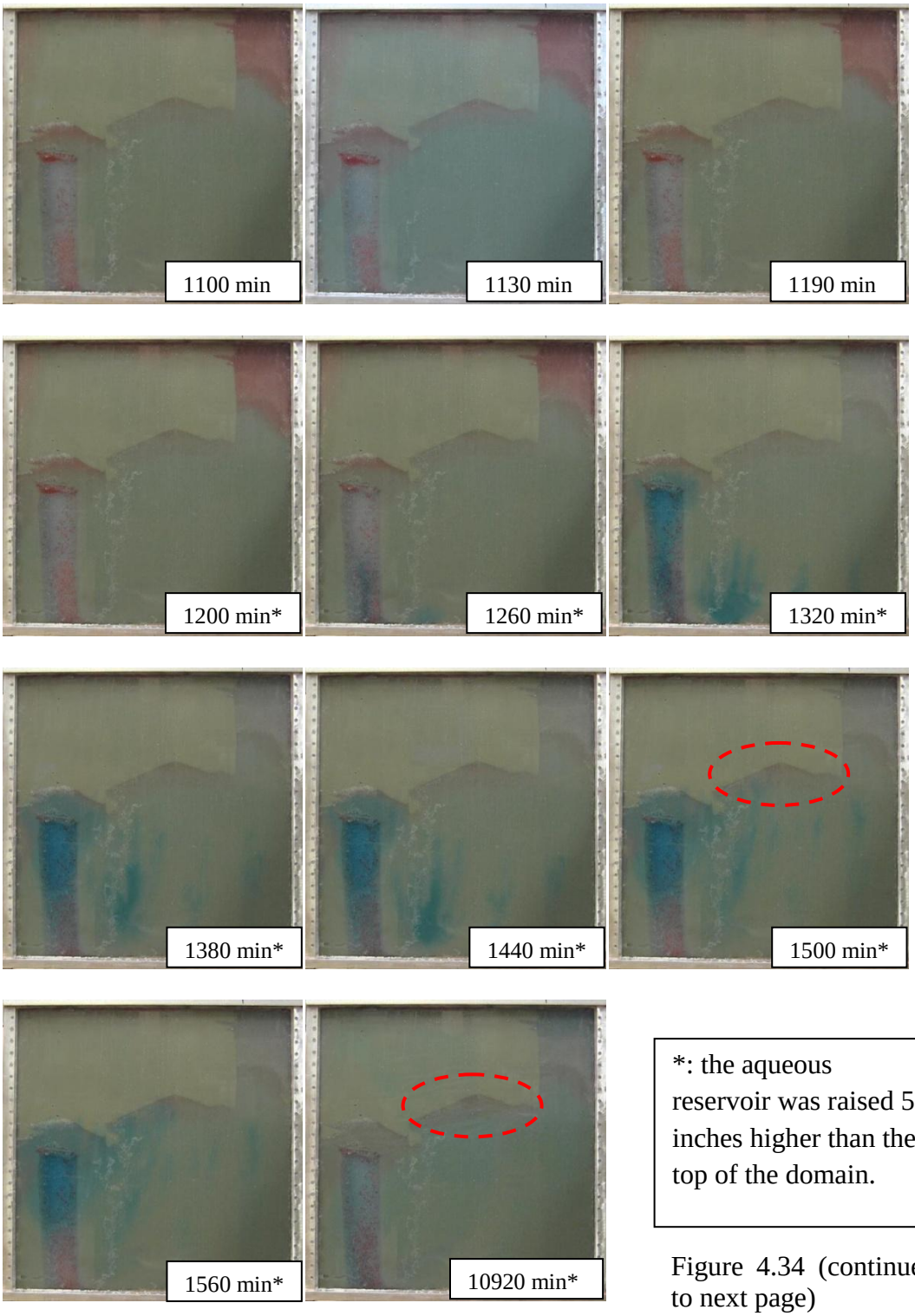


*: the aqueous reservoir was raised 5 inches higher than the top of the domain.

Figure 4.34 (continues to next page)

Figure 4.34: Experiment 10, 1st attempt results, part 2 – imbibition when a simulated fracture induced in the caprock. All valves are open, aqueous reservoir which is connected to the bottom of the domain was kept at the same height as top of the domain to provide constant hydraulic potential. There was no flow for the first 90 minutes, so the aqueous reservoir was raised 5 inches higher to provide a larger potential and to facilitate the flow of blue dyed aqueous phase into the system. At 1440 minutes, the reservoir was lowered to its original position. Finally the system was left for a week, during which no change was observed. The * marks in the time insets indicate that the aqueous reservoir was raised 5 inches higher than then top of the domain to facilitate the flow.

As we can see, the imbibition of blue dyed aqueous phase displaced oil out of the system. While open, the top right port served as an artificial fracture in the capillary seal, through which the accumulated oil escaped via this leakage pathway under pressure exerted by the imbibition.

After all the oil accumulated in the top right trap escaped through the "fracture", a significant amount of oil still remained in the middle trap (indicated by red circle). The system was then left for a week and observed for movement of the fluids. Eventually, the accumulated blue aqueous column in the 3 mm region completely dissipated and distributed to the entire domain. The locally trapped oil remains intact in the middle traps. This shows that even if a fracture occurred in the caprock/seal after storage, it would not affect the stored nonwetting phase in the adjacent traps. This is very important in ensuring the security of stored $CO_2$ in actual aquifers.

**Significance of Experiment 10, 1st attempt:**

1. This experimental procedure better mimics the injection and post-injection stages of a storage process. Experiment 10 didn't require a "flipping" stage. The original line source from the bottom could now be transformed to a "point" source. This offers a better analogy to the storage condition, from the moment of injection to post injection.

2. The complex geometry of heterogeneity / capillary barrier systems can be achieved in the relatively simple experimental apparatus. Basically we can mimic natural depositional patterns in our own sedimentary strata.

3. The fracture in the caprock has little to no effect on retaining nonwetting phase in adjacent capillary traps. This is especially important to the security and total capacity of a site selected for $CO_2$ sequestration and storage.

***Experiment 10, 2nd attempt***

Due to apparent edge effect between 450th minute and 1050th minute the 1st attempt of Experiment 10, most of oil in the 3 mm column had escaped to the top of the domain. In order to avoid the edge effect and to better understand the flow pattern of the uprising oil, 2nd attempt was made with the same arrangement of beads, except the total experiment time was limited to less than 9 hours to minimize the opportunity for edge effects to affect the behavior. The beads used in 1st attempt were discarded. New beads were used to replicate the arrangement for 2nd attempt, thus to keep the domain initial saturation condition consistent.

Initially the aqueous reservoir was placed 40 inches higher than the top of the domain and connected to the bottom of the domain, such that aqueous phase was injected into the system by gravity and thereby saturated the dry porous media. The entire filling up process took about 1 hour. Upon saturation, the aqueous phase imbibes into regions of finer beads faster. This is expected as the smaller the bead size, the larger the capillary pressure, therefore the higher the saturation front will rise compared to its position in adjacent larger beads. Figure 4.35 below illustrates this process.

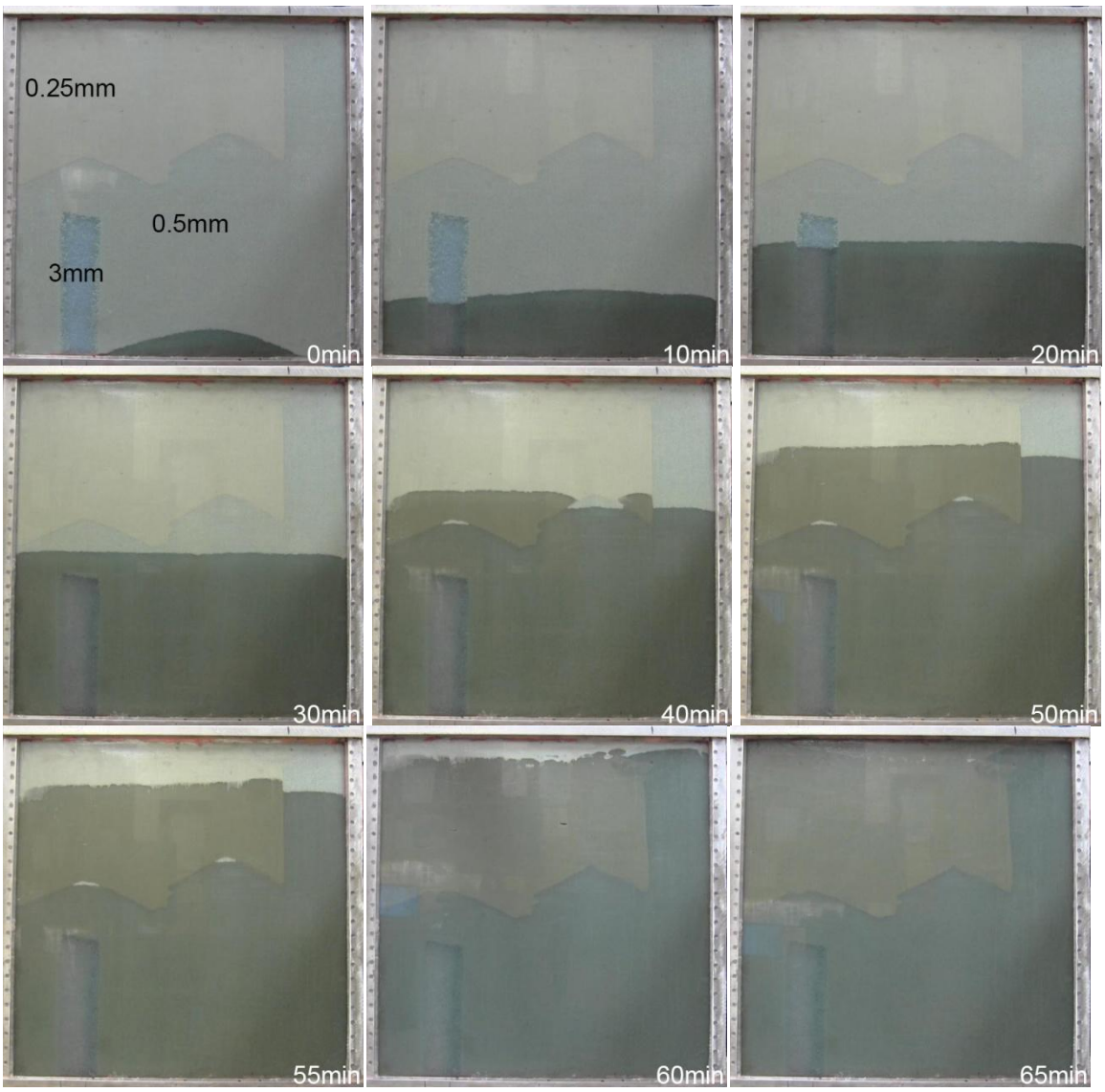


Figure 4.35: Filling up (initial imbibition with aqueous phase displacing air) of Experiment 10, 2nd attempt.

The initial saturation step was then followed by drainage, where the oil reservoir was placed 40 inches higher than the top of the domain and connected to the bottom left valve (as indicated in Figure 4.36). The nonwetting oil phase therefore was injected into the system via gravity. The bottom right valve was open to allow displaced water to leave the system. The other valves remained closed.

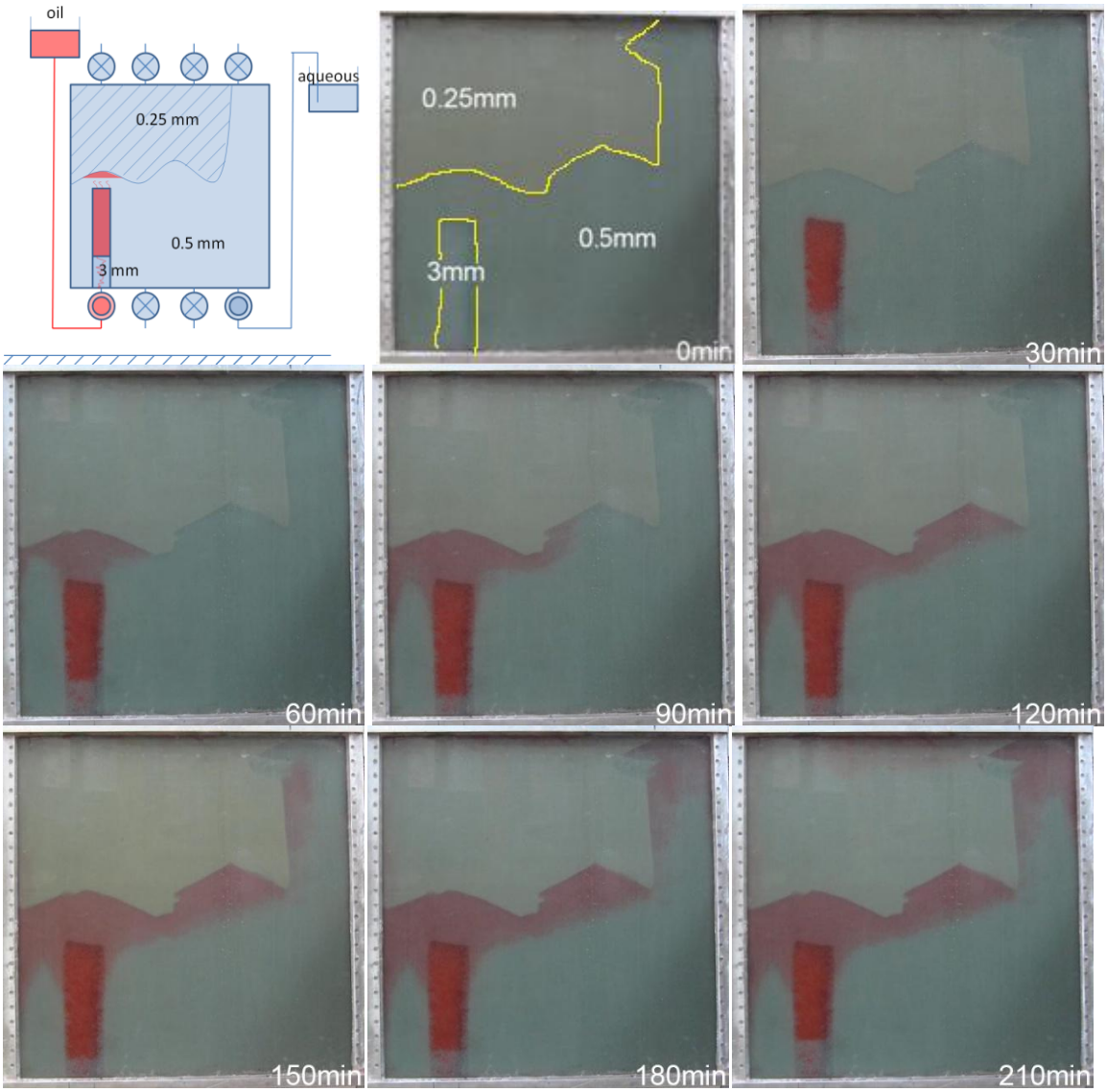


Figure 4.36: Drainage process of Experiment 10, 2nd attempt.

Red dyed nonwetting oil phase first entered the system, and rose along the 3 mm bead column. Due to the relatively large bead size, 3 mm bead column has the smallest capillary entry pressure, therefore served as a preferential flow path for the rising buoyant oil phase. The nonwetting phase reached the 0.5 mm region, and due to higher entry pressure of the 0.5 mm region than the 3 mm region, oil started to accumulate beneath the

0.5 mm region and in the 3 mm column. The nonwetting phase accumulated to a height where its effective capillary pressure exceeded the entry pressure of the 0.5 mm. The nonwetting phase broke through the 0.5 mm region, and started to enter the first capillary trap on the left, which was an anticline-shaped region beneath a capillary barrier made of 0.25 mm beads.

The 0.25 mm bead pack has a capillary entry pressure of 1735 Pa, which could hold up to about 50 cm nonwetting phase column accumulated beneath it. But the nonwetting phase trapped beneath the barrier in this experiment would never reach such height, because it "spilled" to adjacent traps on the right when the first trap was completely filled. This "fill and spill" propagated to the rightmost "trap", a region of 0.5 mm beads continuous all the way to a valve at the top of the domain. The seal for this "trap" is a closed valve, not a capillary barrier, so it differs qualitatively from the local accumulations at the left side and middle of the domain.

A total of 650 ml of oil had been injected into the system; the same volume of aqueous phase was displaced out. Then all valves were closed. The oil reservoir connected to the bottom of the domain was replaced by an aqueous reservoir, and connected to all four valves from the top. The bottom valves were connected to another aqueous reservoir (please refer to following Figure 4.37). Both reservoir liquid levels were kept at the same height as the top of the domain. When the valves were open, these two reservoirs provided hydrostatic pressure gradient to the system, by means of which an open boundary system similar to Nature was mimicked.


Figure 4.37 (continues to next page)

Figure 4.37: Imbibition under hydrostatic potential of Experiment 10 2nd attempt. All liquids displaced out of the domain were collected in a measuring cylinder (on the left hand side of each image). The continuous liquid in the exit line terminates at the same height as the top of the domain, but above the oil level in the collection measuring cylinder. By examining the volume in the cylinder at different point of time, the rate of displacement/injection can be calculated.

The nonwetting phase has a smaller density, therefore the pressure gradient in the apparatus was smaller than the one provided by the aqueous reservoir, hence blued dyed water entered the system through all four valves at the bottom and less dense oil rose and tended to leave the system from the top. A large amount of aqueous phase entered the system through the valve at the bottom left corner because of the lowest capillary entry pressure of the 3 mm bead column. The aqueous phase first displaced out the trapped oil phase in the 3 mm column, and then displaced a portion of trapped phase in the first capillary trap on the left. A significant amount of oil was still trapped beneath the capillary barrier. Due to the persistence of local capillary trapping mechanism, the moving aqueous phase could not displace all oil out of the first trap, and moved to adjacent trap to displace oil out there.

The top right trap was directly beneath a valve, which served as a leakage pathway when opened. It mimicked the breaching seal situation. As we can see in the above Figure 4.37, almost all accumulated oil phase in the right most trap was displaced out of the system through the top valves, leaving only residual oil. But the mobile nonwetting phase in the adjacent traps remained undisturbed. Notice that only oil has been displaced out to this time (note level in the measuring cylinder).

The system reached equilibrium at around 360th minute, as no more aqueous phase entered and no more oil left the system. At 860th minute, the measured displaced

oil out of the system is 520 ml, meaning there were 130 ml oil still remained in the system securely. This demonstrated the persistence of local capillary trapping under constant hydraulic potential.

In order to further test the persistence of local capillary trapping under forced imbibition, at the 1590$^{th}$ minute the aqueous reservoir connected to the bottom was raised 5 inches higher, by means of which the capillary pressure gradient across the domain was increased and a hydraulic potential gradient was established. Therefore aqueous phase again flowed into the system. See Figure 4.38 below.

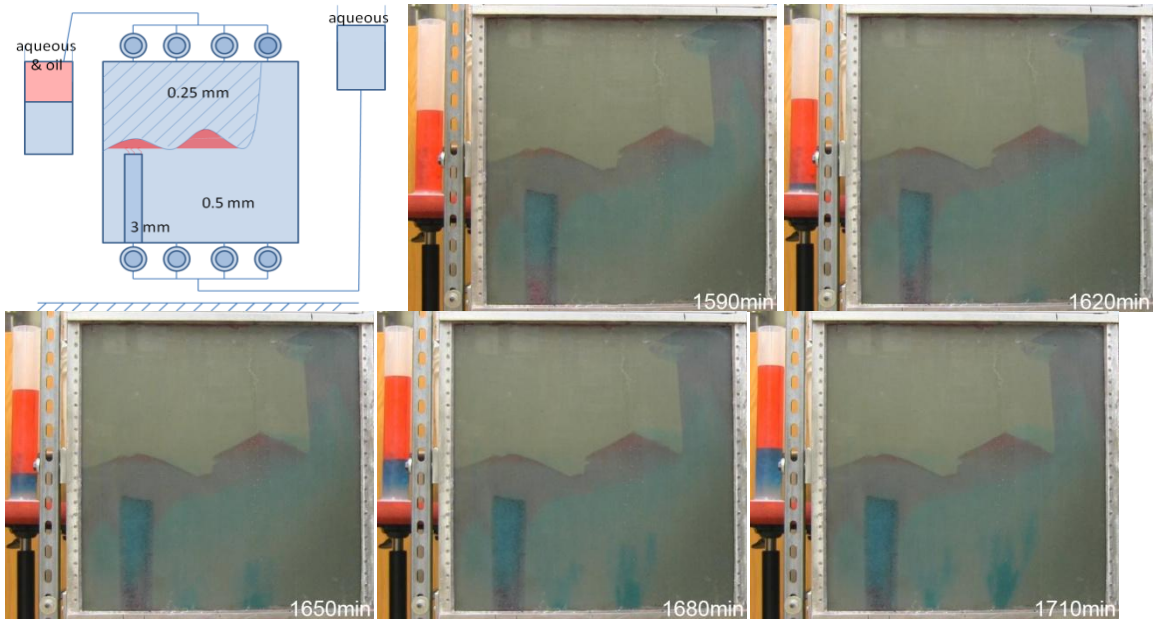


Figure 4.38 (continues to next page)

(Figure 4.38 continued)

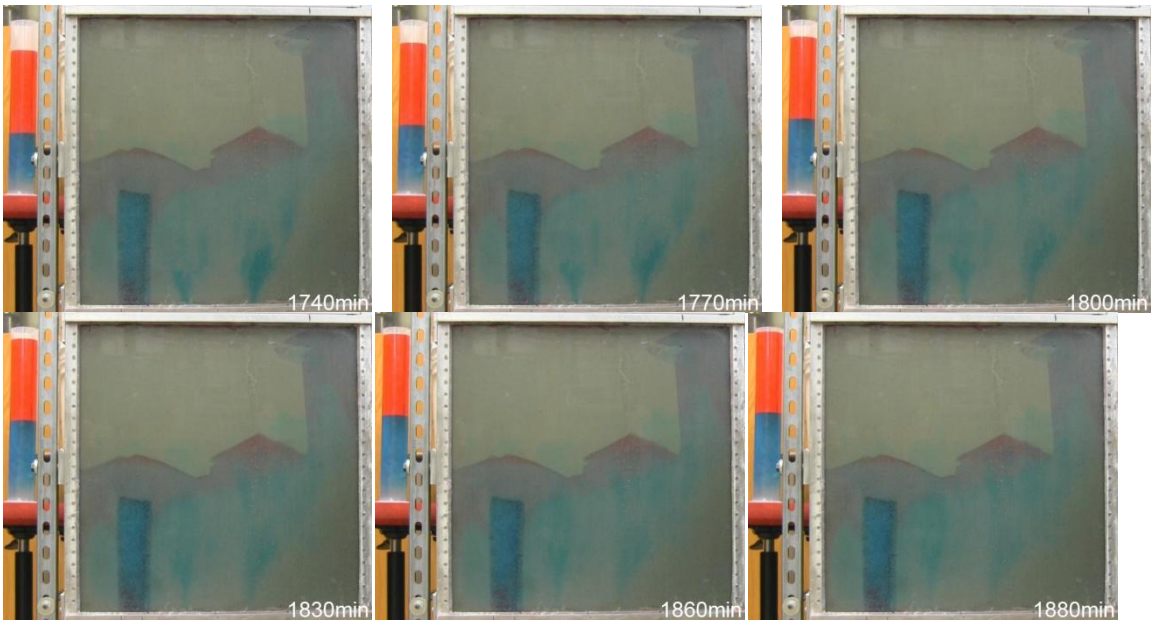


Figure 4.38: Forced imbibition in open boundary system with a higher applied hydraulic potential, Experiment 10, 2nd attempt.

Although the aqueous phase again flows into the system, the oil trapped beneath capillary barriers remained intact. As we can see from Figure 4.38 above, only water is displaced out of the system, the volume of displaced oil (in the cylinder on the left) remained constant.

**Significance of Experiment 10, 2nd attempt:**

1. This is the first ever unequivocal experimental evidence on persistence of local capillary trapping. It demonstrated that Local Capillary Trapping mechanism remains persistence even under forced imbibition. The persistence could be potentially predictable or even quantified if we successfully manipulated the boundary conditions by changing the hydraulic potential / capillary pressure gradient across the system.

2. Majority of the buoyant mobile phase trapped beneath capillary barriers will remain secure in the case when the caprock integrity is compromised. The breach or fracture in the caprock will serve as a leakage pathway for the mobile phase trapped directly beneath it. But mobile phase in adjacent capillary traps will remain undisturbed. This discovery provides strong support for the safety and security of storing $CO_2$ via local capillary trapping mechanism.

3. It shows some clues for quantifying the total $CO_2$ storage capacity in the formation. A sample quantification process for Experiment 10 is shown below:

Experimental value:

Total injected oil volume in the drainage = 650 ml

Total displaced oil volume at the end (when system reached equilibrium) = 520 ml

Total oil volume remained in the domain permanently = 650-520 = **130 ml**

Calculated value:

Inner dimension of the experiment apparatus (glass box) = 63 cm × 63 cm × 2.54 cm = 10080 ml.

Assume a 0.35 porosity of all beadpack regions, so the total pore volume available = 10080 ml × 0.35 = 3530 ml.

Initial pore volume fraction occupied by oil = 3530 ml / 650 ml = 0.184

By observation (read from picture, end of drainage), initial total fractional area of oil occupation to the entire domain is about 0.25.

Assuming that oil displaces aqueous phase down to an irreducible saturation of about 20%, this is reasonably consistent with the calculated value in previous step, i.e. 0.25 × (1- 20%) = 0.20 ≈ 0.184.

Total pore volume occupied by oil = 3530 ml × 0.25 = 882 ml.

Initial oil saturation = 650/882 = 0.74 (this suggests $S_{w,irr}$ = 0.26)

Final oil saturation = 130/882 = 0.15

At the end of imbibition, assume fraction of oil in capillary traps (anticlines) = 0.1, fraction of oil in residual = 0.9,

The amount of oil trapped in the capillary traps = 0.1 × 882 × 0.74 = 65 ml

Assume irreducible oil saturation of the domain = 0.1,

The amount of oil in residual after imbibition = 0.9 × 882 × 0.1 = 80 ml

About 30 ml oil trapped at the top of the domain (in between the seal and top cap of the ant-farm, invisible),

So the total amount of oil left in the system = 65 + 80 + 30 = **175 ml**

The discrepancy between the calculated value (175 ml) and actual experimental value (130 ml) is likely due to inaccurate estimation of porosity of the porous media as well as the area of oil saturation.

# Chapter 5 Conclusions and Recommendations

## 5.1 Conclusions

A variety of heterogeneous porous media made of a range of sizes of loosely packed silica beads are used to validate and test the persistence of local capillary trapping (LCT) mechanism. By adjusting the boundary conditions (fluid levels in reservoirs attached to top and to bottom ports of the apparatus; fluid gradients), the capillary pressure gradient across the domain was manipulated, such that the capillary pressure exerted by the accumulated nonwetting phase column against the capillary barrier was also varied. Experiments were conducted with and without the presence of fracture/potential leakage pathway in the capillary barrier.

The buoyancy driven migration path of the non-wetting phase is significantly influenced by the heterogeneity of the domain. The uprising non-wetting phase plume will selectively fill up the regions with smaller capillary entry pressure (patches, layers or columns made of coarse beads) first, and accumulate beneath the capillary barrier (regions made of fine beads).

Besides heterogeneity, the boundary conditions of the domain also play a crucial role in determining the migration pattern of the immiscible fluids.

i) Closed boundaries which result in counter current flow. In this situation the less dense non-wetting phase rises and the denser wetting phase sinks to fill space originally occupied by the nonwetting phase (Experiment 1 and 2, and part 1 of Experiment 3-8). The effect of this flow regime on LCT is that the top closed valves may aid trapping of fluid by acting as a truly impermeable barrier. So the estimated trapping capacity of the capillary barrier may be larger than the true value.

ii) Open boundaries and hydrostatic gradient which result in counter current flow (Experiment 9). The denser aqueous fluids more easily sink to fill space vacated by the rising nonwetting phase, rather than flow up and out of the system. The effect of this flow regime on LCT is that the down-sinking wetting phase will compete with uprising nonwetting phase for space beneath the capillary barrier, resulting in less volume of trapped nonwetting phase.

iii) Open boundaries and imposed gradients in potential which result in co-current flow. Here the non-wetting phase rises and displaces aqueous phase out of the domain through the top ports. When the hydraulic potential gradient across the domain is increased, either by lowering the ends of the exit tubing from the top domain (part two of Experiment 4) or elevating the aqueous reservoir connected to the bottom (forced imbibition of Experiment 5-10), the wetting and nonwetting phases would flow in the same direction (from bottom to top) in the domain. The effect of this flow regime on LCT is that only the seal is responsible for trapping the uprising nonwetting phase. Forced imbibition results show that trapped nonwetting phase escaped through the barrier due to increased capillary pressure gradient, for which the volume of trapping is smaller but still nonzero.

In addition to domain heterogeneity and boundary conditions, the modes of migration of the nonwetting phase also influence the results. In experiments where a "flipping" of the experiment apparatus is carried out to initiate the buoyancy-driven displacement, the nonwetting phase rises almost as a line source from the bottom of the closed-boundary domain immediately after flipping. In open-state experiments where no

flipping is needed, the nonwetting phase was "injected" from an external reservoir through bottom ports via gravity, similar to point sources. In both cases ("flipping" vs. "injection") the fine bead layer acted as a capillary barrier to trap the uprising nonwetting phase. However, "injection" mode is more analogous to practice in which $scCO_2$ is injected through wells and subsequently rises in a storage aquifer. In the open-boundaries "injection" mode, the capillary barrier is the only one responsible for trapping the mobile nonwetting phase; while in the closed-boundaries "flipping" mode, the closed top valves may aid or influence trapping, potentially introducing an artefact not present in the natural system.

The trapped buoyant phase remained secure beneath the local capillary barriers, as long as the effective capillary pressure $P_c$ exerted by the trapped phase (proportional to column height of the phase) is smaller than the capillary entry pressure $P_{c\_entry}$ of the barrier. Migration of buoyant phase through defects in the barrier such as cracks or gaps occurs when the effective capillary pressure exceeds the entry pressure of those defects. Migration of buoyant phase past the barrier occurs when the effective capillary pressure at the boundary between porous medium and wall of apparatus exceeds the entry pressure of the pores at the bead/wall boundary. These observations apply for hydrostatic gradients, for which the effective capillary pressure of a column of nonwetting phase of height $h_{nw}$ is given by $P_c = (\rho_w - \rho_{nw})gh_{nw}$, and for imposed gradients in potential applied to the aqueous phase, for which the effective capillary pressure of a column of nonwetting phase is given by $P_c = P_{c\_gradient}\ h_{nw} = [\rho_w(1+h_{w\_reservoir\_elevated}/h_{domain\_vertical}) - \rho_{oil}]gh_{nw,}$ where $h_{w\_reservoir\_elevated}$ is the level of aqueous reservoir being elevated and $h_{domain\_vertical}$ is the vertical length of the domain (in this thesis, 2 ft). The calculation for $P_{c\_gradient}$ has been shown at the end of Experiment 8 in Chapter 4.

The amount of nonwetting phase held in local capillary traps is proportional to the column height, so the extent of local capillary trapping is proportional to the entry pressure of the local barriers. Testing this statement for different barriers was not possible in this work as local barriers were always constructed with 0.25 mm beads. However a corollary of this statement was demonstrated in several experiments: if defects extend through the barrier, and thereby reduce the capillary entry pressure at one or more locations, then buoyant phase will not be held under the barrier below these defects.

Orientation of boundaries between regions affects the local trapping behavior. Laterally continuous boundaries serve as good barriers, while vertical bead boundaries serve as a connection between trapped regions and became the preferential paths for migrating flows. Greater lateral correlation length will yield more local trapping: In Experiment 2 which has the longest lateral correlation, all non-wetting fluid gets trapped, but not in Experiment 1 and 3.

Mimicking a seal breach by opening top and bottom boundaries after steady state migration ended yielded following results. When hydrostatic potential was applied, majority of the buoyant mobile phase trapped beneath capillary barriers remained secure. The breach or fracture in the seal/caprock served as a leakage pathway for the mobile phase trapped directly beneath it. But mobile phase in adjacent capillary traps remained undisturbed (refer to part two of Experiment 5 and Experiment 10). The implication is storing $CO_2$ via local capillary trapping mechanism should be secure, since the actual storage aquifers will be at hydrostatic equilibrium, i.e. the hydraulic potential will be constant with depth.

To demonstrate that LCT holds the nonwetting phase at above-residual saturation, the top and bottom boundaries were opened after the nonwetting phase had reached equilibrium state under the closed boundaries. Imposing an upward gradient in hydraulic

potential displaced a significant fraction of the non-wetting fluid out of the local traps. Explanations of the nonwetting phase escape are listed below.

i) In some experiments (example: part 1 of experiment 5, part 2 of Experiment 3 and 6), the displaced fluid was not really in the capillary trap in the first place and was held only by the top closed valves, not by the capillary barriers. So when the top valves are open, this volume of non-wetting is "flushed" out by the newly entered wetting phase at higher potential. This trapping could not be classified as LCT.

ii) In some experiments (example: Region G and H in Figure 4.8 and Figure 4.9, Experiment 3), the remaining trapped nonwetting phase was held by or near a region with smaller $P_{c\_entry}$ than expected. This is because air was in the indicated region and resulted in an undesired three-phase interaction (the research work presented here focuses on two-phase flow). This makes it impossible to determine whether the region would have functioned as LCT in the absence of the air phase.

iii) In other experiments (example: Experiment 8 and 9), initially the nonwetting phase was held beneath the capillary barriers whose $P_{c\_entry}$ is larger than the $P_{c\_oil\ column}$. In this case, when a higher hydraulic potential was applied and $P_{c\_oil\ column}$ reached and exceeded the threshold pressure ($=P_{c\_entry}$), the trapped nonwetting phase invaded into the seal and escaped. This is predicted by LCT and is a strong evidence for persistence of LCT mechanism.

The extent of LCT persistence satisfies the following condition:

$$\boldsymbol{P_{c\_entry}}\,(\boldsymbol{capillarybarrier}) \geq \boldsymbol{P_{c}}\,(\boldsymbol{top\ of\ oil\ column}) = P_c\ gradient \times h_{accumulated\ oil\ column}$$

where $P_{c,gradient} = P_{o,gradient} - P_{w,gradient}$, the base of the oil column is assumed to be at zero capillary pressure and the aqueous phase pressure gradient can be hydrostatic or greater than hydrostatic.

The experiments conducted at imposed potential gradients larger than hydrostatic serve to demonstrate that above-residual trapping occurs. Forced imbibition and larger-than-hydrostatic $P_c$ gradient are not expected in long-term $CO_2$ storage. Therefore, the practical implication of these experiments is to prove that local capillary trapping is capable of holding large saturation of stored $CO_2$ in safe long-term storage, because the accumulated non-wetting phase even survived larger-than-hydrostatic $P_c$ gradient.

This work provides systematic validation of a novel concept, namely the long-term security of $CO_2$ that fills local (small-scale) capillary traps in heterogeneous storage formations: this $CO_2$ remains held in these structures even if the integrity of the caprock is compromised during or after storage. The impact will be a potential reduction in risks associated with long-term storage security, achieved simply by considering the physical implications of geologic heterogeneity.

## 5.2 Recommendations and future works:

1. Continue seeking methods to reduce corner effects. As mentioned in previous sections of this thesis, flat walls create a low-entry pressure preferential flow path at the grain-wall contact where locally regular packing is forced by the flat boundary, such that the rising nonwetting mobile phase bypasses the capillary barrier. This adverse effect is amplified at the corners inside the experimental apparatus where two walls meet. One way to reduce the corner effect is to enlarge the corner angles such that the bead-wall contact is maximized. Figure 5.1 below illustrates this idea.

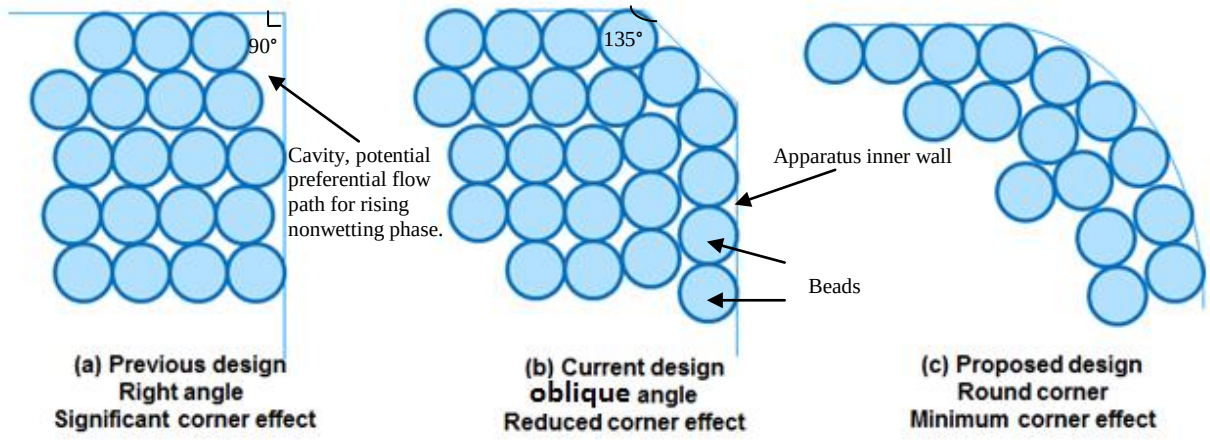


Figure 5.1: Top view of designs to reduce corner effects. Enlarging the corner angle of the experimental apparatus increases the bead-wall contact (b) and reduces the likelihood of cavities formed due to non-uniform packing (a), which serve as preferential flow path for rising nonwetting mobile phase. A smooth transition from one edge to the next (c) should further reduce likelihood of cavities.

Current modification of the apparatus (Figure 4.22) has successfully reduced the corner/edge flow by enlarging the corner angle from $90°$ to $135°$ through inserting diagonally cut aluminum bar at the corner. The future design should achieve round corner to minimize cavity formed.

Another way to reduce corner effect is to use smaller beads to fill up the corners/sides of the domain. Finer bead packs have lower permeability and higher capillary entry pressure. Therefore the rising nonwetting phase will not flow easily through corners/edges.

2. Pre-saturating the domain with wetting phase is strongly recommended for each experiment. Right after the initial dry packing of the beads, wetting phase is injected into the system via gravity and saturates the entire porous media. The initial wetting phase saturation of the entire domain should be 100%. This is very important because it gives the environment similar to the storage aquifer; so later when the non-wetting hydrocarbon phase is injected, it much resembles the situation in which non-wetting $scCO_2$ is injected in a water-wet saline aquifer initially filled with brine. Another reason for this pre-saturation with wetting phase is to prevent packing defects. Saturation of a dry-packed medium requires moving aqueous phase into the medium while air is displaced from the inter-granular spaces. Because aqueous phase is more polar than air, the water-saturated beads are 'pulled' closed to each other by this interaction. Therefore the entire porous medium will settle and leave a large empty space at top of the domain (between top cap and seal). It is very important to refill this empty space by adding more beads from the top of the domain, before the cap is secured. Otherwise when the rotation of the apparatus occurs in closed-boundary-condition experiments, beads will settle and leave a cavity in the porous media (see Experiment 4 & 5), which may hinder the final results. In the open boundary condition experiments where the rotation of apparatus is not required, filling up this top empty space with extra beads is still necessary. Otherwise the nonwetting phase escaped from the capillary barriers below may accumulate in the void space, instead of flowing into the outlet tubes and getting displaced out of system. This will lead to inaccurate estimation of the displaced liquid volume, thus negatively impact

the calculation for trapping capacity. During pre-saturation with aqueous phase, tapping an electric shaker on the wall of the glass containment box is recommended for more thorough settlement of beads inside, bringing firmer and more uniform packing of the porous medium. This will eliminate potential trapping of air bubble in the porous medium, and reduce corner/edge effect.

3. Better quantification methods. Up to this point, majority of the experimental work has been qualitative, in that presence or absence of nonwetting phase was indicated by color, but not quantitative in that saturations of nonwetting phase were not measured. Even though the total amount of oil entering the system and trapped by capillary barriers under open-boundary conditions could be measured, the saturation of nonwetting phase, and hence the amount of nonwetting phase trapping, at a particular time and in a particular region could not be determined. For better understanding and analysis, a method for quantifying the in-situ saturation should be deployed. Option one is to mix the mobile nonwetting phase with fluorescent dye and use light sensor to track the intensity of the moving nonwetting phase at each time each point. Option two is to use current pictures/video clips from experiments to perform an image analysis. Digital pictures of intensity of mobile nonwetting phase against time and position could be generated.

4. Analysis of forced imbibition at the bottom of oil columns in local capillary traps. It may be critical to account for capillary pressure at the oil/water contact at the end of drainage when the oil reaches an equilibrium configuration. This capillary pressure affects the capillary pressure at the top of the oil/water column, which in turn affects the interpretation of the persistence of LCT in forced imbibition experiments. The forced imbibition experiments change the capillary pressure at the top of the column, and when the capillary pressure at the top exceeds the barrier entry pressure and the oil leaks

through the barrier, the capillary pressure at the bottom of the column will also change as imbibition displaces oil from those pores.

5. Further investigation of the anticline-shaped seal/heterogeneity pattern with increased degree of heterogeneity. Previous works from simulation (Ganesh 2012) have suggested that, as the degree of heterogeneity in a storage domain increased, $CO_2$ migration patterns exhibited a spectrum of structures, from 'dispersed' capillary fingers with minimal rock contact to back-filled 'compact' distributions of saturation with much larger storage efficiency. A series of experiments using the bench scale set up would allow researchers to validate this predicted spectrum.

A proof of this concept has been conducted. The system consists of two distinctive sections, the 'seal' and the 'store', each made of a range of sizes of loosely packed silica beads which are mechanically and evenly mixed with prescribed composition. Instead of mono-distributed bead size in each section (as in the experiments reported in this thesis), polydisperse beads were used. This arrangement is a better approximation of naturally occurring storage formations, which have wider pore size distributions than are found in monodisperse bead packs.

A preliminary result appears in Figure 5.2

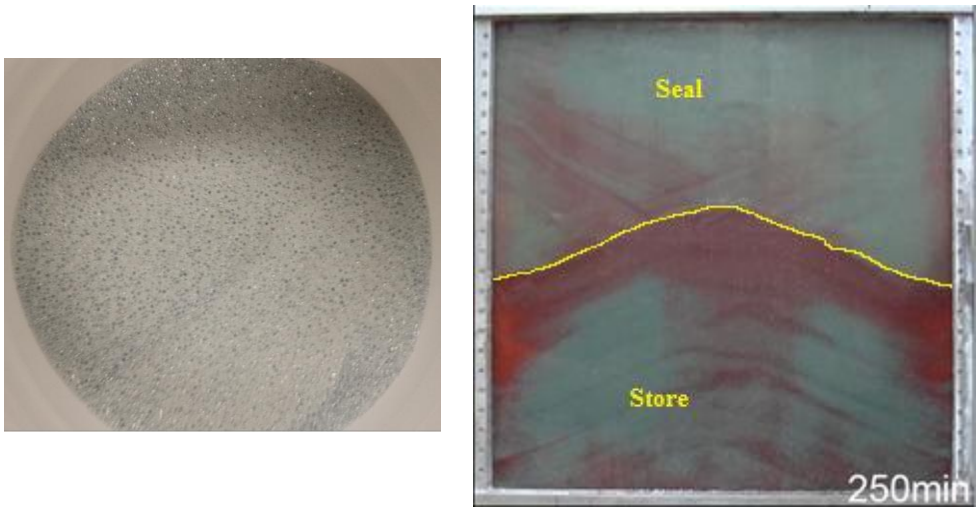


Figure 5.2: **(left)** Mixture of 0.5 mm (50%), 2 mm (25%), 3 mm (25%) beads used to form the store. **(right)** The dry packing process produces local heterogeneity in the form of layers as larger beads roll and settle differently than smaller beads along the top of already settled beads. A seal made of a mixture of 0.25 mm (67%) and 0.5 mm (33%) beads is poured into the domain above the store from the left and right corners at the top. The store was poured from the center position at the top. At end of upward migration of nonwetting phase from the bottom with open boundaries and hydrostatic potential highlights local heterogeneity within both formations, in the form of thin layers of relatively large beads. These layers are conduits for migration because they have smaller entry pressure. Increased degree of heterogeneity blurred the boundary between seal and store.

Degree of heterogeneity and bead size distribution thus has significant impact on the integrity of local capillary trapping mechanism. Table 5.1 below suggests a series experiments to investigate this phenomenon. This could serve as an important initial step in determining the total amount of $CO_2$ that could be stored in a particular heterogeneous storage formation.

| Exp.# | Seal (Caprock) | | | Store | | |
|---|---|---|---|---|---|---|
| | 0.1 mm | 0.25 mm | 0.5 mm | 0.5 mm | 2 mm | 3 mm |
| 11 | | 67% | 33% | 50% | 25% | 25% |
| 12 | | 50% | 50% | 50% | 25% | 25% |
| 13 | | 33% | 67% | 50% | 25% | 25% |
| 14 | 67% | 33% | | 50% | 25% | 25% |
| 15 | 50% | 50% | | 50% | 25% | 25% |
| 16 | 33% | 67% | | 50% | 25% | 25% |

Table 5.1: Experimental plan for influence of bead size distribution on local capillary trapping

# Bibliography

Bryant, S. (1996) "Quantification of Spatial Correlation in Porous Media and Its Effect on Mercury Porosimetry." *Journal of Colloid and Interface Science* 177.1 (1996): 88-100. Print.

Bryant, S. (2007). Geologic co2 storage — Can the oil and gas industry help save the planet? *Journal of Petroleum Technology*, *59*(09), 98 - 105. doi: SPE-103474-JPT

Busch A, Amann-Hildenbrand A, Bertier P, Waschbuesch M, Krooss BM. The Significance of Caprock Sealing Integrity for $CO_2$ Storage, in *SPE International Conference on $CO_2$ Capture, Storage, and Utilization.*2010: New Orleans, Louisiana, USA.

Chalbaud, C. A., Robin, M., & Egermann, P. (2006, January 1). Interfacial Tension Data and Correlations of Brine-CO2 Systems under Reservoir Conditions. Society of Petroleum Engineers. doi:10.2118/102918-MS

Cinar, Y., Riaz, A., and Tchelepi, H. 2009. Experimental Study of CO2 Injection Into Saline Formations. *SPE J.* **14** (4): 588-594. SPE-110628-PA. doi: 10.2118/110628-PA.

Hernandez Thesis

Crowe, Clayton T.. (2005) *Multiphase Flow Handbook*. Hoboken: CRC Press, 2005. EBook Library.

Earth System Research Laboratory, Global Greenhouse Gas Reference network, http://www.esrl.noaa.gov/gmd/ccgg/trends/

Ecofys & ASN Banks, 2010 world GHG emission flow chart http://www.ecofys.com/files/files/asn-ecofys-2013-world-ghg-emissions-flow-chart-2010.pdf

Edlmann, K., Haszeldine, S., & McDermott, C. I. (2013). Experimental investigation into the sealing capability of naturally fractured shale caprocks to supercritical carbon dioxide flow. *Environmental Earth Sciences*. 10.1007/s12665-013-2407-y

Ferer, M., Anna, S. L., Tortora, P., Kadambi, J. R., Oliver, M., Bromhal, G. S., & Smith, D. H. (2011). Two-phase flow in porous media: predicting its dependence on capillary number and viscosity ratio. *Transport in porous media*,*86*(1), 243-259.

Ganesh, P., Bryant, S.L., and Meckel, T. "Characterizing small-scale migration behavior of sequestered $CO_2$ in a realistic 2D geological fabric," CMWR2012.

Ganesh, P. "Geologic drivers affecting buoyant plume migration patterns in small-scale heterogeneous media: Characterizing capillary channels of sequestered CO2" Master's thesis, The University of Texas at Austin, 2012.

Gladkikh, M., and S. Bryant. "Prediction of Imbibition in Unconsolidated Granular Materials."*Journal of Colloid and Interface Science* 288.2 (2005): 526-39. Print.

Green, C. P., and J. Ennis-King (2010), Effect of vertical heterogeneity on long-term migration of CO2 in saline formations, Transp. Porous Media, 82, 31–47.

Hernandez, A. "Observations of Buoyant Plumes in Countercurrent Displacement." Master's thesis, The University of Texas at Austin, 2011.

Hesse, M. A., and A. W. Woods (2010), Buoyant dispersal of CO2 during geological storage, Geophys. Res. Lett., 37, L01403, doi:10.1029/2009GL041128.

IEA, $CO_2$ emissions from fuel combustion 2012 highlights

IPCC 2005, *Special Report on Carbon Dioxide Capture and Storage*. Rep., page 20

IPCC, 2007. Climate Change 2007: Synthesis Report http://www.ipcc.ch/publications_and_data/ar4/syr/en/spms4.html

IPCC, 2007: Summary for Policymakers. In: *Climate Change 2007: The Physical Science Basis. Contribution of WorkingGroup I to the Fourth Assessment Report of the Intergovernmental Panel on Climate Change* [Solomon, S., D. Qin, M. Manning,Z. Chen, M. Marquis, K.B. Averyt, M.Tignor and H.L. Miller (eds.)]. Cambridge University Press, Cambridge, United Kingdomand New York, NY, USA.http://www.ipcc.ch/pdf/assessment-report/ar4/wg1/ar4-wg1-spm.pdf

Kiehl and Trenberth, 1997 "Earth's Annual Global Mean Energy Budget(Kiehl and Trenberth, 1997 )." Earth's Annual Global Mean Energy Budget.

Krevor, S. C. M., R. Pini, B. Li, and S. M. Benson (2011), Capillary heterogeneity trapping of CO2 in a sandstone rock at reservoir conditions, Geophys. Res. Lett., 38, L15401, doi:10.1029/2011GL048239.

Lovoll, G. "Competition of Gravity, Capillary and Viscous Forces During Drainage in a Two-dimensional Porous Medium, a Pore Scale Study." *Energy* 30.6 (2005) : 861-872. Web.

Lovoll, G. et al. "Influence of Viscous Fingering on Dynamic Saturation–Pressure Curves in Porous Media." *Transport in Porous Media* 86.1 (2010) : 305-324. Web.

Mouche, E., M. Hayek, and C. Mügler (2010), Upscaling of CO2 vertical migration through a periodic layered porous medium: The capillary-free and capillary-dominant cases, Adv. Water Resource, 33, 1164–1175.

Nielson, L., Bourg, I., Sposito, G., Predicting CO2-water interfacial tension under pressure and temperature conditions of geologic CO2 storage, Geochimica et Cosmochimica Acta 81 (2012) 28–38

NOAA, National Climatic Data Center (NCDC) US Records 2012 website at: http://www.ncdc.noaa.gov/extremes/records/monthly/maxt/2012/01/00?sts%5b%5d=US#records_look_up.

NOAA Paleoclimatology World Data Centers Vostok Ice Core CO2 Data. N.p., n.d. Web. 05 Mar. 2014. http://www.ncdc.noaa.gov/paleo/icecore/antarctica/vostok/vostok_co2.html

NRDC, The Consequence of Global Warming on Weather Patterns. http://www.nrdc.org/globalwarming/fcons/fcons1.asp

Oldenburg, C., Bryant, S., and Nicot, J.-P. (2007). Certification Framework for Geologic CO2 storage. Paper presented at National Energy Technology Laboratory, 6th Annual Conference on Carbon Capture & Sequestration, Pittsburgh, PA, 7-10 May

Oregon Department of Fish and Wildlife. 2006. The Oregon Conservation Strategy. http://www.dfw.state.or.us/conservationstrategy/docs/climate_change/ClimateChangeEstuaries_Fact_Sheet.pdf

Plug, W. J., and J. Bruining (2007), Capillary pressure for the sand-$CO_2$-water system under various pressure conditions. Application to $CO_2$ sequestration, *Adv. Water Resour.*, 30, 2339–2353.

PSU, Energy, The facts about raising fuel efficiency. N.p., n.d. Web. 30 Mar. 2014

Saadatpoor, E. "Effect of Capillary Heterogeneity on Buoyant Plumes: New Trapping Mechanism in Carbon Sequestraion" Master Thesis, The University of Texas at Austin, 2009.

Saadatpoor, E., Bryant, S. L., Sepehrnoori, K., 2009, *New trapping mechanism in carbon sequestration*, Trans. Porous Media, 82, 3-17.

Saadatpoor, E., Bryant, S. L., Sepehrnoori, K., 2010, *CO2 leakage from heterogeneous storage formations*, Paper 135629 presented at the SPE Annual Technical Conference and Exhibition held in Florence, Italy, 19-22 September 2010.

Saadatpoor, E. "Local Capillary Trapping in Geological Carbon Storage," Ph.D. dissertation, The University of Texas at Austin, 2012.

Schlumberger Oil field Glossary, pressure gradient http://www.glossary.oilfield.slb.com/en/Terms.aspx?LookIn=term%20name&filter=pressure%20gradient

Schlumberger Oil field Glossary, geothermal gradient http://www.glossary.oilfield.slb.com/en/Terms.aspx?LookIn=term%20name&filter=geothermal%20gradient

Shukla et al. 2010 – A review of studies on CO2 sequestration and caprock integrity. Fuel 89 (10), pp. 2651–2664.

Shukla, R., Ranjith, P., Choi, S., and Haque, A. (2011). "Study of Caprock Integrity in Geosequestration of Carbon Dioxide." Int. J. Geomech., 11(4), 294–301.

TWDB. 2012. Texas Water Development Board – Status and Trends of Irrigated Agriculture in Texas. http://twri.tamu.edu/docs/education/2012/em115.pdf

UNFCCC, Kyoto Protocol http://unfccc.int/kyoto_protocol/items/2830.php

US Census Bureau, *Population Clock*. N.p., n.d. Web. 16 July 2013.

US EIA , *Annual Energy Outlook 2013*. Tech. page 60

US EPA, National Greenhouse Gas Emissions Data.

USGS, 2010, The Concept of Geological Carbon Sequestration.

Yan, H., McLaughlin, E., Hanna, Jason. 'Loss of 19 Firefighters in Arizona blaze 'Unbearable,' governor says.' CNN, July 2 2013. http://www.cnn.com/2013/07/01/us/arizona-firefighter-deaths